THE STELLAR CONTENT OF THE PERSEUS GALACTIC ARM IN THE REGION OF h AND chi PERSEI

Thesis by

Robert LeRoy Wildey

In Partial Fulfillment of the Requirements

For the Degree of

Doctor of Philosophy

California Institute of Technology

Pasadena, California

1962

ACKNOWLEDGEMENTS

The sentiments of anyone for whom the composition of this page is the last act in the preparation of the thesis manuscript can be appropriately summed up in two words: "Thank God!". Nevertheless, beyond this candid offering, not a formal but a very real debt of gratitude is owed by the writer to a number of people whose kindness and skill have been drawn upon as decisive factors in obtaining the present results.

I wish to thank Dr. H. C. Arp, who brought the problem of h and chi Persei to my attention, for the many sessions of expert advice, kindly encouragement, and stimulating discussions I have received. Thanks are due to both Drs. Arp and A. R. Sandage, under whom all of the research of my student career has been done, for any skill I may now possess as an observational astronomer. It is a pleasure to thank Dr. P. W. Hodge for taking several 48 inch Schmidt plates of h and chi Persei for me. Thanks are also due to Dr. J. B. Oke for time on, and operation of, the Burroughs 220 digital computer; and also for the use of his photoelectric spectrum scans. The skill of Mr. Eugene Hancock has been indispensible in solving the difficult problem of simultaneously doing astronomy and successfully navigating the Newtonian platform about the north pier of the 100 inch telescope. I wish also to thank my wife, Diane, for graciously enduring many secretarial labors during the course of observation, reduction, and manuscript preparation.

The manuscript was very kindly reviewed by Drs. H. C. Arp, A. R. Sandage, G. Munch and Mr. D. M. Mihalas whose comments were very helpful.

The support of Drs. J. L. Greenstein and I. S. Bowen in the procurement of observing facilities has been indispensible.

I wish to extend a blanket vote of appreciation to the entire staff of the Mount Wilson and Palomar Observatories and the Astronomy Department of the California Institute of Technology for the many kindnesses shown me during my student tenure.

I am grateful for a van Maanen Fellowship held during the academic year 1960-1961.

The hardships endured for the benefit of my education, in later years by my wife and in former years by my parents, have been inspiring demonstrations of selflessness compounded by the grief of my mother's passing before the final culmination of my education. I do, therefore, lovingly and respectfully dedicate this thesis to Lillian Fern Wildey.

ABSTRACT

A total of 944 stars in the general region of h and chi Persei in the Perseus Galactic arm have been observed photometrically in U, B, and V of the Johnson-Morgan photometric system. Supergiants, O stars, giants, subgiants, and their fainter immediate neighbors (used to obtain reddenings) totaling 336 stars have been measured photoelectrically in the general OB association of which the galactic clusters form the nucleus. Within the extreme nuclei of the clusters-proper, photoelectrically calibrated photographic observations have been made with completeness down to about 18th magnitude on an additional 608 stars; however, the photoelectric limit is V = 17.0. Fine structure is exhibited by the stars above the vertical main sequence and a slightly fainter red off-shoot is found. A sequence of stars is found in apparent gravitational contraction but with main-sequence stars extending, nevertheless, to the observational limit. At present the data is best represented by theories of gravitational contraction, hydrogen-burning, and helium-burning, together with a non-unique epoch of stellar condensation. Contraction and nuclear time-scales for the different features are compatible. The differences in apparent evolutionary tracks between the Galaxy, LMC, and SMC are reconfirmed. The 2-color diagram of the bluest stars is of a gray-body character. Sp vs $(B-V)_o$ is monotonic for all stars. The M supergiants are shifted red-ward over previous studies and form a steep 2-color relation.

I. INTRODUCTION

h and chi Persei are a pair of rich open-clusters (NGC 869 and NGC 884) located at R. A. = $2^h11^m.9$, Dec. = $+56^\circ40'$, $l^I = 102^\circ.4$, $b^I = -3^\circ.1$, $l^{II} = 134^\circ.6$, $b^{II} = -3^\circ.7$, and R. A. = $2^h15^m.0$, Dec. = $+56^\circ40'$, $l^I = 102^\circ.8$, $b^I = -3^\circ.0$, $l^{II} = 135^\circ.0$, $b^{II} = -3^\circ.6$, respectively. The right-ascension and declination are for the epoch 1900.0 and the superscript is adopted in accordance with the recommendation of Blaauw, Gum, Pawsey, and Westerhout (1959). The interstellar absorption is extremely patchy in this region making photometric study difficult. Other groups of stars in the Galaxy are known to be as young, but none so far investigated offers the possibility of such a large approximately homogeneous sample for study as the double cluster together with its neighboring stars in the Perseus arm.

A photometric study of these stars is significant in at least four areas of astronomy: (1) the atmospheres of hot stars and supergiants through the colors and spectra, (2) the evolution of massive young stars through the color-magnitude (C-M) and Hertzsprung-Russell (HR) diagrams and the luminosity function, (3) the cosmic distance-scale through the brightest-star criterion, and (4) the history of star formation through the luminosity function and an appropriate theory. In the present study the emphasis is primarily on (2) and to a lesser extent (1).

a) Background

Struve (1927), in a discussion of the Henry Draper Catalogue stars of type B3 or earlier, emphasized a very thick clustering of B

stars in Perseus and suggested that we are here dealing with an actual grouping in space. This suggestion was strengthened when it was discovered that these stars possess interstellar calcium lines of comparable intensity. Although the apparent spatial extension of these supergiants relative to the clusters left them in doubt as cluster members, Shapley (1930) included them in the first HR diagram of h and chi Persei. This diagram, which is uncorrected for reddening, possesses the same general features as the C-M and HR diagrams currently accepted (Johnson and Morgan 1955, and Johnson and Hiltner 1956), except for the M supergiants. Of course, the precision and calibration of the photometry and spectroscopy in the early work is not as good.

A theoretical barrier then (as opposed to the observational barrier presented by the highly variable reddening) in the interpretation of studies of the combination of the clusters and the halo of supergiants, has always been the question of membership. Various criteria have been brought to bear in attempting to solve this problem. Proper motions in the region have been studied by van Maanen (1911, 1917, 1920, 1944); Macklin (1922); Pettit (1919), and others. Radial velocities have been obtained by Adams, Joy, and Humason (1926); Plaskett and Pearce (1933), and others. The number of stars which can be eliminated in this way (proper motions decidedly different from zero and radial velocities markedly different from -43 km/sec) is, however, very small (Oosterhoff 1937). Proper motion determinations based on a much larger separation of epochs would be very helpful, but are not presently available. Oosterhoff (1937) has found a definitive radius

of 11' each for the clusters-proper (nuclei) based on radial counts of faint stars. For the brighter stars (supergiants) the radii are inconclusively established as about the same due to poor statistics.

The extent of the neighboring arm population of supergiants which are hopefully related to the clusters and therefore constituting within themselves a homogeneous group is now established as at least seven degrees across (Bidelman 1943; Johnson and Morgan 1955; Johnson and Hiltner 1956; Blanco 1955, and Sharpless 1958).

Bidelman (1943) reconfirmed Struve's conclusion that a maximum in the concentration of early type stars over this region of the Perseus sky was centered on the double cluster from studies of stars earlier than A2 complete to $m_v = 7.5$ in a region ten degrees by fifteen degrees centered on the clusters. His spectroscopic investigation was complete to mag. 8.5 in a circle six degrees across and to mag. 9.5 in squares 37' on a side centered on each cluster. The latter regions are those in which Oosterhoff (1937) obtained the first C-M diagrams of h and chi Persei.

Oosterhoff's C-M diagrams were uncorrected for reddening and based on pure photographic photometry and the effective-wavelengths of objective-prism spectra. They exhibit the general features of a steep main-sequence curving redward at the top.

Upon first examining Bidelman's (1943) HR diagram one is struck by the separation of the early supergiants from the top of the main-sequence which phenomenon is similar to recent results in NGC 330 of the Small Magellanic Cloud (SMC) obtained by Arp (1958a, 1959a, 1959b). Two aspects of Bidelman's procedure demonstrate that

this is a selection effect. His absolute magnitudes were obtained from the spectra using the luminosity-calibration of Morgan and Keenan (1943). He then used apparent magnitudes to obtain distance moduli. From an examination of the distribution function of stars with respect to distance moduli, stars were rejected which did not lie within reasonable limits of the maximum. This procedure does not permit luminosity to be a continuous function of luminosity class and the stars in Bidelman's gaps are therefore rejected as foreground and background objects. Aside from this, the form of the diagram is in general agreement with the presently accepted version.

Bidelman (1943) included 13 M type supergiants in his analysis which were also found to be concentrated at the double cluster. This had been noted previously by Keenan (1942) who estimated that among the M type variables of small range the material was reasonably complete down to ninth apparent magnitude. Joy's (1939) radial velocity measurements were found to be compatible with the membership of these objects in the association.

The radial velocity-dispersion among the stars of the clusters is about 0.88 km/sec according to Bidelman, who shows dynamically that the supergiants cannot have been expelled into the association from the clusters whose relaxation time is of the order of 10^8 years. The dispersion among the outer stars is evidently not more than 3 or 4 km/sec (Oosterhoff 1937, Bidelman 1943).

The peculiar-motion of the whole group is probably small. Evans (1941) reports that the stellar and interstellar lines agree in giving the same distance which implies that the peculiar-motion of

the stars is small if we assume that the peculiar-motion of the interstellar gas is small. Bidelman, using Oort's constant A = 18 km/sec and assuming that the stellar radial velocity after subtraction of the solar motion is due entirely to the galactic rotation of the Perseus arm, finds a distance of 2180 parsecs corresponding to a true m - M = 11.7 in reasonable agreement with the presently accepted value of 11.8 (Morgan, Whitford and Code 1953a, and Johnson and Hiltner 1956).

Among more recent efforts, the greatest sources of increase of our understanding of these objects have been due to: (1) accurate spectral classification of many of these stars on the MKK system (Johnson and Morgan 1955); (2) application of photoelectric photometry (Stebbins, Huffer, and Whitford 1940) especially the UBV system (Johnson and Morgan 1953) which is accurately transformable to, and with which the reddening may be derived without recourse to spectra (Johnson and Morgan 1955; Johnson and Hiltner 1956); (3) an extension of supergiant member-candidates through surveys (Blanco 1955, and Sharpless 1958); and (4) the interpretation of general features of the C-M diagram in terms of the theory of stellar evolution at constant mass on a hydrogen burning time-scale together with an improvement of the photometric-parallax through the development and proper use of an age-zero main-sequence (Sandage 1957a).

On the basis of the most recent data, exclusive of the present study, then, the following picture of h and chi Persei is presented.

The C-M diagram. An unevolved main-sequence is picked up at $M_V = +2$ (observational limit) and, in a normal manner, becomes bluer as it becomes brighter. At about $M_V = -4$ the main-sequence begins to show the effects of evolution. A "knee" is exhibited beyond which brighter stars become redder. The evolved main-sequence breaks off at $M_V = -7.5$ and $(B-V)_o = 0.1$, corresponding to hydrogen exhaustion in the inner core and an estimated age of a few million years (Johnson and Hiltner 1956; Sandage 1957; and Arp 1958b). The M supergiants which fill the interval $-6 < M_V < -4$, $1.6 < (B-V)_o < 2.0$ roughly linearly represent advanced evolution which we do not understand in detail.

The $(U-B)_o$ versus $(B-V)_o$ diagram. The luminosity-class V stars, of course, fall on the normal relation. The early supergiants (Ia, Iab, Ib) show an ultraviolet-excess of about $0^m.35$ mag. relative to the main-sequence (V) stars and lie roughly parallel to the class V relation. This plot has not been published for the M supergiants. See Johnson (1958).

The $(B-V)_o$ versus Sp diagram. The early supergiants show a color-excess of about $0^m.1$ mag. relative to luminosity-class V from B0 to A0. From A0 to A3 the supergiants cross the class V relation reaching a maximum color-deficit of -0.15. The color-deficit then decreases with the extrapolation again crossing the axis at F8. The "kink" between A0 and A3 is strong enough so that on an absolute plot, between these limits, the intrinsic color becomes bluer as the spectral type becomes later. See Johnson (1958). This plot has

not been published for the M supergiants.

The most satisfactory reddening corrections used to date have been to determine an average correction in the vicinity of the nuclei (Oosterhoff's region), and for the surrounding association the following. Johnson (1958) has plotted the color-excess, $E_{(B-V)}$, versus galactic latitude from early class V stars in the region. The mean curve drawn varies from $0^m.25$ at -6° to $1^m.0$ at $+0^\circ.5$. In conjunction with this curve a second mean relation is given of the correction to be applied to the color-excess, as determined from the first curve, as a function of galactic longitude. This was obtained by plotting the residuals of the first curve. This is tantamount to the assumption:

$$E_{(B-V)} = f(l, b) = g(l) + h(b) \qquad (1)$$

The plots show considerable scatter.

The spiral structure of the Galaxy has been studied from the point of view of the distribution of typical arm objects; for example, HII regions (Morgan, Sharpless, and Osterbrock 1952a, 1952b), and 21 cm HI emission (Schmidt 1957). From the studies of Be stars by Mendoza (1958), O associations by Morgan, Whitford, and Code (1953b), and interstellar polarization by Hiltner (1956), it has been deduced that the local spiral arm is inclined to the Galactic plane. This nourishes our hopes for a scarcity of background contaminants in the region of h and chi Persei. The double cluster has been shown to belong to the Perseus arm (van de Hulst, Muller, and Oort 1954) whose extension at this point is approximately perpendicular to the

line of sight (Bok 1959).

The past investigations (and, as will be seen, the present study) can be represented by the following picture. Consider a reference frame of origin at the Galactic nucleus and rotating with the Perseus arm at the region of the double cluster. Some tens of millions of years ago or more this region of the Perseus arm was populated predominantly by a large cloud of gas and dust of relatively low turbulence. The cloud possessed a maximum density roughly corresponding to the present position of h and chi Persei. This maximum was bounded by a surface within which the material constituted, dynamically, a system of negative energy. Star formation then began in the cloud according to a creation function which need not be severely restricted as to functional form. The material within the proposed closed surface condensed into stars which did not disperse and represent the present clusters-proper. The stars outside this surface have been dispersed somewhat (which gives rise to definitive cluster boundaries) but due to their small peculiar-motion, stemming from the low turbulence and angular momentum of the original cloud, they still show qualitatively the density gradient of the original cloud. This highly heuristic scheme may be the simplest explanation of the situation which exists in the Perseus arm in the region of h and chi Persei. The hypothesis cannot be proved and will not be discussed further.

b) The Present Study

The primary reasons why further value can be obtained from the present study are: (1) the greater detail given to the determination

of the reddening of bright stars whose intrinsic color-color relationship is not well known; (2) the increased information on the nature of the population of the supergiant halo (neighboring arm population) through the measurement of faint stars there; (3) the extension with completeness to fainter magnitudes in the extreme nuclei of the clusters; (4) the large increase in the number of data points, which makes possible the detection of the dependence of possible departures from homogeneity on galactic latitude and longitude.

By intrinsically-unreddened we shall mean that the star in question was traced back along its known reddening trajectory to its intersection with the unreddened two-color relationship for luminosity-class V. By extrinsically-unreddened we shall mean that the reddening for a given star was obtained from the color-excesses of its fainter neighbors.

The important bright-stars of the general region of the surrounding Perseus arm population which are subjects for extrinsic-unreddening have been divided into three groups: (1) the supergiants, (2) the O stars, and (3) a sample of giants and sub-giants of early type. All of these stars have accurate spectral classifications and unobjectionable radial velocities except for those untested M supergiants not on Bidelman's (1943) list of 13, which remain admirable candidates for high-dispersion spectroscopy. The O stars have been grouped separately because very few of them have been classified with respect to luminosity. These three groups of stars have been compiled from lists of Johnson and Morgan (1955); Johnson and Hiltner (1956); Blanco (1955), and Sharpless (1958). They are bounded by

R. A. (1855) = 1^h50^m, R. A. (1855) = 2^h43^m, Dec. (1855) = $53^\circ10'$, and Dec. (1855) = $61^\circ00'$. The material is reasonably complete as far as the M supergiants are concerned, and probably within a factor of about two as far as the early supergiants are concerned. With regard to the absence of stars in the range AV to K9 the scarcity in the early part of the range is probably real according to the catalogue of R. E. Wilson (1941) while further work is needed for the later types. The investigation of the completeness of the entire upper part of the C-M diagram in supposed horizontal evolution is planned by the writer for the near future.

The intrinsically-unreddened stars (neighbors) used to find color-excesses for the individual bright-stars of the above three groups were selected according to the following criteria: (1) at least two neighbors per bright-star; (2) the neighbors should be as close to the bright-star as possible without requiring unduly rare seeing conditions for photometry; (3) the stars should be sufficiently faint so that if they are not at a greater distance and not much older than the bright-star, they can be assumed to be unevolved; (4) stars which appear obviously red for their brightness on the blue and red prints of the National Geographic-Palomar Sky Survey are rejected (few neighbors were excludable in this way), and (5) the neighbors should fall on opposite sides of the bright-star. The inclusion of binaries in this sequence will not have serious consequences unless the straight line-segment, joining the two points in the two-color diagram corresponding to the intrinsic-colors of the individual binary

components, deviates significantly from the class V two-color relationship. Any gravitationally-contracting stars included in this sequence, unless too near the sun to be of value, will not be late enough to have their intrinsic-colors depart from the class V relationship (Walker 1956, 1957, 1959, 1961, and Johnson and Mitchell 1958).

Within the extreme nuclei of the clusters a sufficient number of stars have been intrinsically-unreddened to plot contours of equal reddening over the sky. Such a curve will hereafter be referred to by the shortened work, isocrypt, from the Greek words for "the same" and "hidden or obscure."

Through an essentially morphological approach to the C-M diagram the present study "solves by avoidance" the problem of membership. According to the theory of stellar interiors in its most general form (Chandrasekhar 1957; Schwarzschild 1958; Arp 1958b) the departure of star plots in the $(\log T_e, M_{bol})$ plane from a unique sequence can only arise through a dispersion in one or the other or both of (1) the initial chemical composition, and (2) the age. This neglects such things as internal magnetic field, rotation, and acretion (see Mestel 1959; Lambrecht 1959; Wentzel 1961, and Schatzman 1960) which is probably reasonable. By appeal to the general theory of stellar atmospheres this principle becomes immediately extendable to the C-M diagram since no new parameters are introduced by this theory. That is to say; given the initial chemical composition and the mass, the subsequent history of M_{bol}, T_e, and R hence g is uniquely determined. Inasmuch as the emergent

monochromatic flux is a function only of T_e, g, and present chemical composition hence initial composition and age, then color-index and bolometric-correction are also specified throughout time for the same given star. Thus the Russel-Vogt theorem is as rigourously valid in the C-M diagram as it is in the M_{bol}- log T_e diagram. [This does not preclude the possibility that dispersion in the C-M diagram may consistently preserve uniqueness in the (log T_e, M_{bol}) plane (Sandage and Eggen 1959; Melbourne 1960; Burbidge, Burbidge, Sandage and Wildey 1959, and Wildey, Burbidge, Sandage and Burbidge 1961).] Finally, since it is the color-apparent magnitude diagram with which we must observationally deal rather than the color-absolute magnitude diagram, we must introduce (3) the distance moduli of stars.

Throughout the present study it will be assumed that the chemical composition of all stars in the direction of h and chi Persei (general region) that are capable of coalescing into major sequences in the color-apparent magnitude diagram are of the same chemical composition and that this composition is negligibly different from the solar neighborhood composition as far as the C-M and two-color diagrams are concerned. This disposes of (1).

In order to keep from being misled by (3) we must refrain from basing any interpretation on isolated points in the color-apparent magnitude diagram.

We shall regard the uniqueness of age (2), then, as a hypothesis to be tested in our interpretation.

In order to be effective, such a program requires that the

range in absolute magnitude of the subject matter be as independent as possible of galactic lattitude and longitude. This is afforded by the same technique which improves our reddening correction for the bright-stars.

II. THE PHOTOELECTRIC OBSERVATIONS

The supergiants, O stars, and giants-and-subgiants are listed in Tables 1, 2, and 3 respectively (Appendix I). Column 1 gives the number according to the present study. Column 2 gives the Henry Draper number when available. Column 3 gives any other common designation. Numbers preceded by Oo are Oosterhoff numbers. Columns 4 and 5 give the right-ascension and declination for 1960. Column 6 gives the spectral type on the MKK system. Column 7 gives the absolute visual magnitude determined in the present study. These stars are identified in Figures 1, 2, and 3 (Appendix II). The number in the lower left hand corner of each square is from column 1 of the foregoing tables, and corresponds to the bright-star in the center of the square.

Tables 4, 5, and 6 (Appendix I) list these three groups of bright-stars again in the same order. The number in column 1, when underlined, corresponds to the same number in column 1 of Tables 1, 2, and 3. Immediately following each underlined entry in column 1 of Tables 4, 5, and 6, a sequence of integer designations, in cardinal order, and always beginning with 1, is listed. Each such sequence refers to the faint-neighbors of the bright-star referred to by the immediately preceding underlined number. Each sequence is indicated in the appropriate square of Figures 1, 2, and 3. Occasionally, in column 1 of Tables 4, 5, and 6, an Oosterhoff number, which is <u>not</u> underlined, follows the small-integer sequence of one of the underlined numbers. This means that this star, which has already been measured by Johnson (Johnson and Morgan 1955), is

close enough to the bright-star it follows in the list and is itself faint enough so that it is of value in extrinsically-unreddening said bright-star. Columns 2, 3, and 4 of Tables 4, 5, and 6 give the adopted photoelectric magnitudes and colors from the present study. They are the evenly weighted means of the individual measurements of the present investigation, and, for some of the bright-stars, the published values of Johnson and Morgan (1955) and Johnson and Hiltner (1956).

In addition to the above, a sequence of faint stars midway between the cluster nuclei was selected for photoelectric measurements. This sequence, together with previously published nuclear stars of somewhat brighter magnitude, provides the photoelectric calibration of the photographic investigation of the extreme nuclei. This faint sequence is indicated in Table 7 (Appendix I). Column 1 gives the identifying letter. Columns 2 and 3 give the offset coordinates of these stars from Oosterhoff 1818 (FZ Persei) in seconds-of-arc. The material for these columns was obtained using a sixty-inch direct plate and the two coordinate measuring engine of the Mount Wilson Observatory. The plate scale was 27.12 "/mm. Columns 4, 5, and 6 give the V, B, and U magnitudes respectively together with their formal probable-error.

The photoelectric observations were obtained using the 60-inch, 100-inch, and 20-inch telescopes of the Mount Wilson and Palomar Observatories according to the following schedule. 20-inch observations: November, 1959, 6 nights; December, 1960, 8 nights. 60-inch observations: November, 1959, 7 nights; August, 1960, 11

nights; September, 1960, 4 nights. 100-inch observations: November, 1959, 3 nights; October, 1960, 5 nights. There were thus a total of 44 nights out of which 33 were photometric with good seeing conditions. All of the observations were made during the dark-run except for the first run on the 20-inch. During moonrise and moonset and after astronomical twilight a given star was observed in the sequence star-sky-star to allow for the rapidly changing sky brightness. The maximum value of secant Z was approximately 1.6, while the minimum value, as h and chi Persei crossed the meridian, was nearly 1.0. Each star of Tables 4, 5, and 6 was observed on two different nights. The stars of Table 7 were observed at least six times each. The diaphragm for selective admission of light to the photometer was accurately placed in the focal plane (Newtonian-focus) by using the aperture boundary as a knife-edge. The aperture diameter was maintained at three times the apparent diameter of the seeing-tremor-disk, which proved sufficiently inclusive of all starlight.

The photometer employed a dry-ice refrigerated RCA 1P21 photo-multiplier behind a Fabry lens which focused an image of the objective-mirror of optimum size for quantum-yield onto the photo-cathode. The 1P21 was operated at an accumulated potential drop of 960 volts provided by a voltage-regulated power-supply. The photometer signal was fed into a General Radio d.c. amplifier whose gain ranged from 10 to 27.5 magnitudes. The amplifier output was fed into a Brown strip-chart recorder.

The production-model amplifier has a range of Victoreen input resistors which proceeds in two-and-one-half magnitude steps.

The amplifier has been modified by the incorporation of a range of precision wire-wound feedback resistors which results in overall loop-gain steps of one-half magnitude. The amplifier has provision for internal calibration of the two-and-one-half magnitude gain steps. The one-half magnitude gain steps were calibrated using the photometer and a radium source. The calibration was found not to vary from night to day. The power was maintained uninterrupted throughout a given observing run.

The equipment has been described elsewhere (Walker 1957, and Varsavsky 1960).

The filters used were 2-mm Corning 9863 in the ultra-violet, 1.3-mm GG13 plus 0.7-mm BG12 in the blue, and 2-mm GG11 in the yellow. The deflections were transformed to the Johnson-Morgan UBV system by the simultaneous observation of standard stars from their list (1953) and a fainter list of secondary standards kindly provided by Dr. Arp. Since it was convenient to do so, as many as 35 standard stars were measured for a given transformation. The number was never less than 15. The extinction correction and transformation to the UBV system were both secured on a Burroughs 220 digital computer through the program of Arp (1959c) modified to the exclusion of the iteration of extinction coefficients.

Thus was adopted the policy of Johnson (1951), Hiltner (1956), and Arp (private communication), to the effect that the most suitable values of extinction coefficients are means based on a large number of good nights, since these will generally be closer to the true values on any other good night than those derived on that night alone. We

may further quote photoelectric pioneers Stebbins and Whitford (1945):

"It is impractical to determine extinction thoroughly and accomplish anything else."

The magnitudes and colors read out were subjected to the following final correction procedure. Two local-standard stars were chosen (Oo1162 and Oo1187) and measured several times each night. Their average read-out values over all runs were the same as the published magnitudes and colors of Johnson and Morgan (1955). Using these values and the individual read-outs, residuals were plotted as a function of time from which corrections to each set of magnitudes and colors read out were obtained. These corrections were applied to all the unknowns before averaging. Although the region studied is too large for individual telescope settings to be placed on the observer's slow-motion itinerary, it is still small enough that the telescope's hour-angle remains a reasonably unique function of time. Any dependence of the above residual plots on hour-angle was masked by their general similarity to noise-with-a-long-time-constant (i.e. slow random variability), thus showing the advisibility of the present use of mean extinction coefficients. Although the two local-standards do not differ in color by a great deal, they indicated that only the gray term of atmospheric extinction varied.

The averaged formal probable-error of all the photoelectric stars excluding those of Table 7 is shown in Table 8 (Appendix I). Reference is thus to a single entry in Tables 4, 5, and 6.

III. THE PHOTOGRAPHIC OBSERVATIONS

The 60-inch telescope, when diaphragmed to 32 inches, has a photometric field large enough to include the nuclei of both clusters. A total of 608 stars were chosen in circled areas 6 minutes-of-arc across in the extreme nuclei of h and chi Persei. Completeness was achieved down to about V = 18. These stars are indicated in Tables 9 and 10 (Appendix I), and Figures 4 and 5 (Appendix II). Column 1 of the tables gives the present designations which appear in the figures. Columns 2, 3, and 4 give the photographically derived magnitudes and colors on the UBV system.

The photographic observations were made on 5 nights in September, 1960, and 4 nights in July, 1961. All observations were made at the Newtonian-focus of the 60-inch telescope. A total of 53 plates were taken, ranging in exposure from 15 seconds to 2 hours, and are catalogued in Table 11 (Appendix I). Secant Z was never greater than 2.

The telescope was collimated by taking an out-of-focus exposure of a bright star-cloud and identifying the position where the toroidal images were symmetrical about their centers. Knife-edge focusing was used with filter-offsets from an empirical relation due to Baade (communicated to Arp).

The filter-emulsion combinations used were Kodak 103a-D plus 2-mm GG11 for the yellow, 103a-O plus 2-mm GG13 for the blue, and 103a-O plus 2-mm either UG2 or Corning 5840 for the ultraviolet. These combinations reproduce the bandpasses of the UBV system

for normal secant Z (Johnson and Sandage 1955; Sandage and Walker 1955; Johnson, Sandage, and Wahlquist 1956; Sandage 1958; and Walker 1961). The plates were developed for 4 minutes in D-19 with mechanical agitation. This was followed by 15 seconds of acetic acid short-stop. Two hypo solutions were used; a first until clearing and a second of equal duration. The plates were washed for one hour.

The plates were measured on the Sartoris iris-diaphragm photometer of the Mount Wilson and Palomar Observatories. The 6 best plates (2 per color) of the longest exposures were measured first (all 608 stars). The photoelectric-sequence used to calibrate these measurements is given in Table 7 (Appendix I) and Table 12 (Appendix I). The magnitudes in Table 12 are due to Johnson and have been published elsewhere (Johnson and Morgan 1955). Column 1 of Table 12 gives the present designation (corresponding to column 1 of Tables 9 and 10) if it exists. Column 2 gives the Oosterhoff designation. Columns 3, 4, and 5 are self-explanatory. The calibration-curves of magnitude versus iris-diameter were obtained from the photoelectric-sequence and the unknowns were read off in the usual way (Wildey 1961).

By a combination of eye-inspection of the images and the agreement between the measurements, overly crowded stars were selected for remeasurement on shorter exposure plates. A few stars were (1) too crowded on long exposure plates and (2) below the plate limit on shorter exposure plates. The rejection of these few is estimated to have a negligible effect on the completeness.

Inspection of the differences between the photoelectric and photographic values for those stars of the photoelectric-sequence representing the extreme range in (1) distance from the optical-axis and (2) color revealed no systematic effects due to (3) comatic distortion or (4) the presence of a color-equation.

It will be noted that the photographic material extrapolates the photoelectric data by about one magnitude. It is estimated that the systematic accuracy in the extrapolated region is about $0^m.2$ in V, $0^m.5$ in B-V, and $0^m.6$ in U-B. Stars in this region are suitable only for the luminosity function and determining the number of sequences present in the C-M diagram.

For the majority of stars, which are photographically-interpolated, the estimated probable-errors are $0^m.02$ in V, and $0^m.03$ in B-V and U-B, obtained by analysis of the residuals from the mean of the two independent photographic measurements per color for a sample of thirty stars.

IV. THE INTERSTELLAR ABSORPTION AND REDDENING CORRECTION

In general, one expects the reddening-trajectory in the U-B vs B-V diagram to be non-linear and dependent on $(B-V)_o$ since

$$S_\lambda \neq \delta(\lambda - \lambda_o) \tag{2}$$

and

$$\kappa = f(\lambda) \neq \text{constant} ; \tag{3}$$

where

S_λ = the response-function of the U, B, or V bandpass;

$\delta(x)$ = the Dirac delta function

and

κ_λ = absorption-scattering coefficient per unit mass due to interstellar matter.

The non-linearity has been found observationally by Hiltner and Johnson (1956), who have well determined the coefficient of the second-order term as 0.05. The variation of the coefficient of the first-order term (the slope) with intrinsic-color or spectral type has been found observationally by Walker (1957); Johnson (1958), and from the analysis of Lindholm (1957). Johnson (1958) has reviewed the data and, assuming

$$\frac{E_{(U-B)}}{E_{(B-V)}} = X + 0.05\, E_{(B-V)} , \tag{4}$$

he has tabulated X as a function of $(B-V)_o$ for the range $-0.32 < (B-V)_o < 0.10$.

Aside from the fact that X has not been obtained for intrinsic-colors as red as some of those in which we are interested; one cannot obtain the color-excess, for a star of a given intrinsic-color, from the color-excess of an adjacent intrinsically-unreddened star, of different intrinsic-color, without recourse to both (1) the reddening-trajectories and (2) the loci-of-constant-mass-of-interstellar-absorbing-matter. The second relation is not presently available.

For these reasons the following program was instituted. The interstellar absorption A_v may be rigorously written

$$A_v(\rho\ell) = 2.5 \log\left[\frac{\int_{\lambda_a}^{\lambda_b} S_\lambda F_\lambda (1-\eta_\lambda) d\lambda}{\int_{\lambda_a}^{\lambda_b} S_\lambda F_\lambda (1-\eta_\lambda) e^{-\kappa_\lambda \rho\ell} d\lambda} \right]; \qquad (5)$$

where

$F_\lambda(1-\eta_\lambda)$ = the monochromatic emergent flux of stellar radiation;

F_λ = the flux from the continuous spectrum only;

η_λ = the line-blanketing coefficient;

$\rho\ell$ = the integral of the density of interstellar absorbing matter along the line of sight (κ_λ is thus assumed independent of space coordinates);

and λ_a and λ_b are the cut-off wavelengths of the band. Similar expressions can be written for B and U. The following cut-off wavelengths were adopted: U(λ2943-4086); B(λ3641-5475); and V(λ4853-6690). They were estimated from S_λ taken from Code (Melbourne 1959).

Thus, given the spectral energy distributions of a few stars of known intrinsic-colors and the interstellar-reddening law we can develop (1) A_V, $E_{(B-V)}$, and $E_{(U-B)}$ as a function of the amount of interstellar dust; (2) the reddening-trajectories in the two-color diagram, and (3) the loci-of-constant-interstellar-dust in the two-color diagram. The first two are sufficient for all corrections needed in the present study. κ_λ has been taken from the work of Stebbins and Whitford and is tabulated by Oke (1961a).

Absolute-energy-distributions obtained from photoelectric spectrum scans were very kindly provided by Dr. J. B. Oke. A continuum and a fictitious-continuum were provided for the O9 star HD214680 and the K0III star δ Tauri. The intrinsic-colors of these stars are $(B-V)_o = -0.35$ and 0.98 respectively. The writer measured the line-blanketing coefficient on the original scans and used it to depress the continuum of each star; at the same time applying a degree of smoothing with respect to wavelength which was appropriate to the mesh-fineness of the numerical integration method to be used. This yielded $F_\lambda(1 - \eta_\lambda)$.

Integrations on both stars were carried out for values of $\rho\ell$ equal to 1, 3, 6, 9, and 12 (arbitrary units). An $n = 5$ Gaussian quadrature was used (see Margenau and Murphy 1956, pages 479-482). The integrand factors and the integration parameters are tabulated in Tables 13 and 14 for HD214680 and δ Tauri respectively. Terms undefined in the present paper are defined in Margenau and Murphy.

In addition to the two above, a third integration was carried out using the sun (center of the disk). A detailed integration using

the ordinary summation-of-slim-rectangles approximation but with a mesh-fineness of 25 A was employed. The blanketing coefficient was taken from Wempe (1947), and Michard (1950). The continuum, from model atmospheres, was found by interpolation in the tables of de Jager and Neven (1957). In earlier calculations of blanketing-vectors in the two-color diagram, the differences between results obtained using this continuum and results found using the empirical continuum of Minnaert (1953) had been found to be only a few thousandths of a magnitude. The tabulations of the integrations, except for the factor $e^{-\kappa_\lambda \rho \ell}$ which is straightforward, are from the blanketing-project (Wildey, Burbidge, Sandage, and Burbidge 1961) and will not be reproduced here.

The results of the integrations are found in Table 15 (Appendix I) and are plotted in Figure 6 (Appendix II). In order to best interpolate and extrapolate the three curves of Figure 6 into the network of the one-parameter family of curves shown, the data in Table 15 was used to plot color-excess versus intrinsic-color $(B-V)_o$ for constant values of $\rho\ell$. These plots are shown in Figures 7 and 8. A straight line was fitted by eye to the points. The fit is excellent. The linear-relations shown in Figures 7 and 8 were thus used to extend the curves of Figure 6. The horizontal dashed lines shown in Figures 7 and 8 are asymptotes corresponding to infinitely blue (not infinitely hot) and infinitely red stars. They are obtained by assuming monochromatic magnitudes at the blue and red cut-off wavelengths of the bandpasses. Due to the gentle sloping foot of the red side of the V bandpass, the cutoff wavelength shown on page 23, which was

used for the integrations, was replaced by the wavelength intercept of the linear tangent at half-maximum. One would expect these asymptotes to be crossed and approached from the outside, since the second-derivative of the spectral energy distribution would be positive at all finite wavelengths as either extreme was approached. These asymptotes are fictions presented for purposes of comparison and orientation.

a) The Intrinsic-Unreddening

All intrinsic-unreddening was performed graphically using the network of reddening-trajectories and intrinsic color-color relationship (class V) shown in Figure 9 (Appendix II). This figure is presented for general use and the reader is advised to extend the grid across the figure by pencil. The class V relationship shown was taken from that of the Hyades (Johnson and Knuckles 1955, and Johnson and Heckmann 1956) whose mean relationship is tabulated by Sandage and Eggen (1959) over the range available. Outside this range the relationship is from the solar neighborhood (Johnson and Morgan 1953). The network of reddening-trajectories was drawn using equation 4 and Johnson's tabulation of X for its available range. Redward of this the trajectories were obtained from the curves in Figure 6 with the following stipulation. It was immediately noted that the trajectory predicted by Figure 6 for $(B-V)_o = 0.1$ was much steeper than that indicated by Johnson. Johnson's tabulation of X is force-fitted to give the well-known value of 0.72 for O stars. It was found that by multiplying $E_{(U-B)}$ in Figure 6 by 0.802 an

excellent fit was obtained. Since Figure 6 predicted an absorption-to-reddening ratio for early stars that was in good agreement with observation, the discrepancy was concluded to originate in the ultraviolet and the somewhat heuristic factor 0.802 was adopted generally.

The above discrepancy is interpretable as (1) a spuriously long base-line characteristic of the present calculations for $E_{(U-B)}$, and/or (2) a spuriously high value of κ_λ in the ultraviolet. With regard to the first situation, if S_λ adopted in the present calculations extends further into the ultraviolet than the real U bandpass, then the factor 0.802 is merely the scale-factor in the color-equation connecting the real U-B and the fictional one in which $E_{(U-B)}$ of Figure 6 is expressed. Insofar as such a color-equation is universally valid, it should be obtained by fitting at the other extreme, $(B-V)_o = -0.32$. It is found, however, that such a fit leads to a factor of 0.86. The universality of the color-equation for scale-factors so far from unity in bandpasses which both contain the Balmer jump is in sufficient doubt that the problem remains unsolved. It may be approximately calculated that <u>if</u> the U response-function <u>is</u> the source of the discrepancy, then the effective-wavelength of U is about 3700 A rather than the often quoted value of about 3600 A.

Regarding the second possibility, insofar as our $\rho\ell$ is everywhere spuriously high in the U bandpass by the same amount, the effect is indistinguishable from too long a base-line. But if the second situation does exist then it is also likely that we have adopted too steep a rise of κ_λ as one progresses to shorter wavelengths. This means that we will predict a spuriously large second-order term in the redden-

ing trajectory. It appears that we have predicted it to be too large by about the same factor as we have overestimated the first-order term. Rogers (private communication) has recently obtained provisional results from an investigation of the reddening law with a photoelectric scanner which seems to confirm the earlier results of Stebbins and Whitford. Approximation, using the concept of effective-wavelengths, indicates that an explanation of the discrepancy in terms of the reddening law requires that the difference in absorption, in magnitudes, between the U-region and the B-region must be lowered by 20 percent; which is equivalent to - 0. 058 U-magnitudes per magnitude of visual absorption. The solution to the problem awaits further study.

In order to avoid confusion, the reddening-trajectories in Figure 9 were represented by solid lines from the top of the figure down to the first tangency with the intrinsic two-color relation. From there to the second tangency dashed lines have been used. Beyond the second tangency dotted lines are used.

Thus a star is intrinsically-unreddened by translation along its reddening-trajectory until intersection with the intrinsic class V relation. In the event the determination is two-valued the decision is made on the basis of the mutual consistency of normalized color-excesses of close neighbors.

b) The Extrinsic-Unreddening

When the most mutually consistent set of color-excesses has been obtained for the faint neighbors of a bright-star (as defined on page 10) of the general region of h and chi Persei, the color-excess of the bright-star is found in the following way. The color-excesses

are averaged and applied to the bright-star thus obtaining for it a provisional intrinsic-color. Each faint-neighbor's color-excess is then normalized to this provisional intrinsic-color as follows. Each neighbor's $(B-V)_o$ and $E_{(B-V)}$ determines a point in Figure 6. This point is then moved along the vertical line-of-constant-$\rho\ell$ until intersection with the curve identified by the provisional intrinsic-color of the bright-star. A new color-excess corresponding to this point is then read off of the curve. A similar procedure exists for normalizing the ultraviolet color-excess. Thus for this particular purpose Figure 6 is only used differentially. The new color-excesses are applied to the bright-star leading to an improved intrinsic-color. The procedure converges on the true intrinsic-color. In practice a single iteration is sufficient. Finally Figure 6 yields A_V from $(B-V)_o$ and the value of $\rho\ell$ determined by $(B-V)_o$ and $E_{(B-V)}$ for any star. The intrinsic magnitudes and colors together with the absolute magnitudes found from the distance modulus (discussed later) are given for the stars of Tables 4, 5, and 6 in Tables 16, 17, and 18 (Appendix I) respectively. The column headings are self-explanatory.

Similar results are presented for the stars of Tables 9 and 10, of the extreme nuclei, in Tables 19 and 20 (Appendix I) respectively. The reddening was handled as follows. A sufficient number of stars (those in Tables 19 and 20 whose entry under $(B-V)_o$ is parenthesized) were intrinsically-unreddened in B-V so as to construct isocrypts which are indicated in Figures 10 and 111 (Appendix II). The color-excesses were normalized to $(B-V)_o = 0.00$. These figures show that the size of the isocryptic-gradient can be quite severe indicating

severe fluctuations in the density of interstellar dust-clouds. Serkowski (1958) has applied an autocorrelation analysis to the residual variation of color-excess and polarization in the cluster nuclei after the general variation with galactic-latitude has been removed and concluded that the micro-scale of the fluctuation in density of the interstellar absorbing matter has an upper limit of 1.75 parsecs.

The indications are that over the general region the isocryptic-gradients are usually not quite so high. Nevertheless we can expect that due to the inability to choose faint neighbors always close enough to a bright star to overpower the isocryptic-gradient, an error will appear that will be, on the average, about $0^{m}.025$.

It is mentioned in passing that the present integrations produce data-points which fall well outside of a range in $(B-V)_o$ where small departures from the linearities assumed in Figures 7 and 8 (Appendix II) can be expected (in spite of the good fit) due to a maximum in the strength of the hydrogen lines confluent at the Balmer limit. This range, which effects only U-B, is included in the range for which Johnson tabulates X. It might at first appear that the proper procedure would be to apply the differential correction for intrinsic-color difference only to $E_{(B-V)}$, using Figure 6, and then to obtain $E_{(U-B)}$ using equation 4. It should be born in mind, however, that this intrinsic-color range is also where differences due to luminosity-class, whose effect on the reddening-trajectory has been tacitly omitted in the present integrations, would be most important.

The correct procedure for extrinsically-unreddening a supergiant, whose hydrogen lines are narrower for a given $(B-V)_o$, would lie somewhere between (1) adopting $E_{(U-B)}$ (with scale correction) as fixed in Figure 6 by $(B-V)_o$ and $\rho\ell$ from $E_{(B-V)}$ and $(B-V)_o$, and (2) adopting $E_{(U-B)}$ from equation 4 and $E_{(B-V)}$. The net effect of the method adopted is to decide in favor of procedure 1 when the faint-neighbor is outside of the intrinsic color range in question, and in favor of procedure 2 when the intrinsic-colors of both faint neighbor and bright star are identical. Otherwise a degree of compromise is exacted. The methods are, in principal, identical outside the questionable range. Systematic accuracy, in any event, will not be effected by more than about 0.01 magnitudes from these considerations.

V. RESULTS

a) The Color-Color Relation

The intrinsic-colors from Table 16 of the early and later supergiants have been plotted in Figure 12. The early supergiant plot appears to describe a roughly linear relationship from $(U-B)_o = -1.04$, $(B-V)_o = -0.22$ to (0.00, 0.12). The mean class I relationship for supergiants that fall in other areas of the diagram (Arp 1958b) has also been plotted, together with the class V relationship and the relationship for black-bodies (Arp 1961a). The new relationship, in the mean, agrees with the old relationship at the lower end of the early supergiants. At the upper end it is found to lie very slightly closer to the class V relation. The class Ia stars are represented by open circles, class Iab by half-filled circles and class Ib by filled circles. It is not possible to separate the subclasses in the diagram. A few remarks are in order regarding individual scatter:

Oo2589, A2Ia, (-0.34, 0.11). The reddening of both faint-neighbors in single-valued and in perfect agreement.

HD15690, B1.5Ib, (-0.92, -0.24). The two faint-neighbors give normalized color-excesses differing by 0.06 magnitudes. V_o and $(B-V)_o$ places them probably together in space.

HD17145, B8Ia, (-0.52, 0.04). Two of the faint-neighbors are fairly bright and appear well photometered. Their reddening determinations agree to 0.04. A third neighbor, which is much fainter, gives a color-excess 0.20 magnitudes higher. It has been given zero-weight.

Oo2178, A1Ia, (-0.45, -0.08). The three neighbors give color excesses

for this supergiant which fall in a range of 0.07 magnitudes.

The M supergiants show a larger scatter, some of which is undoubtedly due to intrinsic variability. Blanco (1955) in the course of observation of some of these stars on two different occasions has noted magnitude differences of 1^m and color differences of over $0^m.2$. The writer has noted comparable variations of color, but with smaller variations in V, about 0.5 magnitudes. In the mean, the stars appear to describe a relation which is roughly linear from (1.80, 1.68) to (2.16, 1.94) at which point it bends over and becomes very steep. A few remarks may be made concerning the individual scatter:

BD + 57°524, M0.5, (2.28, 1.87). Of the five faint-neighbors, three, when unreddened, appear to be together in space and yet present widely differing color-excesses. Their $E_{(B-V)}$s are single valued determinations and the range is 1 magnitude. Evidently an extreme isocryptic-gradient prevails.

HD14404, M1Ib, (2.21, 1.80). Only one of the neighbors chosen was not a nearby unreddened star. Its resulting intrinsic magnitude and color place it at a distance comparable to those of stars giving reliable reddening. The photometric agreement of the primary measurements for this neighbor is 0.02 magnitudes in range.

HD14826, M3Iab, (1.92, 1.67). The four neighbors give normalized $E_{(B-V)}$s that fall within a range of 0.15 magnitudes.

T Persei, M2Iab, (2.27, 1.89). The reddening determinations agree to within 0.03 magnitudes for both faint neighbors.

RS Persei, M4.5Iab, (1.79, 1.83). The two usable neighbors give normalized color-excesses agreeing to 0.03 magnitudes.

S Persei, M4eIa, (2.09, 2.05). The reddening determinations are 0.03 magnitudes apart.

YZ Persei, M2.5Iab, (2.19, 1.64). The two reddening determinations are 0.03 magnitudes apart in $E_{(B-V)}$.

BD + 58°373, M0, (2.44, 1.87). Two reddenings are 0.06 apart.

BD + 60°478, M2Iab, (3.08, 2.17). Only one of the chosen neighbors was not a member of the solar neighborhood. The reddening found for this star is commensurate with the determinations for the nearest bright-star subjects on either side. The measurements of the supergiant itself are discordant to an unusual extent if its variability is regarded as comparable to that of the others. Moreover the discordance does not decrease in the order V, B, U as expected (Payne 1930, and Gaposchkin and Gaposchkin 1938) but rather V, U, B. This portion of the sky contains some HII emission, which is uncharacteristic of the region in general, all of which lies to the South. This supergiant does not have a published radial velocity. It is not used to draw any conclusions regarding the stellar content of this region of the Perseus arm.

The remaining bright-stars are shown in Figure 13 (Appendix II). The O stars in general fall on a sequence not previously discovered except for the fact that the two O stars which define the blue end of the normal class V relation fall on the new relation at the point of intersection with the class V relation. The O star sequence is closely parallel to Arp's black-body relation and nearly coincidental with it. Except for the single very blue star (HD12993 - No. 14 in Table 17) at (-1.49, -0.71) the sequence terminates very

near the terminal point of the black-body relation which corresponds to infinite black-body temperature. This sequence has been transformed to Figure 12. The two bluest supergiants fall on this sequence quite well. The mean relationship for the early supergiants is also shown in Figure 13. The isolated, bluest point in the O star plot is HD12993, an O5 star. The two neighbors give individual reddening determinations differing by 0.01 magnitudes. The group is not in an HII region.

The giants and subgiants in Figure 13 have been divided into two plots; the class II stars and the stars of classes III and IV (filled circles for III and open circles for IV). Most of the stars in both plots do not fall noticeably away, in the mean, from the ordinary class V relation. The bluest members of both groups, however, fall to the upper left in the fashion of the O stars. With regard to the class III and IV plot, the appearance of this feature, whose slope is slightly less than the O star sequence, is apparently not vitiated by a manipulation of reddening determinations within a reasonable range. In the class II plot, the isolated point in this region of the diagram falls below stars of comparable $(B-V)_o$ of classes III or IV or the O stars. In this case it seems possible to explain the deviation in terms of the isocryptic-gradient being perhaps too large for the spatial resolution afforded by the proximity of faint-neighbors.

b) The Spectral Type Versus Color Relation

The difference between intrinsic B-V color corresponding to

a given spectral (temperature) type for luminosity-classes I and V has been plotted against spectral type in Figure 14 (Appendix II). The supergiants of the present study are indicated by filled circles (luminosity class V is from Arp's (1958b) tabulation). A linear fit has been made which runs from (B1.5, +0.07) to (A3, 0.00). The adopted relation has been abruptly returned to the abscissa just early of B1 for reasons which will be discussed in the next section. Through the detailed reddening correction the scatter has been considerably reduced over the best previously available plot (Johnson 1958). The open circles in Figure 14 are supergiants in M29 and nearby supposedly unreddened supergiants taken directly from the previous plot of Johnson. The crosses are from Feinstein's (1959) determination of the lower envelope of B-V versus Sp for nearby supergiants. The x points are from Kraft's (1961) intrinsic-colors for Ib stars based on an analysis of classical cepheids in galactic clusters and binaries. Kraft's relation has been adopted and a smooth transition curve connecting it to the early supergiant relationship has been drawn.

This curve has been transformed to the absolute $(B-V)_o$ versus Sp diagram where the supergiants have been individually plotted, this time with delineation in regard to luminosity sub-class (open circles for Ia, half-filled circles for Iab, and filled circles for Ib). This is shown in Figure 15 (Appendix II). Of primary importance in the new relationship for the early supergiants as demonstrated here is the fact that $(B-V)_o$ is a <u>monotonic increasing</u> function of spectral type (defining positive as early-to-late). The previous relation with

its pronounced kink is also drawn as is the relation for luminosity class V.

The M supergiants fall well below the class V relationship, with large scatter, and a slight, roughly horizontal concentration centering around (M2, 1.85). At the present time it does not appear that these stars can be treated more satisfactorily than to have the center of their plot connected to the late limit of Kraft's relation by a straight line.

The giants, subgiants and the O stars are shown in Figure 16, from which it appears that for stars this hot $(B-V)_o$ is too sensitive to Sp for a good correlation. The O stars and classes III and IV are drawn as filled circles. Class II are open circles. A concentration of stars in the extrapolated region of Arp's class V relation (solid line) is evident as is another immediately below. Considerable scatter is evident from which it is difficult to draw conclusions.

c) The Color-Magnitude Diagram

All of the purely photoelectric observations made in the present investigation, which constitutes Tables 16, 17, and 18 for the general region and the intrinsically-unreddened values for Table 7 of the faint photoelectric-sequence of ten stars between the cluster nuclei, have been plotted twice in the color-apparent magnitude (intrinsic) diagram. In Figure 17 (Appendix II) the stars have been divided into two groups with respect to declination (open circles north of $57^{\circ}10'$ and filled circles south). We note that the clusters-proper fall completely

in the southern region. In figure 18 the division is made in right-ascension; open circles west of 2^h18^m (1855) and filled circles east. Also shown in Figure 17 are (1) the fitted age-zero main-sequence (Sandage 1957a) and (2) a group of bright BV stars published previously (Johnson and Morgan 1955, and Johnson and Hiltner 1956) which are representative of the same general area. These stars have been intrinsically unreddened according to the present study. They are indicated by x points and are presented to show that the gap they fill is a result of the selection effects deliberately imposed in the present study (see page 11).

The two figures show a normal main-sequence from V_o = 7.5 down to V_o = 13.5. At the bottom a few stars are scattered on the blue side of the main-sequence. A number of stars appear to fall above and to the right of the main sequence from V_o = 8 to V_o = 13 with a suggestion that the deviation is greatest at the bright end. A large number of stars fall in the center of the diagram roughly toward the faint end. They do not fill a well-defined region and some are undoubtedly in the solar neighborhood, although many of them give the same reddening as co-neighbors which fall on the main-sequence. The apparent scarcity of faint stars in the interval of $(B-V)_o$ between 0.0 and 0.2 is a result of the fact that the stars have been intrinsically-unreddened and the reddening-trajectories run nearly parallel to the intrinsic class V two-color relation in this interval.

The M supergiants scatter about a roughly linear relation running from V_o = 6, $(B-V)_o$ = 1.7 to (8, 2.2). Two isolated M super-

giants are at (5.07, 1.64) (YZ Persei) and (9.02, 1.95) (K100172). Their reddening determinations are good. The latter has not had its radial velocity measured.

Beginning at $V_o = 7.5$ on the main-sequence and proceding brightward, the stars fan out into a definite cosmic scatter or fine-structure. Once we admit the presence of something more than a simple main-sequence break-off, the possibility of the structural detail being on a scale of the order of the separation of the points and their probable errors introduces a hazard into attempts at delineation. Thus some sequences which ought to be separated may be connected and others which ought to be connected may be separated. In this way a reordering of morphological trends may be necessary in order to reveal the true evolutionary or physical trends. One can only observe the principle-of-parsimony and proceed. It seems possible to delineate at least two sequences at the top of the main-sequence of Figures 17 and 18. A "blue-elbow" branch turns blueward with decreasing magnitude (increasing brightness), beginning at about $V_o = 7.5$. It reaches a blue extreme of about $(B-V)_o = -0^m.5$ at about magnitude 6.5 and then becomes red with decreasing magnitude until it terminates at about (4, 0.1). A "hollow" branch of some sort of duality indicated by the name arcs redward from the main-sequence at about $V_o = 7$ and proceeds to an extreme position of roughly (5.25, 0.1).

Examination of Figures 17 and 18 shows no definite dependence on the C-M plots on celestial coordinates except in Figure 18 where the eastern stars in the upper main-sequence and the blue-elbow

branch appear to lie slightly bluer than the western stars.

The feature of stars arcing blueward at the top of the main-sequence is not as unprecedented as it might at first appear. We may cite the following references where stars in other regions of space yield C-M diagrams with points in the blue-elbow region which have not been emphasized due to a paucity-of-points imposed by the lack of richness of the region in stars or the thoroughness of the investigation; (1) the association I Geminorum (Crawford, Limber, Mendoza, Schulte, Steinman, and Swihart 1955); (2) the association III Cephei (Blaauw, Hiltner, and Johnson 1959); (3) the association II Persei (Seyfert, Hardie, and Grenchik 1960). This is not an exhaustive list. In some instances where the reddening has been obtained using O stars, the O stars themselves will fail to appear in the blue-elbow region by any substantial amount if they have only been moved along their reddening-trajectories until intersection with the old class V two-color relation. Stars have fallen in the blue-elbow region in previous investigations of h and chi Persei, to-wit the reference to the "blue stragglers" by Massevitch (1957). They are seen in the C-M diagram of Johnson and Hiltner (1956) and the HR diagram of Johnson and Morgan (1955) though nearly all the O stars are omitted from these diagrams and the filling of the region is not well defined. Kopylov (1958) has presented two HR diagrams; one based on trigonometric and spectroscopic parallaxes and the other compiled from 13 clusters and associations. They both have blue-elbow regions which are very well defined and show a definite arcing away from the vertical main-sequence. The sequence does

not re-curve toward the red as does the blue-elbow branch of the present study. In addition, Kopylov's diagrams show a short branch arcing away toward the red from the top of the main-sequence in general similarity to the hollow branch of the present study.

The cross in Figures 12, 17, and 18 is the A5Ia star HD17378 which was added to the study later. Its reddening has been determined from the spectral type versus intrinsic-color relation derived in the present study.

In order to show the C-M diagram for the class I stars alone (thus excluding, principly, the O stars) and at the same time demonstrate the relative importance as sources of error of (1) unaccountable isocryptic-gradient and (2) the enforced collapse of possible fine-structure in the intrinsic two-color plot of class I stars, Figure 19 (Appendix II) was plotted. The C-M diagram on the left was plotted as Figures 17 and 18 were plotted, while the diagram on the right shows supergiants which were "intrinsically-unreddened" assuming equation 4 and the mean intrinsic color-color relation found for class I stars in Figure 12. In the unprejudiced opinion of the writer's wife the diagram on the left appeared more systematic. The x points are the same ones appearing in Figure 17. These points are observed to show less scatter than the stars of the present program which fall in the same magnitude interval, which is undoubtedly due to the following factors. (1) Leastwise, the probable errors of the photometry of Johnson et al. are slightly smaller than those of the present study. (2) The stars of the present program which fall in

this region are mostly extrinsically-unreddened. (3) The essential reason is cosmic; the x points are luminosity-class V stars whereas most of the stars of the present study in this range are from luminosity-classes II, III, and IV.

The photographic observations in the extreme nuclei (Tables 19 and 20 of Appendix I) have been used to plot the C-M diagram of Figure 20. h Persei is represented by filled circles and chi Persei by open circles from which it is immediately apparent that there is no systematic difference between the two clusters. The fit of Sandage's age-zero main-sequence is indicated in the figure as is the approximate photoelectric-calibration limit. The blue-ward trend of the stars in the extrapolated region is a systematic error due to the fainter plate limit (for say A0 stars) of the blue plates. The diagram shows stars on the main-sequence all the way to the faint limit of the data. Nevertheless an apparent-contraction-sequence with a fairly well defined upper envelope is converging onto the main-sequence more than two magnitudes above this limit. From about $V_o = 13$ this envelope rises steeply in a red-bright direction, levels off at a maximum at approximately $V_o = 12.1$, $(B-V)_o = 0.3$, proceeds in a gently sloping red-faint direction and gives some indication of curving back up into a red-bright direction beyond about $(B-V)_o = 1.0$.

The main-sequence extends normally up to between magnitude 6 and 7. Above this there is one B supergiant at (4.75, - 0.14) which appears where one would consider a proper position at the top of an evolved main-sequence. In order to avoid being misled by this

single bright supergiant, those bright-stars of Tables 1, 2, and 3 which fall within the region determined by Oosterhoff's dynamical cluster radii have been plotted as crosses. The result is too poor in statistics to be used for more than refuting a hasty conclusion based upon the lone B supergiant that the nuclei do not possess the age-dispersion of the general region. We also see that one M supergiant is added to the one already present in this way.

We also notice that the red off-shoot tendency found for the main-sequence of the general Perseus arm population is indicated also for the extreme nuclei, and, unfortunately, with the same paucity of points.

The single very red star at $V_o = 10.26$, $(B-V)_o = 2.41$, has not been discovered before and is not discussible beyond this point.

In order to obtain maximum definition of the major sequences and in the interest of general clarity, all of the stars of Figures 17, 18, and 20 were plotted in the color-absolute magnitude diagram of Figure 21 (Appendix II). All of the previously pointed-out sequences are reenforced except for the so-called contraction-sequence whose upper envelope has been slightly confused by the greater number of solar-neighborhood stars added in the general arm investigation.

In particular the fainter (third brightest) red off-shoot of the upper main-sequence becomes definitive. Its branching-off begins to be noticeable at about $M_v = 0$ and it terminates at about $M_v = -4.3$, $(B-V)_o = -0.02$. It possesses the general character of what has normally been referred to as evolved-main-sequence (the top defining core-hydrogen exhaustion). The writer reexamined

Oosterhoff's earlier C-M diagram which was characterized by stellar richness (over 2000 stars) and found such a sequence present and well-defined in spite of the lack of precision of the earlier methods employed and the neglect of reddening.

d) The Hertzsprung-Russell Diagram

The HR diagram of the bright-stars of Tables 1, 2, and 3 together with the bright BV stars which were plotted as x points in Figure 17 are shown in Figure 22 (Appendix II). Among the early stars the sequences correspond closely with those of the C-M diagram (Figure 21). We note in addition the appearance of a separation between the red end of the hollow branch and its blue end, which becomes closely allied with the top of the vertical main-sequence. It can be produced in Figure 21 by disregarding the single point (or moving it 0.04 magnitudes blue) at $M_V = -6.03$, $(B-V)_o = -0.17$, which gap is then enhanced by the non-linearity of the mapping from the C-M diagram to the HR diagram.

The main mass of M supergiants appears nearly symmetrical about (- 5.2, M2) with a slight suggestion of sloping along a steep line from early-bright to late-faint. The mass as a whole defines a vertical sequence.

We notice that the luminosity-classes congregating at a given absolute magnitude are very sensitive to temperature-class earlier than about B2.

Figures 21 and 22 are morphologically very compatible.

e) The Luminosity Function

Figure 20 was used to obtain the luminosity function shown in Figure 23. The lower, dashed histogram is due to stars in the immediate vicinity of the main-sequence. The upper, solid-line histogram is obtained from all stars. Since the contraction-sequence grades continuously into the main-sequence, it has not been easy to pick out those stars in this magnitude range which are main-sequence stars. The boundary of the main-sequence was somewhat arbitrarily set as the straight line running from (0.7, 0.04) to (4.1, 0.68). The previous luminosity function of Sandage (1957) for h Persei is in good agreement with the results of the present study over the overlapping range, providing the upper histogram is adopted. This comes as no surprise, since Sandage's luminosity function was based upon a transformation of Oosterhoff's photographic results.

The dashed curve is a normalized van Rhijn function (whose integral between the limits $M_V = -7.0$ and $M_V = 4.5$ is the same as that of the solid histogram) which is computed from Sandage's (1957b) tabulation. Of current theories of star formation, that due to Schmidt (1959) appears to be based upon the most realistic physical assumptions. The two solid curves are from Schmidt's derived creation-spectrum for the case of a square dependence of the rate-function on the interstellar gas-dust density. 2 has the same normalization as the van Rhijn function while 1 has been normalized to the dashed histogram over the range (- 7.0, 3.5). The ambiguity evident for the dashed histogram fainter than $M_V = 3.5$ is a deliberate device to indicate that no attempt was made to separate the sequences in this

region. Both Schmidt-functions represent their corresponding histograms better than the van Rhijn function represents its.

f) The Distance Modulus

In order to determine distance moduli Sandage's age-zero main-sequence was inked to proper scale on a piece of plate glass, and, with proper superposition of color-indices, translated parallel to the ordinate axis of the C-M diagrams until a good fit to the unevolved portions of main-sequences was obtained. For Figure 17 the fit was made in the range $-0.5 < M_V < 1.0$. The fit was made several times and the average taken. It was found to be $m-M = 11.8$. The average deviation-from-the-mean of a single determination was 0.1 magnitudes.

The same fitting procedure was used on the extreme nuclei in Figure 20. There the range used was M_V from - 1 to 3.3. The average deviation was about the same and the results were $m-M = 12.0$.

The agreement is satisfactory by ordinary standards and we present the mean, $m-M = 11.9$, as a final result. We may remark, however, that <u>if</u> we assume, <u>heuristically</u>, that the deviation is at least partially real, then the sense would indicate either (1) stars 8.5 magnitudes below the brightest star of the diagram were non-negligibly evolved, or (2) the clusters, as viewed from a position on a line intersecting the clusters at right-angles to the solar line-of-sight, were not in the center of the surrounding concentration of early stars but toward a side away from the sun (contrary to their central position as viewed from the earth), or (3) the bright end of Sandage's age-zero

main-sequence is systematically faint.

The previously accepted distance modulus has been 11.8 (Johnson and Hiltner 1956).

VI. DISCUSSION

a) The Stellar Colors and Spectra

The possible sources of opacity in early-type stellar atmospheres was studied in detail by Greenstein (1942) who showed that the absorption effects of helium and other light elements were negligible compared to atomic hydrogen for stars of normal elemental abundances. Greenstein also pointed out that observations which indicated an absolute magnitude effect in the Balmer jump might be explained by the influence of electron scattering which he found to be a non-negligible contributor to the continuous absorption coefficient in the high and low extremes, respectively, of the temperature and electron pressure ranges which he considered. The sense of the effect is compatible with the suggestion that it may be the source of the ultraviolet-excess of the early supergiants in the two-color diagram. The influence of electron pressure on the negative hydrogen ion absorption coefficient also provides the sense of deviation necessary to explain the ultraviolet deficit of F supergiants. With regard to electron scattering in the early supergiants the author has made first order theoretical calculations of the differential effects based on Greensteins theoretical variation of Balmer jump with electron pressure for a star of temperature $10,000^{\circ}$. The crude model which I developed assumed (1) that the stellar energy distribution was describable by a Planck function with separate temperatures for each side of the Balmer jump, (2) that the Balmer jump occurred at approximately the median wavelength of the stellar radiation, and (3) that magnitudes are monochromatic at an effective wavelength and that departures therefrom are totally com-

pensated for by a simple color-equation for the real base-line lengthening of U-B when the Balmer jump is reduced. The results yield an ultraviolet excess of $\Delta(U-B) = -0^m.33$ in comparison to an observed value of $-0^m.35$. The agreement is fortuitously better than one would hope for from such a crude model.

Another effect due to electron pressure which varies from dwarf to supergiant with the proper sign for explaining the ultraviolet excess of supergiants is the stark-broadening of the hydrogen lines in confluence at the Balmer limit. The difference in blanketing-effect from dwarf to supergiant requires some amount of class I ultraviolet excess. While it is not necessary to invoke the effect as non-negligible in order to account for the ultraviolet excess of early supergiants, the absence of the hump in the class I two-color relation which is a striking feature of the class V relation and believed due to the hydrogen lines, suggests that differences in Stark effect may nevertheless be important in the interpretation of broad-band photometry.

With regard to the behavior in the two-color diagram of the bluest stars (O5-B0) of the present study, we note that they are well within the temperature range where electron-scattering is a non-negligible contributor to the continuous-absorption-coefficient (Greenstein 1942; Aller 1960). It would thus seem immediately clear that the hottest stars should possess very accurately gray-atmospheres due to the independence of wavelength of the electron scattering coefficient, and would therefore be expected to fall on a two-color relation closely resembling the one for black-bodies, which is pre-

cisely what is observed. While wavelength-insensitive electron scattering can produce an emergent flux in good agreement with that of a gray-body, it can not happen in the simple manner which might at first be imagined. Because electron-scattering is a pure-scattering process rather than a pure-absorption process, the source function is decidedly non-Planckian; Kirchoff's law does not hold since the photons being expelled by the fundamental atmospheric particles are independent of any kind of local temperature, and we do not have a classical gray-atmosphere at all. The electron-scattering can only preserve, with negligible blurring, the continuous energy distribution which arises from the pure-absorption processes obtaining, which are not likely to be independent of wavelength. How then does a gray continuum eventually emerge from the star?

It is a characteristic of non-gray atmospheres in which true local-thermodynamic-equilibrium holds that the departure from grayness in the observed energy distribution can arise only through the fact that the finally emerging stream of photons has been emitted from a collection of atoms whose range in temperature is different from zero. It is also true that sufficiently below the surface, such that the specific intensity does not differ very much from the mean intensity, the matter and radiation will be in local-thermodynamic-equilibrium and the radiation density will be Plackian even if the predominant source of opacity is electron-scattering. This arises because photons remain within a given region long enough for residual true-absorption processes to bring matter into equilibrium with them and is tantamount to the widely accepted assumption made in the

theory of stellar interiors for stars of high mass. Lastly, the predominance of electron-scattering makes it the source of optical-depth independent of whether it were an absorption or scattering process. We may thus conclude that a gray-body energy distribution emerges from the star from either of two points of view. (1) Electron-scattering forms a gray blanket over the atmosphere which promotes Kirchoff's law (for absoprtion only) and a black-cavity distribution of radiation at the local temperature at depth through the reduction of the escape of radiation, which blanket does not contain enough purely-absorbing atoms to significantly alter the distribution of the radiation which does escape. (2) If we assume that throughout the atmosphere there exists a temperature parameter which governs the true-absorption processes, notwithstanding the predominance of electron-scattering, through Kirchoff's law; then the energy distribution of the emergent photons will be determined by the temperature distribution of the atoms from which they were previously emitted, regardless of how many subsequent scatterings each suffered, before emerging from the star. Thus the responsibility of electron-scattering for the optical depth requires that the final absorption-emission process which occurs before emergence must occur with an atom that is not too close to the boundary but at the same time cannot extend over a very large range in depth. This tends to reduce the temperature range for atoms of the final absorption-emission process and therefore promotes a gray-body energy distribution in the emergent flux.

The required physical conditions may be more rigorously summarized. The equation of transfer including pure isotropic scattering where the absorption occurs under LTE may be written

$$\mu \frac{dI_\nu}{d\tau_\nu} = I_\nu - \left(\frac{\kappa_\nu}{\kappa_\nu + \sigma}\right) B_\nu(\tau_\nu) - \left(\frac{\sigma}{\kappa_\nu + \sigma}\right) J_\nu \qquad (6)$$

The usual Eddington variable definitions are assumed. Multiplying equation 6 by $1/2$ and integrating over μ from -1 to 1 with an interchange of the order of integration and differentiation, we obtain the equation for the change of monochromatic-flux with optical depth due to residual absorption,

$$\frac{dH_\nu}{d\tau_\nu} = \left(\frac{\kappa_\nu}{\kappa_\nu + \sigma}\right)(J_\nu - B_\nu) \qquad (7)$$

which also shows that monochromatic-radiative-equilibrium prevails under conditions of pure-scattering.

The criteria for the emergence of a gray-body continuum as discussed in the preceding paragraphs may be expressed quantitatively:

There exists τ_o such that

$$\left| \frac{I_\nu(\tau) - J_\nu(\tau)}{J_\nu(\tau)} \right| < m_1, \text{ for } \tau \geq \tau_o, \text{ all } \mu, \qquad (8)$$

and

$$\left| \frac{H_\nu(\tau) - H_\nu(0)}{H_\nu(0)} \right| < m_2, \text{ for } \tau \leq \tau_o, \qquad (9)$$

where m_j is a small positive number, much less than one, corresponding to a reasonable observational limit to the accuracy of the

test of agreement with a gray-body.

Integrating equation 7, using the fact that the absorption is much less than the scattering and the good approximation that $d\tau_\nu = d\tau$, we obtain for inequality 9:

$$\left| \int_0^\tau \frac{\kappa_\nu}{\sigma} \left[\frac{J_\nu(\tau') - B_\nu(\tau')}{H_\nu(0)} \right] d\tau' \right| < m_2, \text{ for } \tau \leq \tau_o . \qquad (10)$$

Evidently inequality 10 will be true if

$$\left(\frac{\kappa_\nu}{\sigma} \right)_{\max} \left| \int_0^\tau \frac{J_\nu(\tau') - B_\nu(\tau')}{H_\nu(0)} \, d\tau' \right| < m_2, \text{ for } \tau \leq \tau_o. \qquad (11)$$

With respect to inequality 8 we may rewrite equation 6 to a high degree of approximation:

$$\frac{I_\nu(\tau) - J_\nu(\tau)}{J_\nu(\tau)} = \frac{\mu}{J_\nu(\tau)} \frac{dI_\nu(\tau)}{d\tau} + \frac{\kappa_\nu}{\sigma} \frac{B_\nu(\tau)}{J_\nu(\tau)} . \qquad (12)$$

Since at the depths implied in equality 8 $J_\nu(\tau) = B_\nu(\tau)$, we may simplify equation 12 and substitute in inequality 8 to obtain:

$$\left| \frac{\mu}{J_\nu(\tau)} \frac{dI_\nu}{d\tau} + \frac{\kappa_\nu}{\sigma} \right| < m_1, \text{ for } \tau \geq \tau_o. \qquad (13)$$

Since κ_ν/σ is independent of μ, and since the expression on the left side of 13 must satisfy the inequality for the value of μ at which it is a maximum ($\mu = 1$), we further require

$$\frac{\kappa_\nu}{\sigma} + \frac{dB_\nu(\tau)}{B_\nu(\tau)\, d\tau} < m_1, \text{ for } \tau \geq \tau_o, \qquad (14)$$

where we have also simplified the expression on the left using the approximation $J_\nu = I_\nu = B_\nu$, which obtains at the depths considered.

From 11 and 14 we summarize the criteria for gray-body continua due to electron-scattering.

There exists τ_o such that

$$\left(\frac{\kappa_\nu}{\sigma}\right)_{max} < \left| \frac{m_2}{\int_0^\tau \frac{J_\nu(\tau') - B_\nu(\tau')}{H_\nu(0)}\, d\tau'} \right|, \text{ for } \tau \leq \tau_o \qquad (15)$$

and

$$\left(\frac{\kappa_\nu}{\sigma}\right) < m_1 - \frac{d \ln B_\nu(\tau)}{d\tau}, \text{ for } \tau \geq \tau_o \qquad (16)$$

where m_j is a suitably chosen small positive number much less than one.

Lemma: The fundamental assumption for the region of validity of inequality 8 that makes inequality 8 a meaningful criterion is that the approach of the radiation field to isotropy implies that the mean intensity J_ν approaches the Planck function B_ν at the local temperature. This may be made more rigorous from the following argument. Evidently no generality is lost by approaching isotropy from within a first order range in μ. We may thus write:

$$I_\nu(\tau_\nu, \mu) = a_\nu(\tau_\nu) + b_\nu(\tau_\nu)\mu,$$

hence $J_\nu(\tau_\nu) = a_\nu(\tau_\nu)$ which yields

$$I_\nu(\tau_\nu, \mu) = J_\nu(\tau_\nu) + b_\nu(\tau_\nu)\mu,$$

and

$$\frac{dI_\nu}{d\tau_\nu} = \frac{dJ_\nu(\tau_\nu)}{d\tau_\nu} + \mu \frac{db_\nu(\tau_\nu)}{d\tau_\nu} \quad .$$

Substituting this expression into the transfer equation 6 and integrating over μ,

$$\frac{dJ_\nu}{d\tau_\nu} \int_{-1}^{+1} \mu \, d\mu + \frac{db_\nu(\tau_\nu)}{d\tau_\nu} \int_{-1}^{+1} \mu^2 d\mu$$

$$= \int_{-1}^{+1} I_\nu \, d\mu - \left(\frac{\kappa_\nu}{\kappa_\nu + \sigma}\right) B_\nu \int_{-1}^{+1} d\mu - \left(\frac{\sigma}{\kappa_\nu + \sigma}\right) J_\nu \int_{-1}^{+1} d\mu \, ,$$

which simplifies to

$$J_\nu - B_\nu = \frac{1}{3}\left(\frac{\kappa_\nu + \sigma}{\kappa_\nu}\right) \frac{db_\nu(\tau_\nu)}{d\tau_\nu} \quad .$$

Since $b_\nu(\tau_\nu)$ must approach 0 asymptotically with increasing τ_ν

$$\lim_{\tau_\nu \to \infty} J_\nu = B_\nu, \quad \sigma, \ \kappa_\nu \text{ finite.}$$

The construction of model atmospheres upon which to apply these criteria is beyond the present degree of elaboration. It may be pointed out that the derivative on the right side of 16, in the range indicated, will go as the product of (1) a term inversely proportional to the square of the local temperature and (2) the local value of the temperature gradient, and can therefore be expected to approach zero for all atmospheres with positive-finite temperature-gradients. A real value of κ_ν/σ can therefore be expected to exist which satisfies

16 corresponding to stars above a certain effective-temperature. Evidently the same can be said of 15 so long as the denominator does not become infinite, which is reasonable even if conditions are laxed to the extent of replacing the Planck function by a generalized source-function-for-pure-absorption which would be requisite for the outermost layers of a star.

The behavior of the bluest stars in the two-color diagram is thus explained. According to Woolley and Stibbs (1953) the gray-body and black-body energy curves are negligibly different for effective-temperatures above 20, 000°K. This would imply that real stars cannot have colors bluer than those of the blue tip of the black-body relation in Figure 12 (Appendix II) (Arp 1961) which corresponds to a black-body of infinite temperature. Nearly all of the stars studied fulfill this apparent requirement. The two apparently reliable deviations fall on the extrapolated relationship very nicely. The emission lines ordinarily observed in Be stars do not appear capable of providing the desired sense of the deviation. Neither has the writer an explanation of the fact that there is such an overlap in the two-color diagrams of O stars and B giants.

The spectra of the M supergiants are dominated by a general confluence of atomic lines and molecular bands, with doubtless the concurrence of a continuous-absorption-coefficient due to the photo-ionization of metals and the photodissociation of molecules and free-radicals. The physical explanation of the sequences delineated in the two-color diagram for stars in this temperature range is very difficult. As one goes to the coolest stars among the dwarfs, the relative redden-

ing in $(U-B)_o$ compared to $(B-V)_o$ is less than for a black-body, which may be best explained in terms of the negative-hydrogen-ion-absorption-coefficient with a more or less uniform blanketing of lines. The general feature of supergiants falling off steeper in the diagram and lying below the class V relation is understandable in terms of the growth with decreasing temperature of much stronger TiO bands in the supergiants than in the dwarfs, which bands are strongest in V, then B and finally U. It is noticed that the reddest supergiants fall over into a quite steep relation. All of these stars are in a temperature and electron-pressure range where Rayleigh scattering is a non-negligible contributor to the continuous-absorption-coefficient (Aller 1960). One can imagine for the coolest most voluminous supergiants an envelope so tenuous and unenergetic that little exists to impede the passage of radiation except Rayleigh scattering. This phenomenon is presently under study by Dr. R. P. Kraft. The writer knows of no published model atmospheres for M stars, which is easily understandable.

A further remark is in order concerning the scatter of the blue supergiants in the two-color diagram. If we assume that all the stars in Figure 12 are of the same chemical composition, then their position is fixed by their effective-temperature and surface gravity. Through the Russell-Vogt theorem there should be a one-to-one correspondence between the color-color diagram and the color-absolute magnitude diagram. Consequently the result derived in the present study that the supergiants lie on a complicated sequence in the C-M diagram where M_V is a multi-valued function of $(B-V)_o$

would indicate that the scatter in the two-color diagram (and the color versus spectral type relation) is in large measure cosmic. This is also suggested by the discussion of some of the individual points of wide scatter in the preceding section. Also, if the M supergiants are engaged in thermonuclear reactions in sequences of everything from carbon burning to the iron group as suggested by Hayashi and Cameron (1961), we would not be surprised if their true relation in the two-color and C-M diagrams were in fact quite intricate.

The differences between class I and class V in the Sp - $(B-V)_o$ relation can be somewhat understood in terms of how one would set up a two-dimensional classification system in terms of the visual examination of spectral features. To the extent that one is devising a temperature-sequence that is ultimately based on a collection of stellar prototypes, and the examination and ordering of the prototypes are independent operations for the different luminosity-classes except at certain intercalibration points on the temperature-class scale, one can expect the two scales to be independent and apparently-systematic differences can be the arbitrary result of a personal equation. This in no way questions the validity of the classification scheme since its fundamental basis and requisite for repeatability in classifying stars is the collection of prototypes and a well defined set of classification criteria rather than the measurement of a physical parameter. On the other hand to the extent that higher luminosity stars of the prototype collection are classified by the criteria which have already been applied to lower luminosity stars and by direct comparison with the lower luminosity stars, we may expect the systematic differences

shown in Figures 14 and 15 to be related to physical atmospheric parameters in a reasonable way.

The ordinary assumption that $(B-V)_o$ is a good indicator of effective-temperature while Sp is a good indicator of excitation-temperature leads to the conclusion, assuming $T_{ex} < T_e$ in all cases, that the difference between the two temperatures is less for supergiants than for dwarfs in the ranges B0 to A3 and F7.5 to M4.5, whereas the reverse is true in the middle range. On the other hand if we assume that Sp is a good indicator of T_{ex} and that the difference between the two kinds of temperature parameters is independent of luminosity-class, we derive that for a given effective-temperature the dwarfs are systematically bluer than the supergiants in the early and late range and redder in the middle range. This may be restated that for a given $(B-V)_o$ the effective-temperature of a supergiant is higher than the T_e for a dwarf in the early and late range, while in the middle range the supergiants are cooler. The first hypothesis seems tenable in the middle range on the general grounds of the greater extension of supergiant atmospheres. The second hypothesis is reasonable in the early range where for a given $(B-V)_o$ the ultraviolet-excess of the supergiants would lead to a higher T_e. It may be added with respect to the early supergiants that a temperature classification based on the equivalent-widths of the hydrogen lines without separate rules for different luminosity-classes would place the dwarfs further in temperature (and therefore $(B-V)_o$) away to either side of that corresponding to A2 (where the

hydrogen lines reach a maximum) due to the larger Stark-effect. Restated, this means that to obtain a given hydrogen line equivalent-width (and therefore a given temperature type) for stars earlier than A2 a supergiant must be chosen that is cooler (redder) than the corresponding dwarf, while for classification later than A2 the supergiant must be chosen hotter (bluer) than the dwarf. This is precisely what is observed and this explanation is probably the most satisfactory for stars earlier than about F. A similar situation can exist for the M supergiants where if one considers the TiO bands to increase with decreasing temperature a given bandstrength (much higher for the supergiants over the whole range) will be achieved by a hotter supergiant than corresponding dwarf. This prediction leads to the opposite of what is observed, however, though it may be pointed out that the problem is much more complicated for the late than early supergiants. A reliably exact explanation for all of the differences observed in Figures 14 and 15, if at all possible, requires a detailed analysis of the individual classification criteria with regard to the effects of both effective-temperature and surface gravity, and special consideration of possible stratification effects in supergiant atmospheres.

The curve in Figure 14 has been forced to the abscissa at O9 in accordance with the expected confluence of all luminosity-classes in the region where electron-scattering dominates the continuous-absorption-coefficient and all gray-bodies converge on the black-body sequence.

b) The Color-Magnitude Diagram

The powerful tool of comparison is inhibited in a study of h and chi Persei. No other objects of the Galaxy with published investigations are anywhere near as rich in stars for the age-group considered. There are a number of sparsely populated associations and NGC 457 which contains three supergiants (B6Ib, F0Ia, and M0Ib) (Pesch 1959). Aside from being compatible with the present results, these objects offer no source of understanding of the present results. Neither the luminosity functions for these objects nor the van Rhijn function offers sufficient statistics to provide illumination; in particular the semi-empirical evolutionary tracks cannot be constructed in the usual way (Sandage 1957c).

Insofar as the evolution at bright magnitudes can be considered sufficiently rapid that the star sequences themselves indicate the topology of the evolutionary tracks, one can make useful comparison of h and chi Persei with some older groups in the Galaxy and others of more closely the same age in the Large Magellanic Cloud (LMC) and the Small Magellanic Cloud (SMC). The resulting composite C-M diagram does not help decide how one is to divide the morphological sequences in h and chi Persei into an age distribution and its corresponding evolutionary sequences, but it is useful in examining the nature of evolutionary tracks in different galaxies.

The boundary of the major sequences in the C-M diagram of the present study of h and chi Persei has been drawn in Figure 24 (Appendix II). Also shown are the schematic C-M diagrams of

M11, κ Crucis, and NGC 1844 (LMC) from the study of Hodge (1961). The schematic C-M diagram of NGC 330 (SMC) has been obtained by the writer from the published C-M diagram of Arp (1958a, 1959a, 1959b). The distance modulus used for the SMC was 18.25 (Arp and Kraft 1961).

Before beginning the comparison of the diagrams a few remarks are in order regarding the physical significance of the schematic diagram of h and chi Persei alone. The principle sequences have been pointed out in the preceding section. First, it has been shown that the bright stars of the general Perseus arm population surrounding the clusters are part of a general star field that is at the same distance as the clusters and which possesses roughly the same age-distribution. Within these limits it has been shown that a component of age-gradient exists parallel to right-ascension with none noticeable along declination. In particular it has been shown that nearly all of the stars of the blue-elbow region of the blue-elbow branch are in the eastern half of the region, and none are in the dynamically bound region of the clusters although the statistics are too small to warrant an age restriction or other physical conclusion for the clusters-proper through consideration of the latter point. The stars in the eastern section on the more normal vertical main-sequence near the top also show signs of being in general younger. The hollow branch and the red end of the blue-elbow branch appear to be populated equally by stars from all parts of the region. This lends support to the possibility that the red end of the blue-elbow branch is a part of the same evolutionary sequence as the hollow branch all of

the stars of which are roughly the same age which is slightly older than the age characterizing the blue-elbow region of the blue-elbow branch which is supposed to be a separate and younger evolutionary sequence. Certainly the apparent main-sequence break-off point at $M_V = -4.3$ is best explained as the evolutionary sequence of a group of still older stars (somewhat older than the κ Crucis cluster). It may be pointed out here that with respect to this break-off the three cepheids in h and chi Persei, VX Persei, UX Persei, and UY Persei are of normal absolute magnitude whereas they are anomolous when considered with respect to the brightest stars of the region. (The use of these stars in the calibration of the Cepheid period-luminosity relation should now be given renewed consideration.) Further evidence for the multiplicity of ages for the stars of the present study exists in the appearance of main-sequence stars well below the magnitude of convergence of the contraction-sequence onto the main-sequence.

One may ask what the expected number of field stars in Figure 20 should be, especially with regard to the interpretation of the apparent contraction-sequence. In the present context, however, the term 'field star' cannot be immediately equated with 'stellar contaminant' in the C-M diagram of h and chi Persei. By 'field star' one means the isolated star belonging to no gravitational complex smaller than, and within, the Galaxy; and which star, with other members of its class, can be roughly identified with the smooth distribution of stars over the celestial sphere. Such stars, however, usually form the population of either the local or some adjacent spiral arm. For

the present study, estimates of true stellar contaminants must distinguish between field stars of the Perseus arm and those of the local arm and even, perhaps, a few from the arm beyond Perseus. The author knows of no such detailed field star tabulations. It is nevertheless interesting to examine the predicted abundance of field stars according to the tables of van Rhijn (1929). van Rhijn gives the number of stars per square degree brighter than a certain magnitude (international photographic) as a function of galactic latitude and longitude. Taking our reddened photoelectric limit as $V = 17^m$ and saying that the contracting sequence has a mean reddened color-index of about B-V = 1 gives the corresponding m_{pg} as about 17.5 (Arp 1961b). The number of field stars in the two circular areas 6 minutes-of-arc in diameter whose area is thus 0.0157 square degrees is therefore predicted to be 56.4. The actual count of stars in the contraction sequence above the indicated magnitude limit is 93. This number is conservative since there is a tendency to label some contracting stars near the main-sequence as main-sequence stars. It may be pointed out that stars in the contraction region of Figures 17 and 18 were used to give reddening values cooperatively and consistently with main-sequence stars of comparable brightness. Rather than base a conclusion on so-called field-star-counts, it is felt that this type of data is best brought to bear in the investigation of rich clusters at higher galactic latitude where it can be less ambiguously interpreted.

It thus appears that most of the sequences in h and chi Persei can be represented by a series of relatively sharp maxima in the rate of star formation in the region, with only the very youngest stars

showing any preference for spacial position. Each age has a relatively simple sequence unless we insist that the red end of the blue-elbow branch is geneologically connected to the hollow branch instead of the blue-elbow region of the blue-elbow branch. In the latter event the second-youngest group of stars would be concluded to follow a much more complicated evolutionary track than the youngest group which is represented in sufficient number that it would exhibit the appropriate fine structure if it were there. The presence of a slight age-gradient for the youngest stars seems rather well founded, but the proposition that the red end of the blue-elbow branch shows a different dependence on spatial position and therefore age than the bluer stars of the branch is open to question due to a paucity of points.

It has been assumed without discussion up to now that the faintest red off-shoot from the main-sequence in the stars of the present study represents a contraction-sequence. This seems reasonable since the total age-dispersion is much less with this interpretation than if we were to believe these stars represented an advanced stage of hydrogen exhaustion. The thermonuclear interpretation would place this sequence comparable in age to the Hyades, Praesepe, and Coma Berenices. These three clusters, however, show a Hertzsprung gap whose blue end is bluer than $(B-V)_o = 0.3$ and whose red side is at about $(B-V)_o = 1.0$ -- see the composite C-M diagram of Sandage (1957a). The contraction-sequence in h and chi Persei does not show this scarcity in distribution of stars but fills rather evenly the gap. It does show an increase in the concentration of stars as one comes

within close proximity of the main-sequence, which is expected from theory (Henyey, Le Levier, and Levee 1955) for gravitationally contracting stars.

In the composite schematic C-M diagram of Figure 24 the general character of the population of the clusters of the Galaxy over most of the diagram is that they exhibit horizontal evolutionary tracks. The evolutionary tracks slope slightly downward toward the red for the most massive stars and upward toward the red for the least massive stars with a continuous monotonic trend between the extremes of mass. With present knowledge it is also indicated that the Hertzsprung gap grows continuously wider with increasing mass (decreasing magnitude). Evidently part, at least, of the population of the SMC and the LMC disagrees with the Galactic picture. This has been previously pointed out in the case of NGC 330 by Arp (1958c) and in the case of NGC 1844 by Hodge (1961). NGC 330 has a separate early supergiant branch which extends too red into the Hertzsprung gap, and a red supergiant branch which is marginally too blue at its blue end and appears to slope opposite to what is expected in the Galaxy. The blue stars in NGC 1844 are normal by Galactic standards but the red giants are far too blue and appear to define a vertical evolutionary track. Hodge has suggested three possible meanings for the vertical sequence of red giants. (1) The evolutionary tracks in the Large Cloud are indeed vertical at the red end. (2) The sequence represents stars returning to the main-sequence on their way to the white-dwarf region. (3) The sequence does not represent the direction of the evolutionary tracks because of its reflection of

the finite formation-time of the cluster. Proposition 3 has consequences for the dynamics of star formation in low density stellar systems as compared to high density systems such as the Galaxy. The difference to be explained is not quite so ominous when it appears that even in the Galaxy, according to the present study, single-epoch star formation for clusters may not be universal, although its lack of universality is not revealed in h and chi Persei in the same way it is in NGC 1844 if this is the correct explanation. On the other hand propositions 1 and 2 reflect a fundamental difference in the stellar content of the galaxies which, judging from the positions of the tops of the main-sequences, is only explainable in terms of a difference in initial chemical composition. Such an explanation is made difficult by three considerations. (1) NGC 330, NGC 1844, and the clusters of the Galaxy indicate that the three galaxies each exhibit unique evolutionary patterns, which would require the variation of one parameter to explain a very wide range of phenomena. (2) Feast (1960) and Feast, Thackeray, and Wesselink (1960) have indicated that no peculiar spectroscopic abundances exist among the high luminosity stars of either Cloud. (3) Aller (1961) has concluded from a spectroscopic investigation of gaseous nebulae that the Galaxy, LMC, and SMC all have the same excitation patterns and probably the same chemical composition. Even if proposition 3 straightens out the evolutionary tracks into non-contradiction, one must have recourse to a variation in chemical composition in order to explain the difference in the geometry of the Hertzsprung gap which would still be left too narrow in the Clouds. The spectroscopic and photometric investiga-

tions in the Clouds overlap in subject stars so that no alleviation in the conflict between the photometric demand for composition differences and the spectroscopic indications of normalcy is afforded by the undoubted variation in chemical composition within the individual Clouds. It appears that we must either revise our ideas as to the physical factors which are of major importance in stellar evolution or else revise our observational picture of the Hertzsprung gap in the Galaxy. For this reason the size of the Hertzsprung gap in h and chi Persei is presently under investigation by the writer. It has been indicated that the red end of the early supergiant sequences is not likely to be revised by such an investigation, although the possible discovery of G and K supergiants is less remote due to the emphasis in early surveys on either very blue or very red stars. The writer is indebted to Dr. P. W. Hodge for providing him with several 48 inch Schmidt plates of h and chi Persei which are being used in the investigation. Provisional results should be available shortly after the next observing season.

c) The M_{bol}-Log T_e Diagram

In order to compare the observations with the predictions of the theory of stellar interiors it is necessary to apply bolometric-corrections and an effective-temperature scale to the observational parameters. The uncertainties in these scales have been thoroughly reviewed by Popper (1959) and his arguments will not be reproduced here. Suffice it to say that in the extreme temperature ranges where our observations are most important the scales are much in need of

improvement. For the reddest of our M supergiants it has been necessary to extrapolate the compilations which have been made in the present study in an attempt to obtain the most reliable scale of effective-temperatures and bolometric-corrections. A number of recently proposed B. C. and T_e scales have been drawn in Figures 25 and 26 respectively (Appendix II). We will now briefly review the source of each in chronological order. (1) Arp (1958b) has conducted the most recent review and compilation which extends over the entire observational range of temperature. From B2 early-ward the B. C. s have been obtained from the prediction of B. C. and Sp from the model atmospheres of Underhill and McDonald. Later than B5 the B. C. s are from the early comparison of the radiometric magnitudes of Pettit and Nicholson with the corresponding photovisual magnitudes. For the T_e scale model atmospheres are again used early through B2. For later stars the scale is based on an interpolation by six-color photometry between the sun, beta Aurigae (eclipsing binary), and T_e's based on interferometric diameters of giants and supergiants. (2) Popper (1959) has revised the B. C. s chiefly by changing the argument of the scale from Sp to $(B-V)_o$ (photoelectric), and returning to the original radiometric data of Pettit and Nicholson and subtracting photoelectric V magnitudes. The radiometric data of Emberson with an adjusted zero-point was also used. For the effective-temperatures, beyond the improvement afforded by the revised B. C. s, an improvement is incurred through the measurement of the diameter of Sirius by Hanbury Brown and Twiss. Popper also advocates the termination of empirical B. C. s as late as F0 because

of atmospheric extinction and draws on model atmosphere predictions in this range (Hunger, Osawa, Saito, and Underhill and McDonald). (3) Schmalberger (1960) gives B. C. s and T_es for O and B stars from the model atmosphere computations of Sp, B. C., and T_e from Pecker, Underhill, McDonald, and Traving. (4) Bless (1960) has made photoelectric spectrum scans of AV stars and obtained the T_e on the basis of several predicted (model atmospheres) and measured criteria. The criteria chosen were the Balmer discontinuity and the monochromatic wavelength differences: m(λ4600) - m(λ4190); m(λ5600) - m(λ4400), and m(λ6000) - m(λ5000). (5) Oke (1961b) has obtained photoelectric spectrum scans for various phases throughout the light-cycle of delta Cephei. With concurrent high-dispersion spectrograms he has measured the line-blanketing at various wavelengths and corrected the scans to obtain the true continuum as a function of phase. He has fitted model atmospheres to each continuum and thereby obtained the T_e and B. C. as a function of phase hence $(B-V)_o$. These have then been corrected for the blanketing-effect giving the parameters for the true star as opposed to its continuum.

The reader is referred to the above five authors for reference to authors referred to by them.

In the present compilations, when T_es and B. C. s of other authors are given as a function of Sp the argument is changed to $(B-V)_o$ by the Sp versus $(B-V)_o$ relation of the present study when available and otherwise from the tabulations of Arp (1958b).

The adopted relation is indicated in Figures 25 and 26 and is

considered by the writer to be as reliable a choice as is possible at the present time.

Using the presently adopted effective-temperature and bolometric-correction scale, the schematic C-M diagram of h and chi Persei shown in Figure 24 has been mapped into the M_{bol}-Log T_e plane and is shown in Figure 27. Under the effects of the transformation the red tips of the blue-elbow branch and the hollow branch are no longer the brightest features of the respective sequences. The elbow of the blue-elbow branch emerges as the brightest feature of the diagram. The hollow branch becomes nearly horizontal and its red tip becomes horizontally opposite the blue tip of the M supergiant branch.

Also shown in Figure 27 are a number of theoretical evolutionary tracks corresponding to the following physically expected periods in the life of a star: (1) gravitational contraction out of the interstellar medium, (2) hydrogen burning on the main-sequence, (3) hydrogen exhaustion with increasing importance of gravitational contraction, (4) gravitational contraction with hydrogen shell burning, (5) helium burning on the triple alpha reaction in the core with hydrogen shell burning, and (6) the onset of carbon-neon burning at the center. On each of the theoretical tracks the direction of evolution has been indicated by the sense of the arrow-heads superimposed on the track. The masses (solar units) corresponding to each evolutionary track have been indicated in the figure, on the left for thermonuclear tracks and on the right for gravitational contraction tracks, with the exception of the contraction track labeled

to indicate that it corresponds roughly to the youngest just-contracted main-sequence star in h and chi Persei. The chemical composition assumed for each track is indicated in the figure.

The gravitational contraction tracks have been obtained from two sources. For masses 1. 25, 1. 549, and 2. 291 the tracks are due to Henyey, Le Levier, and Levee (1955). The irregular track that terminates at $M_{bol} = 0.8$ is the result of a homology transformation (i. e. the track has been moved parallel to itself) of the very elaborately computed pre-main sequence evolutionary track for the sun which includes deuterium burning and which is due to Brownlee and Cox (1961). It may be rightly pointed out that the elaborate nature of the latter computations, especially since they include provisions for a variety of possible pre-main sequence thermonuclear reactions, tends to vitiate the application of a homology transformation which is based on a pure Kelvin contraction. However, the result should be superior to calculations which assume homology from the beginning and also to those of correct mass whose degree of elaboration is considerably less than Brownlee's and Cox's.

The hydrogen burning tracks have been drawn from several authors and represent a rather wide variety of computational methods, initial chemical composition, and opacity assumptions. The well known fact that such differences result primarily in a change of time-scale is born out by the good agreement between the tracks. For masses 1. 5, 2. 0, 3. 5, 6. 0, 11. 0, 20. 0, and 30. 0 the tracks are due to Henyey, Le Levier, and Levee (1959). For masses 1. 52, 3. 89,

and 30.1 they are due to Hazelgrove and Hoyle (1956). For masses 28.2 and 62.7 they are due to Schwarzschild and Härm (1958). The track for the mass 15.6 is due to Sakashita, Ōno, and Hayashi (1959).

The Hertzsprung gap has been widely interpreted as a physical separation of stars which are burning hydrogen and stars which are engaged in more advanced post-hydrogen thermonuclear core reactions, except, of course, for those stars which are on the red side of the gap but which have evolved brightward from low masses below the gap rather than horizontally redward from the blue side of the gap. Stars of the latter type are exemplified by the red giant branches of globular clusters and M67 and are believed to be still engaged in hydrogen burning (Hoyle and Schwarzschild 1955). It was suggested by Hoyle (1959) that for the more massive stars helium firing begins not far to the right in the HR diagram as formerly believed, but quite soon after quitting the main-sequence. Preliminary calculations of helium burning were made for a star of mass 15.6 by Hayashi, Jugaku, and Nishida (1960) but did not include provision for the change in mean-molecular-weight in the core due to the formation of the reaction-products. The single evolutionary track of Figure 27 which extends beyond the onset of hydrogen exhaustion through the subsequent gravitational contraction to helium burning and beyond to the onset of carbon-neon burning, with each exhausted core reaction being transferred to an outer shell at the appropriate historical moment, is due to the work of Hayashi and Cameron (1961). The track is for a mass of 15.6 and is thus an extension of the work of Sakashita et al.

One other evolutionary track appears in Figure 27. It begins at about $M_{bol} = -6.7$ and evolves downward, becoming parallel to the main-sequence in the middle magnitude range and curving faintward at about $M_{bol} = 2$. This track is from an alternative theory of stellar evolution where the star evolves at decreasing mass with complete mixing so as to remain chemically homogeneous. The rate of mass loss is balanced against the CN cycle so as to cause the star injected at the top of the evolutionary track to generate the mean empirical mass-luminosity law as its mass and chemical composition change. This yields very closely a mass-loss rate that is proportional to the stellar luminosity. The track is due to Mme. Massevitch (1958). The relative advantages and disadvantages of the evolution-at-decreasing-mass school of main-sequence evolution as compared to the evolution-at-constant-mass school of thought has recently been reviewed by Deutsch (1960) so that such a discussion need not be reproduced here. The present study will be concerned with the observational test of reproducing the main-sequence of h and chi Persei.

The homology transformation of the evolutionary track of Brownlee and Cox seems in fairly good agreement with the contraction-sequence in h and chi Persei. On the whole, evolution is sufficiently rapid that one expects the constant-time-loci to be nearly parallel to the evolutionary track (Huang 1961). Just before the main-sequence is reached, however, the contraction pauses while the He^3 produced in the deuterium burning fires. The thus expected tendency of the observed sequence to over-lie, in parallel fashion, the evolutionary

track which terminates at the convergent point of the sequence onto the main-sequence is observed, though the overall brightness-excess is considerably too large. We note that the observed contraction-sequence increases in luminosity cool-ward of Log T_e = 3.7. This feature is predicted by the theoretical track only as a result of deuterium burning. One may wish to point out that the curvature shown in the M_{bol} - Log T_e diagram was imposed by the transformation from the C-M diagram where it has been drawn linearly, and that therefore, insofar as the linearity in the C-M diagram is a heurism introduced out of respect for the paucity of points, the deuterium hump in the contraction-sequence of Figure 27 may not be real. It was pointed out in the preceding section, though, that a less conservative interpretation of the point distribution in the contraction-sequence of Figure 20 produces the deuterium hump even in the C-M diagram.

Over the middle magnitude range of the unevolved main-sequence, the track for decreasing mass gives slightly better agreement with observation than the loci of the beginnings of the constant-mass evolutionary tracks. We note, however, that agreement can be produced between the two theories by a homologous displacement of the latter theoretical main-sequence, which indicates that most of the difference in their agreement with observation does not arise out of their differences in fundamental physical assumptions. At bright magnitudes, better agreement with observation is unquestionably afforded by the theory of evolution at constant mass; the evolved portions of its evolutionary tracks fall on the upper observed main-

sequence while the evolutionary track of Massevitch falls considerably to the left where no stars are found. The theoretical predictions of the constant-mass evolutionary theory is not necessarily without flaw in the upper main-sequence region, however. If the stars at the elbow of the blue-elbow branch are near hydrogen exhaustion, then those less massive stars in h and chi Persei which are of the same age as the elbow stars should show up as little evolved about three magnitudes fainter. It is found, however, that all of the stars at this magnitude are quite evolved according to the theoretical H-burning interpretation. The point is well-taken that something more complex than has yet been suggested may be taking place in the blue-elbow branch, but the fact that the blue-elbow stars show a space-region preference in agreement with the more normal stars at the top of the vertical main-sequence, and especially that the hollow branch stars do not seem to show a preference, seems to indicate that any other alternative interpretations of the blue-elbow branch should continue to keep it younger than the hollow branch.

The helium burning portion of the evolutionary track of Hayashi and Cameron is in good agreement with the hollow branch of the observed diagram. The zig-zag nature of the track is theoretical concurrence with the observationally concluded presence of fine structure in the sequence manifested in the vacancy depicted in the center of the hollow branch. We further note that the time spent between $\text{Log } T_e = 3.9$ and $\text{Log } T_e = 3.56$ is one percent of the total time spent in helium burning. The onset of carbon-neon burning corresponds remarkably well with the beginning of the M supergiant-

sequence considering the uncertainties in the B. C. and T_e scale in this temperature range. The theoretical time-scales involved are 15. 6 million years for hydrogen burning and 1. 2 million years for helium burning. For the only C-M diagram of the present study characterized by completeness (Figure 20) the statistics at bright magnitudes are not good enough to confirm these time-scales but compatibility is clearly indicated. The gravitational contraction-time between hydrogen exhaustion and helium firing is of the order of 10^5 years, so that one would expect to find a gap between the top of the main-sequence (as far as stars of the appropriate common origin in time are concerned) and the hollow branch. The observational basis of this gap was discussed in the preceding section. It appears in the HR diagram.

Neither the red end of the blue-elbow branch nor the apparent main-sequence break-off at $M_{bol} = -5.0$ appears well represented by hydrogen burning evolutionary tracks. The latter is observed not to protrude unusually far into the Hertzsprung gap in Figure 26. One thus feels justified in suggesting the possibility that not only the red end of the blue-elbow branch and the apparent main-sequence break-off at $M_{bol} = -5.0$ correspond to evolution beyond hydrogen exhaustion, but that some of the brightest blue stars in other bright clusters and associations may have been mis-identified as burning hydrogen and that some of the ages of these objects may warrant revision.

A word of caution is in order in regard to the good agreement of the observations with the theory of Hayashi and Cameron. The

structure of the helium burning evolutionary track is very sensitive to the ratio of energy generation in the shell (hydrogen) to that in the core (helium). With the advances that can yet be expected in nuclear physics, it is conceivable that improved cross-sections and new completion chains may considerably alter the track shown in Figure 27. It may be pointed out that such a high sensitivity of evolutionary track configuration to energy production ratios implies a strong dependence of evolutionary tracks on chemical composition which seems to be requisite to any attempted explanation of the differences in the stellar content of galaxies in terms of chemical composition.

d) The Age Distribution

It is not wished to engage in a discussion of the general theory of star formation, or in particular the universality of the initial mass-spectrum. What seems to be required in the present study, unless one resorts to horribly complicated evolutionary tracks whose comprehension is hopeless and disregards the evidence for an age-gradient, is that either (1) stars were formed in different parts of the region at different times and then well-mixed, thus explaining why only the very youngest stars indicate an age-gradient, or (2) some age-gradient whose general time dependence is unknown may exist, but the region as a whole, without spatial dependence, is characterized by a star formation rate that is not a Dirac delta function, and which may be a sum of several delta functions for different epochs, but has at least shown several fairly pronounced maxima in the past.

A third possibility is that there is a strong component of age-gradient with depth, which is in keeping with the fact that we are looking across the Perseus arm at this point, and that there is a general tendency for interstellar dust to concentrate along the leading edges of spiral arms (Hubble Atlas, Sandage 1961).

Considering the appearance of main-sequence stars below the point of convergence of the contraction-sequence onto the main-sequence in the C-M diagram of the dynamically bound clusters proper (Figure 20), the second proposition would seem to be preferable. We can say something about the mixing-time for the region. If we assume that the mean peculiar-velocity in the general region of the surrounding association is about 3 or 4 km/sec (Bidelman 1943) and that the angular diameter of the region in which mixing must take place is about 5 degrees (210 parsecs using the present distance modulus), then the length of time it would take the average star of the region to travel this distance is about 60 million years. This is a lower limit since no encounters are considered, although a mean-free-path using the formula from Chandrasekhar (1960 page 76) and assuming star density conditions similar to the solar neighborhood came out to be about 200,000 parsecs.

Main-sequence stars below the contraction-sequence have been definitively found in the Pleiades (Johnson and Mitchell 1958). Arp (1958b) has pointed out that more stars fall off of the major sequences of the halo globular clusters than can be explained by field star contamination; especially, there are a number of apparent main-sequence stars which lie brighter than the turn-off to the giant branch.

The situation within the globular clusters is probably not comparable to h and chi Persei because of the construction of the younger stars out of the remains of the older stars of the same globulars.

Using the time-scales of the models in Figure 27, we proceed to read off the ages of the major sequences of h and chi Persei.

The Blue-Elbow Branch. The results are, according to the following assumptions: (1) The red end of the branch implies hydrogen exhaustion, hence the age is 6.3×10^6 years. (2) The red end of the branch is engaged in helium burning and the hydrogen burning probably ends at about $M_{bol} = -9.5$ which implies an age of 4.0×10^6 years.

The Hollow Branch. The results are one of two. (1) Hydrogen burning ends at the red end of the hollow branch and therefore the age of this group is 8.9×10^6 years. (2) Helium burning ends at the red tip. In this instance Hayashi's and Cameron's combined hydrogen and helium age is 1.7×10^7 years. Their hydrogen age of 16 million years, which is based on more recent nuclear data than other ages presented in this section, is 6 million years longer than the age of Henyey et al. and Schwarzschild and Harm for the same final M_{bol}.

The Apparent Main-Sequence Break-Off Ending at $M_V = -4.25$, $(B-V)_o = -0.01$. If the break corresponds to hydrogen exhaustion, then the age is 2.0×10^7 years. If the break corresponds to the exhaustion of a more advanced fuel, probably helium, then the age assessment awaits further theoretical study. A rough guess on the basis of the second assumption which is made by extrapolating the sequence back to a more reasonably evolved position above the age-zero main-sequence

turns out to be about 40 million years.

The Upper Envelope of the Contraction-Sequence. Using the mass-radius-time and mass-luminosity-time relation for stars on a Kelvin-contraction from Schwarzschild (1958, page 163), we obtain, with a little algebra, the following homology transformation for age.

$$\text{Log}\left(\frac{\tau}{\tau_o}\right) = 1.635\ \text{Log}\left(\frac{T_e}{T_{e_o}}\right) + 0.418\ (M_{bol} - M_{bol_o}) \qquad (17)$$

Using the parameters for the primordial sun published by Brownlee and Cox and transforming the C-M coordinates of the youngest just-contracted star in h and chi Persei to the M_{bol}- Log T_e plane (0.80 and 3.970 respectively) the contraction ages turn out to be (1) 3.4×10^6 years with no deuterium burning, and (2) 6.2×10^6 years with deuterium burning assuming meteoritic abundance. We mention in passing that an interpretation of hydrogen exhaustion for this sequence leads to an age of about 3×10^8 years.

The Faintest Main-Sequence Star in the C-M Diagram. The contraction age for this point ($M_{bol} = 3.45$, Log $T_e = 3.826$), which represents a lower bound on the star ages of the immediate neighborhood of this point of the C-M diagram, is (1) 2.6×10^7 years with no deuterium, and (2) 4.6×10^7 years with deuterium firing.

We may summarize the ages, assuming that helium burning represents the supergiants, and that contracting stars undergo deuterium firing. With H-time scales homologously transformed to agree with Hayashi's and Cameron's, we obtain (1) nuclear ages of

7, 17, and 60 million-years, and (2) contraction ages of 6 and at least 46 million-years. Considering the difficulty in delineating contraction-sequences intermediate between those corresponding to the ages given here, the agreement between the nuclear and gravitational dating methods is quite satisfactory.

e) The M Supergiants as Distance Indicators

Insofar as an analogy with less massive stars is appropriate, the use of such highly evolved stars as M supergiants as distance indicators without a method of evaluating and correcting for chemical composition differences would seem to be invalid. It has been shown both theoretically (Hoyle and Schwarzschild 1955, and Kippenhahn, Temesvary, and Biermann 1958) and observationally (Sandage and Wallerstein 1960, and Wildey 1961) that the absolute magnitude of ordinary red giants is strongly dependent on the initial metal abundance. Attempts to invalidate the analogy might be based on the ideas that (1) sufficiently heavy elements have been transmuted in the cores of the M supergiants that the initial metal abundance is of negligible significance there, (2) the temperature and density range in the core may be such that the electron-density is at the limiting value imposed by pair-production (Sampson 1959), and/or (3) the masses of these stars is fixed by the maximum stable mass a proto-star can have and successfully contract to the main-sequence. These possibilities seem vitiated by the expected dependence of the extension of the convective envelope on chemical composition, which might leave bolometric magnitude insensitive to composition because of the insensitivity of the

core solution to the low-energy envelope solution; but any heterochromatic magnitude would be expected to show the effect of composition because of its effective-temperature dependence. With regard to the third possibility, aside from the fact that the M supergiants of the present study appear below both the theoretical limit and the observational limit of mass, it has been shown that theory predicts a considerable dependence of maximum stable mass on chemical composition (Schwarzschild and Härm 1959).

With regard to the effect of age (essentially mass) alone, if we have correctly interpreted the blue-elbow branch and the hollow branch of the present study as differing in age, then considering both as the suppliers of the M supergiants we conclude that the latter show the mass dispersion much less than the early supergiants. On the other hand, the possibility exists that the one anomalously bright M supergiant at $M_V = -6.7$ is the only one associated with the blue-elbow branch and that for stars this massive the M supergiant stage is very shortlived. By the same token the anomalously faint M supergiant at $M_V = -2.8$ may be an advanced stage of evolution corresponding to the apparent main-sequence break-off at $M_V = -4.25$, in which case the paucity of the single M supergiant is explainable in terms of the generally observed scarcity of stars of this age group. This, of course, should be regarded as pure speculation.

Assuming that the above objections can somehow be met, then the requirements for these supergiants to be good distance indicators when the only measured parameter is a single heterochromatic magnitude (whose bandpass still recognizes the blue M supergiants as

the brightest) can be summed up as follows. (1) The evolutionary tracks on which these supergiants lie in the C-M diagram must approach an upper envelope asymptotically with increasing mass. (2) A well defined observational range of mass must exist within which the evolutionary tracks are sufficiently close to the asymptotic track that the derived distance will not be strongly dependent on the value of n if one is averaging the n brightest stars. Especially must this be true so that the brightest star in a given galaxy can be safely assumed to be on the asymptote. (3) The blue end of the red supergiant branch must correspond to the abrupt onset of some physical process so that its observational definition will not be seriously effected by the richness of the star sample. (4) This point must approach the corresponding point on the asymptotic evolutionary track as a limit and be within a sufficiently small neighborhood of the limit-point in a well-defined observational range of mass. The fulfillment of all of these criteria is open to question, as far as the results of the present study are concerned, except for possibly the third. Theoretically, we have seen that the blue end of the M supergiant sequence should correspond to the onset of carbon-neon burning. Observationally, we find the following basis for fulfillment of criterion 3. For the 15 brightest M supergiants (excluding the two isolated stars) we find an average absolute visual magnitude of -5.07 with an average deviation of $0^m.34$. For the ten brightest M supergiants we obtain an average M_V of -5.31 and an a. d. of $0^m.20$. For the five brightest we get -5.50 and 0.13. For the brightest four we get -5.57 and 0.09. For the brightest three and two we get -5.61,

0.06 and - 5.66, 0.01 respectively. A source of doubt which must be removed is the possibility that G or K supergiants may extend the sequence blueward and that these stars have not been previously discovered because of selection effects in previous star surveys in the region. The writer's forthcoming investigation of the Hertzsprung gap at bright magnitudes should answer this question.

One observational test is possible. Shapley and Nail (1948) have found 15 M supergiants in the 30 Doradus association of the LMC. The selection is believed to be complete. Assuming the LMC as a whole presents negligible absorption, their mean intrinsic photographic apparent magnitude for these stars is 15.1. For h and chi Persei the average photographic absolute magnitude of the 15 brightest stars referred to in the preceding paragraph is - 3.17 using the present UBV photometry and reddening corrections and color-equation 3 from Arp (1961b). The resulting distance modulus is 18.3, which would be decreased by the discovery of an overall reddening correction for the LMC. The distance modulus based on cepheids found by de Vaucouleurs (1955) and independently by Hodge (1961) is 18.7.

The prospects do not seem encouraging, considering all that has been discussed, but the fundamental basis for the refutation as for the establishment of an M supergiant brightest-star distance criterion must be purely empirical. The problem requires further observational work. Unfortunately, little can be done within the Galaxy to solve the problem. Although quite a few M supergiants exist, very few are known in association with other stars whose distance can be

reliably determined. We must therefore look mostly among the near-by galaxies for a solution.

VII. CONCLUDING REMARKS

It has been reasonably shown that the general concentration of stars, whose nucleus is dynamically bound, in the Perseus spiral arm about 45° from the anticenter of the Galaxy is a group all of whose members are fairly young, but whose luminosities and colors demand, as theory stands at present, a multiplicity of epochs of stellar condensation and the operation of the three physical processes of gravitational contraction, nuclear hydrogen burning, and helium burning. The colors also indicate the predominance of electron-scattering as the source of opacity in the atmospheres of O stars. The variation of the color with spectral class for the stars of similar effective temperature but different luminosity seems understandable in terms of the classification criteria for the early stars while the more complicated analysis for the M stars has not been attempted.

The present study has pointed out lines of further research. The investigation, with completeness, of the Hertzsprung gap over the entire region investigated in the present study and the observation in UBV of the light curves of the M supergiants over a 2 or 3 year period has been pointed out previously and is already on the writer's observing program. It is probably necessary for definitive bolometric-corrections that the M supergiants be given individual radiometric measurements. Preliminary studies are under way for the procurement of this end. A method of obtaining the reddening of stars that involves measurements only on the star in question without the necessity to know its intrinsic UBV colors would be desirable. Such a requirement implies the measurement of narrow-band features.

Ordinary interstellar-absorption lines due to the interstellar gas have not demonstrated good correlation with color-excess. The possibility of using narrow-band absorption features of the interstellar dust through interference-filter techniques to obtain color-excesses will be reported on in a later paper by the author.

REFERENCES

Adams, W. S., Joy, A. H., and Humason, M. L. 1926, Astrophysical Journal, Vol. 64, 225.

Aller, L. H. 1960, Stellar Atmospheres, ed. J. L. Greenstein (Chicago: University of Chicago Press), p. 237.

_____. 1961, Astronomical Journal, Vol. 66, 37.

Arp, H. C. 1958a, International Astronomical Union Symposium No. 10, p. 53.

_____. 1958b, Handbuch der Physik, ed. S. Flugge (Berlin: Springer-Verlag), Vol. 51, 75.

_____. 1959a, Astronomical Journal, Vol. 64, 175.

_____. 1959b, ibid., p. 254.

_____. 1959c, Astrophysical Journal, Vol. 129, 507.

_____. 1961a, ibid., Vol. 133, 874.

_____. 1961b, ibid., p. 869.

Arp, H. C., and Kraft, R. P. 1961, Astrophysical Journal, Vol. 133, 420.

Bidelman, W. P. 1943, Astrophysical Journal, Vol. 98, 61.

Blaauw, A., Gum, C. S., Pawsey, J. L., and Westerhout, G. 1959, Astrophysical Journal, Vol. 130, 702.

Blaauw, A., Hiltner, W. A., and Johnson, H. L. 1959, Astrophysical Journal, Vol. 130, 69.

Blanco, V. M. 1955, Astrophysical Journal, Vol. 122, 434.

Bless, R. C. 1960, Astrophysical Journal, Vol. 132, 532.

Bok, B. J. 1959, The Observatory, Vol. 79, 61.

Brownlee, R. R., and Cox, A. N. 1961, Sky and Telescope, Vol. 21, 251.

Burbidge, E. M., Burbidge, G. R., Sandage, A. R., and Wildey, R. 1959, Liege Symposium, Vol. 16, 427.

Chandrasekhar, S. 1957, Stellar Structure (New York: Dover Publications), pp. 252, 281, 457.

_____. 1960, Principles of Stellar Dynamics (New York: Dover Publications), p. 76.

Crawford, D., Limber, D. N., Mendoza, E., Schulte, D., Steinman, H., and Swihart, T. 1956, Astrophysical Journal, Vol. 121, 24.

Deutsch, A. J. 1960, Stellar Atmospheres, ed. J. L. Greenstein (Chicago: University of Chicago Press), pp. 544-545.

Evans, D. 1941, Astrophysical Journal, Vol. 93, 275.

Feast, M. W. 1960, The Observatory, Vol. 80, 104.

Feast, M. W., Thackeray, A. D., and Wesselink, A. J. 1960, Monthly Notices of the Royal Astronomical Society, Vol. 121, 337.

Feinstein, A. 1959, Zeitschrift fur Astrophysik, Vol. 47, 218.

Gaposchkin, C. P., and Gaposchkin, S. 1938, Variable Stars (Cambridge: Harvard College Observatory), pp. 133-134.

Greenstein, J. L. 1942, Astrophysical Journal, Vol. 95, 299.

Hayashi, C., and Cameron, R. C. 1961, Astrophysical Journal, in press.

Hayashi, C., Jugaku, J., and Nishida, M. 1960, Astrophysical Journal, Vol. 131, 241.

Hazelgrove, C. B., and Hoyle, F. 1956, Monthly Notices of the Royal Astronomical Society, vol. 116, 527.

Henyey, L. G., LeLevier, R., and Levee, R. D. 1955, Publications of the Astronomical Society of the Pacific, Vol. 67, 154.

_____. 1959, Astrophysical Journal, Vol. 129, 2.

Hiltner, W. A. 1956, Astrophysical Journal Supplements, Vol. 2, 389 (No. 24).

Hiltner, W. A., and Johnson, H. L. 1956, Astrophysical Journal, Vol. 124, 367.

Hodge, P. W. 1961, Astrophysical Journal, Vol. 134, 226.

Hoyle, F. 1959, Liege Symposium, Vol. 16, 446.

Hoyle, F., and Schwarzschild, M. 1955, Astrophysical Journal Supplements, Vol. 2, 1.

Huang, S. 1961, Astrophysical Journal, Vol. 134, 12.

Hulst, H. C. van de, Muller, C. A., and Oort, J. 1954, Bulletin of the Astronomical Institute of the Netherlands, Vol. 12, 117.

Jager, C. de, and Neven, L. 1957, Annales de l'Observatoire Royale Belgique, Vol. 8, Part 1.

Johnson, H. L. 1951, Astrophysical Journal, Vol. 114, 522.

_____. 1958, Lowell Observatory Bulletin, Vol. 4, 37.

Johnson, H. L., and Heckmann, O. 1956, Astrophysical Journal, Vol. 124, 477.

Johnson, H. L., and Hiltner, W. A. 1956, Astrophysical Journal, Vol. 123, 267.

Johnson, H. L., and Knuckles, C. F. 1955, Astrophysical Journal, Vol. 122, 209.

Johnson, H. L., and Mitchell, R. I. 1958, Astrophysical Journal, Vol. 128, 31.

Johnson, H. L., and Morgan, W. W. 1953, Astrophysical Journal, Vol. 117, 313.

_____. 1955, ibid., Vol. 122, 429.

Johnson, H. L., and Sandage, A. R. 1955, Astrophysical Journal, Vol. 121, 616.

Johnson, H. L., Sandage, A. R., and Wahlquist, H. D. 1956, Astrophysical Journal, Vol. 124, 81.

Joy, A. H. 1939, Astrophysical Journal, Vol. 89, 356.

Keenan, P. C. 1942, Astrophysical Journal, Vol. 95, 461.

Kippenhahn, R., Temesvary, St., and Biermann, L. 1958, Zeitschrift fur Astrophysik, Vol. 46, 257.

Kopylov, I. M. 1958, International Astronomical Union Symposium No. 10, p. 41.

Kraft, R. P. 1961, Astrophysical Journal, Vol. 134, 616.

Lambrecht, H. 1959, Liege Symposium, Vol. 16, 318.

Lindholm, E. H. 1957, Astrophysical Journal, Vol. 126, 588.

Maanen, A. van 1911, Recherches Astronomique de l'Observatoire d'Utrecht, Vol. 5, 1.

_____. 1917, Popular Astronomy, Vol. 25, 108.

_____. 1920, Contributions of the Mount Wilson Observatory, Vol. 205, 125.

_____. 1944, Astrophysical Journal, Vol. 100, 31.

Macklin, H. E. 1922, Monthly Notices of the Royal Astronomical Society, Vol. 83, 79.

Margenau, H., and Murphy, G. M. 1956, The Mathematics of Physics and Chemistry (New York: D. Van Nostrand Company), pp. 479-482.

Massevitch, A. D. 1957, Astronomical Journal of the USSR, Vol. 34, 176.

_____. 1958, International Astronomical Union Symposium No. 10, p. 89.

Melbourne, W. G. 1959, Thesis, California Institute of Technology.

_____. 1960, Astrophysical Journal, Vol. 132, 101.

Mendoza, E. E. 1958, Astrophysical Journal, Vol. 128, 207.

Mestel, L. 1959, Liege Symposium, Vol. 16, 235.

Michard, R. 1950, Bulletin of the Astronomical Institute of the Netherlands, Vol. 11, 227.

Minnaert, M. 1953, The Sun, ed. G. P. Kuiper (Chicago: University of Chicago Press), p. 88.

Morgan, W. W., Keenan, P. C., and Kellman, E. 1943, An Atlas of Stellar Spectra (Chicago: University of Chicago Press).

Morgan, W. W., Sharpless, S., and Osterbrock, D. 1952a, Astronomical Journal, Vol. 57, 3.

_____. 1952b, Sky and Telescope, Vol. 11, 134.

Morgan, W. W., Whitford, A. E., and Code, A. D. 1953a, Astrophysical Journal, Vol. 118, 318.

_____. 1953b, Astrophysical Journal Supplements, Vol. 2, 41 (No. 14).

Oke, J. B. 1961a, Astrophysical Journal, Vol. 133, 90.

_____. 1961b, ibid., Vol. 134, 214.

Oosterhoff, P. Th. 1937, Annalen van de Sterrewacht te Leiden, Vol. 17, 5.

Payne, C. 1930, The Stars of High Luminosity (New York: McGraw-Hill Book Company), pp. 233-235.

Pesch, P. 1959, Astrophysical Journal, Vol. 130, 764.

Pettit, H. S. 1919, Popular Astronomy, Vol. 27, 671.

Plaskett, J. S., and Pearce, J. A. 1933, Publications of the Dominion Astrophysical Observatory of Victoria, Vol. 5, 197.

Popper, D. M. 1959, Astrophysical Journal, Vol. 129, 647.

Rhijn, P. J. van 1929, Groningen Publications, No. 43.

Sakashita, S., Ōno, Y., and Hayashi, C. 1959, Progress in Theoretical Physics (Kyoto University), Vol. 21, 315.

Sampson, D. H. 1959, Astrophysical Journal, Vol. 129, 734.

Sandage, A. R. 1957a, Astrophysical Journal, Vol. 125, 435.

_____. 1957b, ibid., p. 422.

_____. 1957c, ibid., Vol. 126, 326.

_____. 1958, ibid., Vol. 128, 150.

Sandage, A. R., and Eggen, O. J. 1959, Monthly Notices of the Royal Astronomical Society, Vol. 119, 255.

Sandage, A. R., and Walker, M. F. 1955, Astronomical Journal, Vol. 60, 230.

Sandage, A. R., and Wallerstein, G. 1960, Astrophysical Journal, Vol. 131, 598.

Schatzman, E. 1960, Air Force Office of Scientific Research, Contract AF49(638)-21, Special Technical Report No. 3.

Schmalberger, D. C. 1960, Astrophysical Journal, Vol. 132, 591.

Schmidt, M. 1957, Bulletin of the Astronomical Institute of the Netherlands, Vol. 13, 247.

_____. 1959, Astrophysical Journal, Vol. 129, 243.

Schwarzschild, M. 1958, Structure and Evolution of the Stars (Princeton: Princeton University Press), pp. 97, 163.

Schwarzschild, M., and Harm, R. 1958, Astrophysical Journal, Vol. 128, 348.

_____. 1959, ibid., Vol. 129, 637.

Serkowski, K. 1958, Acta Astronomica, Vol. 8, 3.

Seyfert, C. K., Hardie, R. H., and Grenchik, R. T. 1960, Astrophysical Journal, Vol. 132, 58.

Shapley, H. 1930, Star Clusters (Harvard Monographs No. 2).

Shapley, H., and Nail, V. M. 1948, Proceedings of the National Academy of Sciences, Vol. 34, 173.

Sharpless, S. 1958, Publications of the Astronomical Society of the Pacific, Vol. 70, 392.

Stebbins, J., Huffer, C. M., and Whitford, A. E. 1940, Astrophysical Journal, Vol. 91, 20.

Stebbins, J., and Whitford, A. E. 1945, Astrophysical Journal, Vol. 102, 318.

Struve, O. 1927, Astronomische Nachrichten, Vol. 231, 17.

Varsavsky, C. M. 1960, Astrophysical Journal, Vol. 131, 623.

Vaucouleurs, G. de 1955, Publications of the Astronomical Society of the Pacific, Vol. 67, 350.

Walker, M. F. 1956, Astrophysical Journal Supplements, Vol. 2, 365 (No. 23).

_____. 1957, Astrophysical Journal, Vol. 125, 636.

_____. 1959, ibid., Vol. 130, 57.

_____. 1961, ibid., Vol. 133, 438.

Wempe, J. 1947, Astronomische Nachrichten, Vol. 275, 97.

Wentzel, D. G. 1961, Astrophysical Journal, Vol. 133, 170.

Wildey, R. L. 1961, Astrophysical Journal, Vol. 133, 430.

Wildey, R. L., Burbidge, E. M., Sandage, A. R., and Burbidge, G. R. 1961, Astrophysical Journal, in press.

Wilson, R. E. 1941, Astrophysical Journal, Vol. 93, 212.

Woolley, R. v. d. R., and Stibbs, D. W. N. 1953, The Outer Layers of a Star (London: Clarendon Press), p. 55.

APPENDIX I

TABLES

TABLE 1

SUPERGIANTS OF THE GENERAL REGION

No.	HD	Other	R.A. (1960)	Dec. (1960)	Sp	M_V
1		BD58°373	$02^h04^m14^s$	58°36.'5	M0	-4.39
2	12856	BD56 429	02 04 56	56 54.2	B0pe	-4.90
3	12953	BD57 494	02 05 43	58 15.0	A1Ia	-8.00
4	13136	BD55 529	02 07 21	56 23.0	M2Ib	-5.20
5	13267	BD56 438	02 08 28	57 28.4	B5Ia	-6.76
6	13402	BD58 396	02 09 55	59 21.2	B0.5I	-6.02
7	13476	BD57 519	02 10 43	58 23.0	A3Iab	-6.83
8	13659	BD56 462	02 12 10	56 45.0	B1Ib	-5.28
9		BD57 524	02 12 14	57 59.1	M0.5	-4.43
10	13744	BD57 526	02 12 57	58 07.0	A0Iab	-6.42
11	13841	Oo3	02 13 49	56 51.4	B2Ib	-5.65
12		Oo16	02 14 03	56 52.1	B1Iab	-6.68
13	13866	BD56°475	02 14 03	56 33.0	B2Ib	-5.31
14		K100172	02 15 05	59 30.0	M1	-2.78
15		Oo662	02 15 38	57 01.4	B1Ib	-5.09
16		Bu Per	02 15 59	57 14.3	M3.5Ib	-4.94
17		Oo1057	02 16 07	56 57.1	B3Ia	-7.05
18		Oo1162	02 16 16	56 57.0	B2Ia	-7.03
19	14142	T Per	02 16 27	58 47.0	M2Iab	-4.68
20		BD58°445	02 17 16	59 29.6	M1	-5.14
21		AD Per	02 17 38	56 48.7	M2.5Iab	-5.44
22	14322	BD55°588	02 17 50	55 44.2	B8Ib	-6.21
23		FZ Per	02 18 07	56 58.6	M1Iab	-4.97
24	14404	BD57°550	02 18 43	57 41.0	M1Ib	-5.67
25		Oo2178	02 19 03	57 03.8	A1Ia	-7.41
26		Oo2227	02 19 09	56 58.0	B2Ib	-5.10
27	14469	SU Per	02 19 16	56 25.5	M3.5Iab	-5.23
28	14489	BD55°598	02 19 28	55 40.6	A2Ia	-7.38
29		RS Per	02 19 32	56 56.0	M4.5Iab	-5.21

TABLE 1 (Continued)

No.	HD	Other	R.A. (1960)	Dec. (1960)	Sp	M_v
30	14528	S Per	$02^h19^m57^s$	$58^\circ24.'4$	M4eIa	-4.46
31		Oo2589	02 20 00	57 04.0	A2Ia	-6.21
32		Oo2621	02 20 07	57 12.5	B8Ia	-6.94
33		BD56°595	02 20 14	56 61.5	M0.5Iab	-5.12
34	14580	Oo2758	02 20 26	57 02.2	M0Iab	-5.52
35	14818	BD55°612	02 22 16	56 26.0	B2Ia	-6.98
36	14826	BD56 611	02 22 22	57 16.2	M3Iab	-5.64
37	14899	BD56 621	02 23 21	57 04.0	B8Ib	-5.74
38	14956	BD57 568	02 23 45	57 31.4	B2Ia	-7.17
39		BD60 478	02 24 08	60 33.4	M2Iab	-3.95
40	15316	BD57 576	02 26 55	57 39.6	A3Iab	-6.59
41		BD60 493	02 27 36	61 01.1	B0.5Ia	-6.71
42	15497	BD57 582	02 28 51	57 32.0	B6Ia	-7.18
43	15620	BD57 584	02 29 49	57 48.2	B8Iab	-6.39
44	15690	BD56 656	02 30 30	57 22.1	B1.5Ib	-6.45
45		YZ Per	02 35 28	56 52.5	M2.5Iab	-6.73
46	16779	BD57°620	02 40 30	57 40.0	B2Ib	-5.79
47	16778	BD59 535	02 40 42	59 40.4	A2Ia	-6.66
48	17088	BD57 632	02 43 46	57 34.9	B9Ia	-6.88
49	16808	BD57 622	02 43 46	56 50.5	B0.5Ib	-5.40
50	17145	BD57 634	02 44 18	57 30.9	B8Ia	-5.99
51	17378	BD56 718	02 46 24	56 55.9	A5Ia	-7.74

TABLE 2

O STARS OF THE GENERAL REGION

No.	HD	Other	R.A. (1960)	Dec. (1960)	Sp	M_V
1	12323	BD54°441	$01^h59^m36^s$	55°26.'7	O9V	-3.98
2		Oo2172	02 19 01	56 43.5	O6	-4.97
3	14442	BD58°455	02 19 07	59 23.5	O5.5	-5.25
4		BD60 470	02 19 59	60 39.7	O8V	-4.72
5	14947	BD58 467	02 23 43	58 42.2	O6F	-6.31
6		BD60 498	02 28 53	61 24.0	O9V	-4.50
7		BD60 501	02 29 14	61 19.0	O6.5	-4.78
8	15558	BD50 501	02 29 28	61 18.0	O6	-6.55
9	15570	BD60 504	02 29 33	61 13.5	O5F	-6.48
10	15629	BD60 507	02 30 03	61 22.1	O5	-5.96
11		BD60 512	02 30 42	61 14.2	O6	-4.80
12	16429	BD60 541	02 37 35	61 07.0	O9.5III	-6.94
13	16691	BD56 693	02 39 48	56 44.9	O5F	-5.60
14	12993	BD57 498	02 42 48	57 45.0	O5	-5.43
15	13268	BD55 534	02 45 06	55 58.0	O8Vnn	-5.12
16	17505	BD59 552	02 47 41	60 17.0	O7	-6.58
17	17520	BD59 553	02 47 50	60 15.0	O8V	-5.36
18	17603	BD56 728	02 48 40	56 54.1	O7f:	-6.24
19		BD59 562	02 50 07	60 19.2	O8V	-4.66
20		BD60 586	02 50 55	60 29.9	O7	-5.40
21		BD50 594	02 53 39	61 14.7	O9V	-4.63

TABLE 3

GIANTS AND SUBGIANTS OF THE GENERAL REGION

No.	HD	Other	R.A. (1960)	Dec.(1960)	Sp	M_V
1		BD59°388	$01^h59^m39^s$	59°47.'6	B3II	-4.56
2	13051	BD56 432	02 06 30	56 49.3	B1III	-4.23
3	13621	BD54 494	02 11 39	55 08.5	B0.5IV	-4.71
4	13745	BD55 554	02 12 51	55 49.4	B0III	-5.47
5	13831	BD56 469	02 13 43	56 34.0	B0IV	-5.91
6	13890	BD56 478	02 14 14	56 35.7	B1IIIpe	-4.42
7		Oo339	02 15 00	56 54.2	B1IV	-4.62
8		Oo612	02 15 34	56 49.5	B1II	-4.76
9		Oo1187	02 16 26	57 00.0	B2IV	-2.87
10		Oo1586	02 17 24	56 55.0	B1III	-4.65
11	14331	BD55°590	02 17 58	55 38.8	B0III	-5.33
12		Oo1899	02 18 20	56 41.1	B2II	-5.63
13		Oo2138	02 18 57	57 12.4	B0IV:pe	-4.62
14		Oo2246	02 19 11	56 57.6	B2III	-3.37
15		Oo2541	02 19 52	56 54.5	B2II	-4.29
16	15642	BD54°569	02 29 56	55 10.7	B0IV	-4.94
17	16310	BD58 498	02 36 10	58 55.2	B1II:	-6.52

TABLE 4

SUPERGIANTS AND FAINT NEIGHBORS OF THE GENERAL REGION

No.	V	B-V	U-B	No.	V	B-V	U-B
1	8.65	2.22	2.79	12	6.49	0.28	-0.65
I	13.58	0.85	0.30	I	13.20	0.75	0.16
2	14.58	1.05	0.50	2	15.34	0.41	0.16
2	8.55	0.24	-0.77	13	7.52	0.18	-0.63
I	11.25	1.34	1.16	I	12.34	0.20	-0.32
2	11.45	0.49	0.15	2	11.83	0.14	-0.48
3	5.68	0.62	-0.03	14	10.30	2.31	2.51
I	10.17	0.26	-0.37	I	13.97	0.80	0.37
2	8.42	1.28	1.28	2	15.12	1.00	0.49
3	9.49	1.36	1.41	3	13.56	0.68	0.48
4	12.23	0.55	0.15	4	14.62	0.67	0.35
4	7.78	2.24	2.47	15	8.18	0.31	-0.59
I	13.67	0.42	0.28	I	13.21	0.48	0.32
2	14.47	1.21	1.19	2	13.01	0.37	-0.16
5	6.39	0.33	-0.43	16	9.16	2.47	2.63
I	14.45	0.84	0.29	Oo899	10.65	1.27	1.26
2	12.53	0.32	-0.23	1	15.16	0.83	0.53
3	14.74	0.72	0.39	2	14.12	0.87	0.27
4	13.86	0.86	0.43	3	14.56	0.56	0.29
6	8.06	0.60	-0.42	Oo1211	12.58	0.60	0.32
I	12.71	0.58	-0.24	17	6.55	0.47	-0.37
2	14.35	0.76	0.54	I	12.98	0.51	0.02
3	15.01	0.66	0.32	2	11.14	0.35	-0.41
7	6.46	0.59	0.21	3	11.39	0.39	-0.38
I	10.97	0.84	0.38	18	6.66	0.51	-0.45
2	9.61	0.26	-0.52	I	15.50	0.80	0.12
3	9.64	0.45	0.14	2	13.62	0.52	0.16
4	12.17	0.97	0.28	3	13.50	0.60	0.30
5	13.67	1.35	1.36	Oo1166	13.12	0.54	-0.10
8	8.65	0.55	-0.41	Oo1202	12.12	0.44	-0.22
I	12.32	0.59	0.27	19	8.81	2.35	2.75
2	13.98	0.66	0.11	I	12.56	0.57	0.40
9	8.96	2.31	2.74	2	12.53	0.43	-0.16
I	14.91	0.34	-0.74	20	8.35	2.43	2.85
2	15.49	1.11	0.83	I	12.99	0.92	0.42
3	11.07	0.19	-0.50	2	13.55	0.72	0.54
4	15.43	1.30	0.48	21	7.85	2.23	2.43
5	12.44	0.48	-0.19	I	14.03	0.92	0.42
10	7.60	0.74	0.18	2	15.47	0.72	0.48
I	13.98	0.66	0.18	3	13.82	1.24	0.86
2	12.31	0.69	0.40	22	6.79	0.32	-0.34
3	14.82	1.99	2.48	I	13.91	0.34	0.20
4	14.28	1.58	1.44	2	14.74	1.29	0.96
11	7.39	0.23	-0.65	3	10.42	0.42	0.25
I	12.08	0.23	-0.36	23	7.91	2.27	2.57
2	12.38	0.27	-0.37	I	14.22	0.61	0.40
				2	14.17	0.82	0.16

TABLE 4 (Continued)

No.	V	B-V	U-B	No.	V	B-V	U-B
24	7.84	2.27	2.70	36	8.26	2.23	2.50
I	14.26	0.85	0.51	I	14.05	0.56	0.15
2	13.54	1.79	1.53	2	11.28	0.45	-0.39
25	6.38	0.58	0.02	3	12.21	0.57	-0.23
I	12.33	0.54	-0.13	4	15.77	1.19	0.56
2	13.60	0.60	0.21	37	7.40	0.44	-0.11
3	12.26	0.43	-0.30	I	14.27	0.95	0.34
26	8.05	0.34	-0.55	2	11.95	0.42	0.25
Oo2203	14.61	0.50	0.05	38	7.21	0.72	-0.29
Oo2188	14.99	0.71	0.35	I	13.17	0.73	0.04
1	13.28	0.33	-0.16	2	16.24	1.08	0.87
2	13.93	0.42	0.08	3	14.10	0.67	-0.03
27	7.69	2.15	2.37	4	13.90	0.96	0.42
I	12.94	0.39	0.25	39	11.68	3.13	4.22
2	12.76	0.53	0.22	I	15.47	1.25	0.91
3	14.24	0.61	0.40	2	11.00	0.56	0.09
28	5.17	0.37	-0.11	3	10.60	0.42	0.19
I	9.84	0.13	-0.14	40	7.24	0.77	0.42
2	11.65	0.53	0.10	I	13.45	0.54	-0.06
3	10.48	1.15	0.79	2	14.70	1.75	1.90
4	11.54	0.59	0.31	3	14.60	1.79	2.43
29	8.31	2.29	2.28	4	14.94	0.62	0.27
I	13.69	0.49	0.06	5	14.68	1.00	0.30
2	13.17	0.72	0.32	41	8.44	0.79	-0.30
Oo2349	12.81	0.55	0.37	I	14.60	1.03	0.46
30	9.26	2.56	2.63	2	11.76	0.75	0.39
I	15.11	0.63	0.43	42	7.03	0.78	-0.07
2	13.87	0.61	0.31	I	12.84	0.62	-0.06
31	7.44	0.72	0.11	2	15.20	0.82	0.47
I	13.98	0.51	0.03	3	13.58	0.73	0.27
2	12.56	0.42	-0.27	43	8.35	0.92	0.17
3	13.45	0.70	0.29	I	14.26	0.95	0.22
32	7.00	0.61	-0.14	2	15.16	0.83	0.47
I	13.94	0.55	0.09	44	8.00	0.66	-0.27
2	15.18	1.14	0.64	I	13.38	0.67	-0.06
3	14.98	0.97	0.29	2	13.86	0.77	0.06
33	8.29	2.23	2.39	45	7.66	2.35	2.93
I	14.68	0.91	0.41	I	13.34	0.79	0.24
2	14.14	1.68	1.68	2	12.73	0.84	0.31
34	8.31	2.25	2.40	46	8.86	0.74	-0.26
I	12.62	0.51	-0.20	I	12.88	0.83	0.25
2	13.10	0.57	0.10	2	14.69	1.02	0.32
35	6.25	0.31	-0.62	3	11.16	1.18	1.09
I	10.52	0.49	0.34				
2	11.57	0.76	0.22				

TABLE 4 (Continued)

No.	V	B-V	U-B
47	7.73	0.90	0.34
1	14.36	0.83	0.57
2	13.15	1.11	0.81
3	14.15	1.20	0.48
48	7.50	0.82	0.05
1	14.08	0.75	0.10
2	11.57	0.62	-0.23
49	8.60	0.56	-0.47
1	15.07	1.22	0.38
2	13.41	0.58	-0.08
50	8.16	0.82	-0.01
1	12.31	0.66	0.09
2	13.76	1.09	0.63
3	15.14	0.86	0.23
51	6.26	0.89	0.49

No faint neighbors.
Reddening later derived from Sp. See text.

TABLE 5

O STARS AND FAINT NEIGHBORS OF THE GENERAL REGION

No.	V	B-V	U-B
1	8.90	-0.12	-0.93
1	13.01	0.93	-0.48
2	12.35	1.26	1.01
2	8.50	0.16	-0.79
1	15.14	0.50	0.18
2	13.21	1.23	0.40
3	9.21	0.41	-0.61
1	11.82	0.79	0.26
4	9.87	0.70	-0.36
1	14.80	1.89	1.09
2	12.72	0.90	0.56
3	14.35	0.82	0.22
4	13.87	1.09	0.77
5	7.98	0.46	-0.60
1	14.34	1.70	1.21
2	12.19	0.47	-0.38
6	9.92	0.54	-0.46
1	13.28	0.84	0.42
2	12.84	0.74	0.07
2a	13.30	0.76	0.26
7	9.60	0.46	-0.58
3	11.17	0.66	-0.34
4	12.00	0.56	-0.33
8	7.81	0.52	-0.56
5	12.82	0.72	-0.51
6	11.27	0.50	-0.42
9	8.10	0.70	-0.40
1	12.22	0.72	-0.21
2	15.16	1.25	0.55
10	8.43	0.42	-0.62
1	12.77	0.60	-0.27
2	13.67	0.76	0.05
11	9.41	0.50	-0.53
1	14.67	0.86	0.24
2	15.03	0.70	-0.30
3	14.28	0.73	0.33
12	7.67	0.62	-0.38
1	12.33	0.81	-0.15
2	11.54	0.55	-0.42
13	8.70	0.48	-0.55
1	14.04	0.84	0.43
2	13.83	0.64	0.95
3	14.84	1.18	0.54
14	8.95	0.20	-0.79
1	10.93	0.74	0.13
2	12.35	1.11	0.78
15	8.18	0.13	-0.83
1	12.14	0.37	0.27
2	11.87	0.57	0.16
16	7.06	0.40	-0.64
1	12.36	0.61	0.09
2	12.42	0.48	0.24
17	8.27	0.32	-0.68
3	12.53	0.54	-0.25
4	12.23	0.43	0.17
18	8.45	0.64	-0.42
1	11.58	0.72	-0.22
2	11.60	0.64	-0.46
3	13.19	0.77	0.51
19	9.73	0.47	-0.53
1	11.60	1.81	1.55
2	11.57	0.67	0.14
20	8.48	0.30	-0.67
1	12.82	0.60	-0.08
2	13.12	0.46	-0.19
21	9.30	0.36	-0.64
1	10.80	0.37	0.20
2	12.12	0.61	0.12

TABLE 6

GIANTS-SUBGIANTS AND FAINT NEIGHBORS OF THE GENERAL REGION

No.	V	B-V	U-B	No.	V	B V	U-B
1	9.60	0.60	-0.24	10	8.97	0.32	-0.54
I	13.78	0.79	0.20	I	13.56	0.50	-0.82
2	14.11	0.73	0.57	2	12.12	1.95	1.89
2	8.71	0.14	-0.72	epsilon	15.59	1.34	0.86
I	15.31	1.07	0.70	11	8.45	0.17	-0.76
2	14.42	0.35	0.13	I	15.14	0.90	0.13
3	8.11	0.06	-0.78	2	11.89	0.57	0.04
I	13.94	0.30	0.05	12	8.53	0.32	-0.53
2	14.17	0.65	0.30	I	13.38	0.72	0.18
4	7.88	0.17	-0.78	2	14.77	1.26	0.45
I	15.07	0.47	-0.27	13	9.28	0.44	-0.55
2	13.76	0.91	0.37	I	14.71	0.57	0.21
3	13.21	0.89	0.41	2	12.09	0.73	0.40
4	14.44	1.40	1.07	14	9.90	0.32	-0.56
5	8.27	0.09	-0.81	I	13.44	0.36	-0.18
I	15.15	0.66	-0.11	2	15.80	0.89	0.34
2	15.21	0.69	0.29	15	9.15	0.33	-0.55
3	14.98	0.81	0.36	I	14.80	0.59	0.37
6	8.53	0.19	-0.64	2	13.41	0.37	-0.16
I	12.08	0.20	-0.48	16	8.54	0.08	-0.84
2	12.53	0.29	-0.14	I	14.22	0.53	0.28
7	8.85	0.31	-0.61	2	13.19	0.36	0.46
I	12.64	0.31	-0.36	3	10.86	1.18	0.85
2	12.54	0.42	-0.28	17	8.07	0.66	-0.35
8	8.41	0.25	-0.62	I	14.33	0.94	0.25
I	12.72	0.28	-0.35	2	15.70	1.10	0.86
2	15.04	0.56	-0.19	3	15.59	0.71	-0.08
9	10.82	0.39	-0.40				
I	13.62	0.52	0.16				
2	13.50	0.60	0.30				
Oo1166	13.12	0.54	-0.10				
Oo1202	12.12	0.44	-0.22				

TABLE 7

PHOTOELECTRIC SEQUENCE FOR PHOTOGRAPHIC INTERPOLATION - FAINT END

No.	X (sec-arc)	Y (sec-arc)	V	B	U
alpha	216.0 W	99.3 S	14.99 ± 0.011	16.26 ± 0.017	17.02 ± 0.007
beta	170.1 W	41.5 S	15.37 ± 0.008	16.60 ± 0.015	17.32 ± 0.015
gamma	165.7 W	122.2 S	15.42 ± 0.021	17.11 ± 0.020	18.67 ± 0.050
delta	80.8 W	67.3 S	15.49 ± 0.014	16.99 ± 0.012	18.17 ± 0.014
epsilon	192.4 W	189.3 S	15.59 ± 0.016	16.93 ± 0.043	17.79 ± 0.047
zeta	16.8 W	158.8 S	16.03 ± 0.006	16.94 ± 0.006	17.30 ± 0.032
eta	10.3 W	118.0 N	16.79 ± 0.013	17.77 ± 0.014	18.17 ± 0.019
theta	183.9 W	57.0 S	16.98 ± 0.024	18.03 ± 0.006	18.45 ± 0.016
iota	90.1 W	111.1 N	17.04 ± 0.026	18.15 ± 0.012	18.56 ± 0.039
kappa	191.2 W	22.5 S	17.04 ± 0.019	18.17 ± 0.013	18.97 ± 0.014

TABLE 8

AVERAGE PROBABLE ERROR OF PHOTOELECTRIC PHOTOMETRY

Average Probable Error	Mt. Wilson Sixty-inch		Palomar Twenty-inch	
	V < 12	V > 12	V < 12	V > 12
V	0.013	0.023	0.011	0.024
B-V	0.011	0.018	0.016	0.039
U-B	0.017	0.023	0.025	0.046

TABLE 9

STARS OF THE EXTREME NUCLEUS OF h PERSEI

No.	V	B-V	U-B	No.	V	B-V	U-B
1	6.55	0.47	-0.37	47	17.30	0.79	-0.09
2	10.87	0.47	-0.45	48	15.91	0.71	0.53
3	15.35	0.84	-0.42	49	16.36	0.89	0.39
4	14.00	1.01	0.26	50	14.95	0.66	0.37
5	13.52	0.50	-0.24	51	17.60	0.75	0.16
6	13.47	0.43	-0.02	52	14.81	0.86	0.70
7	13.40	0.71	0.01	53	16.91	0.70	0.17
8	15.35	0.83	0.26	54	16.14	0.72	0.32
9	10.57	0.47	-0.53	55	10.59	0.38	-0.44
10	13.21	0.44	-0.01	56	17.60	0.70	0.09
11	10.18	0.36	-0.32	57	17.00	0.87	0.03
12	13.73	0.42	-0.46	58	16.40	0.80	0.21
13	16.65	0.79	0.15	59	14.12	0.82	0.15
14	15.50	0.80	0.49	60	10.26	0.27	-0.39
15	15.13	0.78	0.54	61	12.34	0.44	-0.24
16	14.01	0.75	0.27	62	17.57	0.84	-0.06
17	13.87	0.81	0.32	63	14.55	0.55	0.25
18	14.58	1.32	0.39	64	17.94	0.69	-0.38
19	14.38	1.22	0.33	65	15.62	0.63	0.68
20	13.68	0.40	0.08	66	12.57	0.46	-0.16
21	10.70	0.48	-0.49	67	17.61	0.93	0.03
22	9.31	0.50	-0.48	68	16.92	0.68	0.08
23	9.58	0.52	-0.44	69	15.99	0.69	0.54
24	11.71	0.45	-0.29	70	14.54	0.61	0.41
25	11.28	0.44		71	17.02	0.85	0.18
25b	14.10	0.48	0.12	72	16.24	0.74	0.45
26	15.64	0.82	0.32	73	13.17	0.48	-0.28
27	16.06	0.69	0.31	74	13.37	0.55	-0.23
28	10.33	0.29	-0.41	75	12.93	0.63	0.30
29	14.45	0.73	0.47	76	17.47	0.77	-0.09
30	14.84	0.71	0.63	77	17.60	0.90	-0.17
31	12.54	0.47	-0.21	78	16.93	0.82	0.21
32	15.89	0.89	0.10	79	15.36	0.60	0.58
33	11.95	0.53	-0.47	79b	15.37	0.58	0.46
34	10.55	0.42	-0.46	80	17.56	0.96	-0.10
35	15.35	0.79	0.50	81	13.82	0.44	0.03
36	15.71	0.74	0.58	82	10.57	0.28	-0.10
37	13.52	1.01	0.35	83	14.98	0.65	0.46
38	17.15	0.79	-0.03	84	15.20	0.64	0.54
39	14.04	0.53	-0.13	85	16.01	0.75	0.46
40	16.57	0.78	0.51	86	11.29	0.36	-0.40
41	13.68	0.61	0.15	87	17.34	0.75	0.01
42	15.37	0.75	0.67	88	16.04	1.03	0.45
43	16.11	0.86	0.32	89	16.51	1.11	0.68
44	13.66	0.65	0.03	90	17.72	0.77	-0.19
45	15.69	0.98	0.39	91	17.88	0.71	-0.13
46	16.67	0.80	0.17	92	14.87	0.48	0.32

TABLE 9 (Continued)

No.	V	B-V	U-B	No.	V	B-V	U-B
93	16.84	0.86	0.12	142	16.16	1.34	0.65
94	17.69	0.90	-0.29	143	14.40	0.50	0.18
95	17.24	0.55	0.31	144	17.91	0.65	0.10
96	14.37	0.49	0.27	145	17.51	0.75	0.15
97	12.51	0.37	-0.39	146	14.10	0.44	0.12
98	14.80	0.71	0.50	147	18.08	0.71	-0.08
99	14.65	0.90	0.64	148	17.04	0.87	0.20
100	15.73	1.73	0.88	149	15.85	0.95	0.33
101	17.29	0.89	-0.21	150	17.93	0.49	0.29
102	16.88	0.88	0.16	151	17.53	1.09	0.33
103	15.76	0.75	0.44	152	17.77	0.82	0.19
104	17.68	0.76	-0.05	153	18.01	0.78	-0.01
105	16.74	1.11	0.04	154	17.33	1.30	0.11
106	18.05	0.57	0.11	155	18.11	0.63	0.18
107	14.08	0.49	0.16	156	17.36	0.78	0.18
108	15.05	0.56	0.36	157	18.02	0.51	0.41
109	16.48	0.66	0.66	158	17.39	0.92	0.20
110	16.99	0.90	0.29	159	17.84	0.86	0.01
111	15.39	0.66	0.50	160	18.36	0.38	0.09
112	14.57	0.56	0.29	161	17.23	0.71	0.41
113	17.66	0.74	0.11	162	15.39	0.76	0.53
114	15.26	1.01	0.46	163	18.04	0.70	0.30
115	17.88	0.94	0.03	164	18.00	0.78	0.06
116	17.55	0.90	0.37	165	14.57	0.42	0.17
117	16.59	0.89	0.29	166	17.13	0.99	0.10
118	16.51	0.76	0.41	167	16.25	1.45	0.27
119	12.91	0.51	-0.14	168	15.07	1.78	1.13
120	15.21	0.67	0.54	169	16.89	0.78	0.29
121	17.23	1.16	0.19	170	17.22	0.92	0.24
122	17.88	0.72	0.21	171	17.55	0.72	0.11
123	17.18	1.12	0.17	172	16.75	0.78	0.29
124	14.58	0.53	0.64	173	13.47	0.47	0.33
125	16.56	0.84	0.45	174	14.54	0.77	0.47
126	17.29	1.16	0.21	175	15.80	0.63	0.43
127	17.95	0.89	-0.18	176	17.76	0.77	0.06
128	18.33	0.42	-0.01	177	17.89	0.17	0.17
129	18.34	0.42	0.63	178	12.25	0.36	-0.28
130	17.79	0.78	0.41	179	17.89	0.82	0.09
131	13.57	0.40	0.02	180	16.31	0.84	0.38
132	15.52	0.65	0.57	181	16.19	0.87	0.47
133	13.80	0.85	0.28	182	16.73	0.81	0.30
134	15.26	0.88	0.61	183	16.61	0.80	0.10
135	17.07	0.96	0.35	184	16.38	1.00	0.33
136	15.46	1.83	1.04	185	15.30	0.73	0.51
137	11.04	0.49	-0.22	186	17.30	0.70	0.14
138	15.31	0.77	0.66	187	17.96	0.70	0.06
139	16.16	0.60	0.59	188	14.00	0.62	0.46
140	17.35	0.77	0.14	189	15.68	0.57	0.55
141	15.27	0.60	0.51	190	17.66	0.95	0.47

TABLE 9 (Continued)

No.	V	B-V	U-B	No.	V	B-V	U-B
191	16.37	0.81	0.33	241	17.67	0.69	0.44
192	14.92	1.08	0.62	242	17.89	0.96	0.17
193	10.84	0.26	-0.42	243	18.07	0.75	-0.43
194	14.75	0.56	0.42	244	11.97	0.34	-0.29
195	13.12	0.50	0.24	245	16.95	0.83	0.06
196	15.13	1.15	0.57	246	14.37	0.46	0.24
197	18.25	0.07	0.17	247	17.60	0.62	0.49
198	17.21	1.06	0.48	248	16.55	0.84	0.26
199	10.89	0.32	-0.27	249	13.92	0.27	0.18
200	17.76	0.36	0.49	250	15.43	0.75	0.54
201	13.93	0.34	0.10	251	17.46	0.84	0.02
202	9.37	0.33	-0.65	252	13.25	0.39	-0.14
203	15.00	0.57	0.46	253	15.92	0.80	0.44
204	17.47	0.63	0.45	254	15.38	0.67	0.36
205	12.94	0.50	-0.23	255	15.61	0.56	0.62
206	15.45	0.66	0.40	256	17.68	0.95	-0.10
207	14.63	0.50	0.35	257	17.77	0.85	-0.13
208	14.66	0.58	0.45	258	16.30	0.89	0.04
209	15.28	0.51	0.47	259	9.32	0.31	-0.53
210	16.64	0.83	0.23	260	14.35	0.72	0.32
211	17.62	0.78	0.08	261	15.08	0.68	0.63
212	17.99	0.92	-0.05	262	16.74	0.92	0.04
213	15.49	0.63	0.48	263	11.47	0.36	-0.43
214	Kodak	Star		264	12.40	0.43	
215	15.50	0.59	0.47	264b	12.69	0.47	-0.36
216	17.95	0.77	0.43	265	10.74	0.50	-0.44
217	16.34	0.91	0.35	266	12.31	0.48	-0.41
218	13.43	0.37	-0.03	267	15.91	0.89	0.72
219	14.08	0.35	0.16	268	9.49	0.29	-0.43
220	17.60	0.72	-0.03	269	14.19	0.73	0.43
221	16.64	0.78	0.34	270	12.27	0.34	-0.26
222	17.75	0.70	-0.16	271	14.94	0.77	0.62
223	14.92	0.53	0.35	272	10.66	0.32	-0.11
224	13.19	0.39	-0.03	273	10.59	0.82	-0.41
225	15.91	0.65	0.50	274	15.47	0.79	0.50
226	16.43	1.40	0.52	275	14.09	1.88	0.76
227	17.26	0.91	0.12	276	16.65	0.83	0.27
228	15.49	0.90	0.34	277	17.23	0.62	0.10
229	18.46	0.46	0.28	278	17.00	0.55	0.15
230	17.58	0.97	0.35	279	16.55	0.82	0.23
231	13.74	0.35	0.24	280	14.02	0.45	0.01
232	17.87	0.73	0.35	281	17.57	0.77	0.14
233	16.47	0.77	0.42	282	17.65	0.84	-0.07
234	15.37	0.44	0.52	283	11.39	0.40	-0.08
235	17.52	0.81	0.08	284	12.01	0.39	-0.33
236	18.33	0.42	0.06	285	12.83	0.39	-0.24
237	17.73	0.97	0.42	286	13.00	0.34	0.08
238	16.59	1.02	0.42	287	16.46	0.85	0.34
239	17.04	0.95	0.23	288	13.87	0.43	0.13
240	16.88	0.72	0.22	289	14.73	0.71	0.58

TABLE 9 (Continued)

No.	V	B-V	U-B	No.	V	B-V	U-B
290	13.03	0.43	-0.33	299	16.45	0.71	0.35
291	14.74	1.62	0.97	300	11.99	0.34	-0.23
292	14.26	0.50	0.28	301	14.12	0.49	0.39
293	17.59	0.70	0.20	302	16.07	1.12	0.23
294	17.06	1.05	0.35	303	16.22	0.74	0.35
295	17.58	0.80	0.11	304	10.49	0.45	-0.37
296	17.89	0.69	0.06	305	14.99	0.49	0.76
297	13.08	0.37	-0.28	306	12.68	0.46	0.33
298	11.96	0.37	-0.20	307	15.42	1.29	0.70

TABLE 10

STARS OF THE EXTREME NUCLEUS OF chi PERSEI

No.	V	B-V	U-B	No.	V	B-V	U-B
1	9.66	0.40	-0.59	48	16.03	0.80	0.24
2	17.10	0.50	0.33	49	11.42	0.24	-0.39
3	14.26	0.35	0.00	50	15.55	1.02	0.19
4	16.30	0.93	0.13	51	17.44	0.57	0.36
5	15.91	0.82	0.25	52	17.78	0.18	0.41
6	16.59	0.78	0.31	53	17.31	0.88	0.32
7	17.91	0.46	0.31	54	17.83	0.76	0.03
8	15.20	0.93	-0.02	55	14.28	0.49	0.02
9	17.17	0.95	0.23	56	17.75	0.93	0.14
10	15.89	0.75	0.20	57	18.01	0.86	0.38
11	13.36	0.22	-0.31	58	16.55	1.52	0.84
12	17.17	1.14	0.74	59	15.40	1.67	0.31
13	17.20	1.09	0.58	60	8.26	2.46	2.42
14	18.87	0.51	-0.22	61	13.80	0.48	-0.06
15	16.05	0.77	0.32	62	16.95	0.92	0.22
16	16.02	0.73	0.37	63	16.46	0.93	0.24
17	16.05	0.98	0.34	64	16.97	1.12	0.44
18	17.01	0.87	0.40	65	16.98	1.18	0.20
19	17.11	0.81	0.18	66	15.51	1.63	0.59
20	15.61	0.63	0.31	67	17.47	1.12	0.12
21	14.06	0.43	-0.03	68	16.69	1.21	0.43
22	17.24	1.01	0.11	69	9.25	0.32	-0.55
23	12.81	0.36	-0.28	70	14.88	1.01	0.16
24	17.41	0.88	0.62	71	17.71	0.74	0.17
25	14.22	0.42	0.08	72	15.68	0.72	0.40
26	13.87	0.25	0.24	73	16.93	0.70	0.24
27	13.08	0.39	-0.20	74	15.47	0.55	0.32
28	14.87	0.81	-0.15	75	17.23	0.98	0.34
29	14.51	0.36	0.23	76	13.84	0.36	0.14
30	12.73	0.35	-0.25	77	13.70	0.32	0.24
31	8.53	0.30	-0.56	78	18.44	0.44	0.61
32	14.50	1.03	-0.04	79	16.63	0.91	0.30
33	16.71	0.71	0.08	80	12.21	0.35	-0.33
34	15.45	1.10	-0.08	81	16.83	0.78	0.24
35	15.10	0.61	-0.33	82	13.47	0.78	0.30
36	9.38	0.30	-0.54	83	13.98	1.05	0.09
37	16.34	0.57	-0.23	84	16.52	1.05	0.36
38	13.97	0.98	0.14	85	18.22	0.73	0.56
39	14.18	0.42	0.08	86	18.39	0.47	0.94
40	17.36	0.72	0.12	87	17.79	1.08	0.46
41	16.56	0.80	0.32	88	17.58	0.76	0.28
42	13.16	0.40	-0.03	89	13.65	0.34	0.07
43	14.82	0.52	0.19	90	14.92	-0.56	0.21
44	16.74	0.89	0.24	91	15.19	1.04	0.29
45	16.17	0.94	0.10	92	18.00	0.73	0.60
46	9.08	0.20	-0.57	93	16.97	0.80	0.25
47	15.59	0.35	0.52	94	15.51	1.43	0.43

TABLE 10 (Continued)

No.	V	B-V	U-B	No.	V	B-V	U-B
95	18.68	0.20	0.32	144	16.82	0.79	0.35
96	18.85	0.08	0.44	145	16.56	0.99	0.41
97	17.13	0.79	0.31	146	17.03	0.87	0.21
98	17.06	0.99	0.36	147	13.45	0.42	-0.13
99	14.92	0.48	0.26	148	15.56	1.25	0.45
100	17.45	0.96	0.42	149	16.04	0.81	0.34
101	13.73	0.79	0.11	150	15.71	0.65	0.49
102	16.58	1.04	0.21	151	15.48	0.68	0.43
103	16.59	0.77	0.41	152	14.06	0.47	0.19
104	16.08	0.78	0.39	153	16.71	0.81	0.30
105	16.03	0.84	0.33	154	15.13	0.50	0.24
106	15.43	0.84	0.59	155	13.14	0.40	-0.25
107	12.12	0.47	-0.29	156	14.64	0.47	0.09
108	13.17	0.52	-0.25	157	14.78	1.06	0.37
109	13.58	0.39	0.17	158	18.36	0.55	0.36
110	14.09	0.34	0.23	159	15.23	1.10	0.37
111	14.00	0.82	0.22	160	15.26	1.65	1.02
112	17.19	1.22	0.78	161	15.21	0.61	0.32
113	12.69	0.90	0.34	162	15.37	0.70	0.33
114	17.86	0.58	0.51	163	15.88	0.61	0.48
115	18.14	0.58	0.47	164	16.74	0.72	0.39
116	15.85	0.82	0.37	165	9.86	0.40	-0.62
117	16.48	1.02	0.41	166	15.54	0.53	0.37
118	18.25	0.44	0.24	167	15.33	0.60	0.22
119	13.95	0.82	0.21	168	11.57	0.32	-0.43
120	12.29	1.11	0.19	169	17.51	0.45	0.21
121	15.64	0.86	0.42	170	16.26	0.86	0.23
122	16.00	0.81	0.31	171	11.08	0.42	-0.43
123	13.05	0.28	-0.19	172	16.90	0.84	0.00
124	13.64	0.59	0.23	172b	10.36	0.49	-0.40
125	15.77	1.20	0.03	173	15.76	0.79	0.24
126	14.68	0.43	0.08	174	10.69	0.19	-0.45
127	15.87	0.56	0.60	175	16.02	0.86	0.28
128	17.46	0.92	0.49	176	17.05	0.88	0.00
129	16.02	0.86	0.56	177	13.90	0.43	0.17
130	16.11	1.61	0.92	178	12.50	0.34	-0.35
131	17.34	0.62	-0.40	179	13.86	0.48	0.04
132	10.38	0.44	-0.60	180	13.61	0.38	0.03
133	17.57	0.58	0.34	181	15.61	0.89	0.32
134	15.87	0.64	0.50	182	13.33	0.50	-0.11
135	15.29	0.98	0.43	183	17.39	0.62	-0.03
136	14.33	0.37	0.01	184	17.89	0.57	0.23
137	17.37	0.41	0.38	185	11.56	0.34	-0.34
138	15.32	1.16	1.35	186	9.36	0.33	-0.55
139	17.53	0.79	0.42	187	9.90	0.32	-0.56
140	17.86	0.65	0.33	188	13.63	0.56	-0.07
141	13.34	0.81	0.10	189	12.04	2.87	0.60
142	15.95	1.17	0.45	190	8.05	0.34	-0.55
143	17.72	0.78	0.53	191	14.61	0.50	0.05

TABLE 10 (Continued)

No.	V	B-V	U-B	No.	V	B-V	U-B
192	14.99	0.71	0.35	241	17.97	0.72	0.12
193	17.70	0.67	0.02	242	16.51	0.89	0.11
194	15.23	0.64	0.43	243	15.28	0.58	0.34
195	17.25	0.96	0.33	244	17.73	0.79	0.33
196	17.43	0.74	0.49	245	12.67	0.36	-0.25
197	18.12	0.46	0.51	246	17.35	0.61	0.06
198	14.34	0.49	0.14	247	17.77	0.57	0.24
199	16.82	0.92	0.32	248	11.11	0.25	-0.54
200	15.13	0.47	0.21	249	15.08	0.57	0.16
201	15.03	1.71	1.30	250	13.19	0.39	-0.19
202	17.62	0.75	0.98	251	12.71	0.41	-0.10
203	14.93	0.95	0.29	252	13.58	0.43	0.02
204	18.58	0.28	0.57	253	16.87	0.84	0.49
205	13.72	0.32	-0.05	254	16.31	0.84	0.24
206	17.13	0.80	0.35	255	18.43	-0.03	0.75
207	16.05	0.79	0.55	256	15.98	0.76	0.27
208	15.12	0.47	0.23	257	15.89	0.81	0.18
209	11.86	0.42	-0.36	258	15.75	0.67	0.32
210	18.13	0.59	0.23	259	15.57	0.65	0.37
211	18.07	0.59	0.33	260	17.56	0.84	0.79
212	17.31	1.08	0.32	261	16.93	0.87	0.26
213	16.94	1.02	0.21	262	14.74	0.33	0.08
214	11.38	0.27	-0.49	263	15.23	0.48	0.22
215	16.89	0.92	0.27	264	17.49	0.97	0.43
216	16.44	0.88	0.27	265	17.54	0.90	0.15
217	16.24	0.87	0.23	266	15.44	0.86	0.35
218	17.38	0.74	0.35	267	17.10	0.85	0.40
219	13.36	0.42	-0.13	268	16.90	0.81	0.79
220	15.99	0.69	0.39	269	15.16	0.62	0.37
221	16.23	0.87	0.30	270	15.93	0.73	0.41
222	12.21	0.33	-0.38	271	15.94	0.77	0.52
223	16.08	0.72	0.37	272	17.57	0.91	0.37
224	17.11	1.09	0.27	273	16.51	0.78	0.23
225	10.83	0.30	-0.49	274	17.84	0.80	0.63
226	13.34	0.41	0.05	275	17.83	0.91	0.06
227	9.45	0.32	-0.65	276	10.92	0.33	-0.25
228	14.51	0.58	0.00	277	13.91	0.62	0.18
229	14.61	0.67	-0.11	278	15.62	0.86	0.22
230	16.94	0.68	0.35	279	17.54	0.74	0.15
231	14.35	0.47	0.29	280	15.44	0.53	0.36
232	16.56	0.77	0.56	281	17.14	0.82	0.43
232b	15.64	0.72	0.44	282	12.98	0.41	-0.15
233	16.75	0.94	0.42	283	17.55	0.88	0.45
234	18.04	0.43	0.53	284	16.40	0.87	0.20
235	17.89	0.72	0.40	285	16.66	0.65	0.41
236	17.51	0.76	0.71	286	14.46	0.51	0.06
237	15.73	0.73	0.44	287	17.92	0.35	0.64
238	11.84	0.44	-0.01	288	16.20	0.77	0.16
239	17.56	0.87	-0.21	289	13.37	0.25	-0.15
240	14.26	0.41	-0.03	290	16.70	0.99	0.30

TABLE 10 (Continued)

No.	V	B-V	U-B	No.	V	B-V	U-B
291	14.06	0.39	0.01	297	15.26	0.56	0.30
292	15.28	0.63	0.30	298	15.10	0.56	0.29
293	18.29	2.02	1.49	299	17.95	0.99	0.51
294	16.23	1.42	0.54	300	17.90	0.76	0.40
295	16.81	1.03	0.30	301	18.27	0.75	0.15
296	15.51	0.71	0.35				

TABLE 11

CATALOGUE OF PHOTOGRAPHIC OBSERVATIONS

Plate No.	Emulsion	Filter	Exposure	Seeing-Remarks
S-3384-W	103a-D	GG11	60m	2; poor
S-3385-W	103a-O	GG13	30m	2-3; poor
S-3386-W	103a-O	RG8	120m	3; error
S-3387-W	103a-O	GG13	30m	2-3; poor
S-3388-W	103a-D	GG11	60m	2-3; poor
S-3389-W	103a-O	GG13	30m	2-3; poor
S-3390-W	103a-D	GG11	60m	2-3; poor
S-3391-W	103a-O	GG13	30m	3; good
S-3392-W	103a-D	GG11	60m	3; good
S-3393-W	103a-O	GG13	30m	3; good
S-3394-W	103a-D	GG11	60m	3; good
S-3395-W	103a-O	UG2	120m	3; good
S-3396-W	103a-D	GG11	60m	3; good
S-3397-W	103a-O	UG2	120m	3; good
S-3398-W	103a-O	GG13	30m	3; good
S-3399-W	103a-D	GG11	60m	2-3; good
S-3400-W	103a-O	UG2	120m	3; good
S-3504-W	103a-D	GG11	1m	2-3; good
S-3505-W	103a-O	GG13	30s	2-3; good
S-3506-W	103a-O	Cor-5840	2m	2-3; good
S-3507-W	103a-D	GG11	1m	2-3; good
S-3508-W	103a-O	GG13	30s	2-3; good
S-3509-W	103a-O	Cor-5840	2m	2-3; good
S-3510-W	103a-D	GG11	1m	3; good
S-3511-W	103a-O	GG13	30s	3; good
S-3512-W	103a-O	Cor-5840	2m	3; good
S-3513-W	103a-D	GG11	2m	3; good
S-3514-W	103a-O	GG13	1m	3; good
S-3515-W	103a-O	Cor-5840	4m	3; good
S-3516-W	103a-D	GG11	2m	3; good
S-3517-W	103a-O	GG13	1m	3; good
S-3518-W	103a-O	Cor-5840	4m	3; good
S-3519-W	103a-D	GG11	2m	3; good
S-3520-W	103a-O	GG13	1m	3; good
S-3521-W	103a-O	Cor-5840	4m	3; good
S-3522-W	103a-D	GG11	30s	2; good
S-3523-W	103a-O	GG13	15s	2; good
S-3524-W	103a-O	Cor-5840	1m	2; good
S-3525-W	103a-D	GG11	30s	2; good
S-3526-W	103a-O	GG13	15s	2; good
S-3527-W	103a-O	Cor-5840	1m	2; good

TABLE 11 (Continued)

Plate No.	Emulsion	Filter	Exposure	Seeing-Remarks
S-3528-W	103a-D	GG11	4^m	2; good
S-3529-W	103a-O	GG13	2^m	2; good
S-3530-W	103a-O	Cor-5840	8^m	2; good
S-3531-W	103a-D	GG11	4^m	3; good, broken clouds
S-3532-W	103a-O	GG13	2^m	3; good, broken clouds
S-3533-W	103a-O	Cor-5840	8^m	3; good, broken clouds
S-3534-W	103a-D	GG11	4^m	2; good
S-3535-W	103a-O	GG13	2^m	2; good
S-3536-W	103a-O	Cor-5840	8^m	1-2; good
S-3537-W	103a-D	GG11	8^m	1-2; good
S-3538-W	103a-O	GG13	4^m	1-2; good
S-3539-W	103a-O	Cor-5840	16^m	1-2; good

TABLE 12

PHOTOELECTRIC SEQUENCE FOR PHOTOGRAPHIC INTERPOLATION - BRIGHT END

h No.	Oo No.	V	B	U	chi No.	Oo No.	V	B	U
1	1057	6.55	7.02	6.65	190	2227	8.05	8.39	7.84
	1162	6.66	7.17	6.72	31	2296	8.53	8.83	8.27
	662	8.18	8.48	7.89	46	2299	9.08	9.37	8.80
	717	9.28	9.58	9.02	69	2371	9.25	9.57	9.02
259	843	9.32	9.63	9.10	186	2235	9.36	9.69	9.14
	1078	9.75	10.09	9.60	36	2311	9.38	9.68	9.14
82	1015	10.57	10.85	10.75	227	2088	9.45	9.77	9.12
55	978	10.59	10.97	10.53	1	2284	9.66	10.06	9.47
	1187	10.82	11.21	10.81	165	2165	9.86	10.26	9.64
86	950	11.29	11.65	11.25	187	2246	9.90	10.22	9.66
298	869	11.96	12.33	12.13	132	2262	10.38	10.82	10.22
178	800	12.25	12.61	12.33	276	2185	10.92	11.25	11.00
	1000	13.23	13.64	13.66	248	2232	11.11	11.36	10.82
288	982	13.87	14.30	14.43	214	2139	11.38	11.65	11.16
280	935	14.02	14.47	14.48	49	2330	11.42	11.66	11.27
107	837	14.08	14.57	14.73	185	2251	11.56	11.90	11.56
	1040	14.50	15.18	15.58	168	2196	11.57	11.89	11.46
	974	15.43	16.13	16.91	222	2133	12.21	12.54	12.16
103	855	15.76	16.51		245	2200	12.67	13.03	12.78
					251	2253	12.71	13.12	13.02
					23	2349	12.81	13.17	12.89
					250	2269	13.19	13.58	13.39
					219	2167	13.36	13.77	13.64
					147	2194	13.45	13.87	13.74
					252	2241	13.58	14.01	14.03
					39	2270	14.18	14.60	14.68
					198	2147	14.34	14.83	14.97
					191	2203	14.61	15.11	15.16
					203	2134	14.93	15.88	16.17
					192	2188	14.99	15.70	16.05
					298	2250	15.10	15.66	15.95
					194	2170	15.23	15.87	16.30
					167	2155	15.33	15.93	16.15

INTEGRATION TABLES FOR ABSORPTION AND REDDENING

	j	λ_j	v_j	R_j	S_{λ_j}	κ_{λ_j}	TABLE 13 HD214680 $F_\lambda(1-\eta_\lambda)$	TABLE 14 δ Tauri $F_\lambda(1-\eta_\lambda)$
U	0	2982	0.0338	0.0857	0.375	0.671	1.74	0.221
	1	3137	0.1694	0.1804	1.84	0.654	1.669	0.282
	2	3378	0.3807	0.2340	3.61	0.634	1.542	0.423
	3	3651	0.6193	0.2340	4.035	0.606	1.379	0.641
	4	3893	0.8306	0.1804	1.46	0.573	1.189	0.553
	5	4047	0.9662	0.0857	0.105	0.554	1.054	1.147
B	0	3703	0.0338	0.0857	0.13	0.599	1.341	0.666
	1	3952	0.1694	0.1804	2.79	0.564	1.139	1.051
	2	4340	0.3807	0.2340	3.93	0.519	0.910	1.426
	3	4778	0.6193	0.2340	2.40	0.462	0.679	2.088
	4	5164	0.8306	0.1804	0.92	0.412	0.519	1.971
	5	5413	0.9662	0.0857	0.115	0.388	0.452	2.050
V	0	4915	0.0338	0.0857	0.37	0.443	0.609	2.037
	1	5164	0.1694	0.1804	2.86	0.413	0.518	1.970
	2	5552	0.3807	0.2340	2.86	0.375	0.421	2.177
	3	5991	0.6193	0.2340	1.305	0.334	0.335	1.668
	4	6379	0.8306	0.1804	0.28	0.300	0.287	1.409
	5	6627	0.9662	0.0857	0.05	0.280	0.254	1.280

TABLE 15

INTEGRATION RESULTS FOR ABSORPTION AND REDDENING

HD 214680, Sp/O9, $(B-V)_o$/-0.35

$\rho\ell$	1	3	6	9	12
$E_{(U-B)}$	0.115	0.349	0.712	1.091	1.486
$E_{(B-V)}$	0.144	0.428	0.847	1.255	1.652
A_V	0.396	1.225	2.460	3.684	4.898

THE SUN (CENTER OF DISK), Sp/GOV, $(B-V)_o$/0.60

$\rho\ell$	1	3	6	9	12
$E_{(U-B)}$	0.137	0.383	0.783	1.192	1.611
$E_{(B-V)}$	0.130	0.391	0.761	1.125	1.496
A_V	0.394	1.218	2.444	3.660	4.852

δ TAURI, Sp/K0III, $(B-V)_o$/0.98

$\rho\ell$	1	3	6	9	12
$E_{(U-B)}$	0.130	0.394	0.805	1.230	1.672
$E_{(B-V)}$	0.124	0.369	0.727	1.074	1.411
A_V	0.392	1.213	2.437	3.651	4.854

TABLE 16

SUPERGIANTS AND FAINT NEIGHBORS OF THE GENERAL REGION

No.	M_V	V_O	$(B-V)_O$	$(U-B)_O$
1	-4.39	7.41	1.87	2.44
I	0.63	12.43	0.50	0.02
2	1.42	13.22	0.62	0.16
2	-4.90	6.90	-0.33	-1.19
I	-1.61	10.19	1.02	0.89
2	-2.00	9.80	-0.07	-0.22
3	-8.00	3.80	0.00	-0.47
I	-2.94	8.86	-0.19	-0.67
2	-3.38	8.42	1.28	1.28
3	-3.89	7.91	0.88	0.66
4	-1.44	10.36	-0.08	-0.26
4	-5.20	6.60	1.91	2.13
I	0.67	12.47	0.01	0.00
2	2.67	14.47	1.21	1.19
5	-6.76	5.04	-0.13	-0.73
I	1.58	13.38	0.50	0.02
2	-0.64	11.16	-0.15	-0.53
3	1.65	13.45	0.30	0.08
4	0.47	12.27	0.34	0.04
6	-6.02	5.78	-0.17	-0.98
I	-1.47	10.33	-0.23	-0.82
2	0.30	12.20	0.01	0.01
3	1.09	12.89	-0.05	-0.16
7	-6.83	4.97	0.10	-0.16
I	-2.31	9.49	0.37	0.02
2	-3.68	8.12	-0.25	-0.88
3	-3.67	8.13	-0.06	-0.19
4	-2.97	8.83	-0.14	-0.46
5	1.87	13.67	1.35	1.36
8	-5.28	6.52	-0.17	-0.93
I	-1.38	10.42	-0.05	-0.15
2	-0.15	11.65	-0.12	-0.41
9	-4.43	7.37	1.87	2.28
I	1.12	12.92	-0.35	-1.26
2	0.92	12.72	0.21	0.13
3	-1.92	9.88	-0.22	-0.79
4	-0.73	11.07	-0.15	-0.52
5	-1.31	10.49	-0.18	-0.64
10	-6.42	5.38	0.00	-0.33
I	-0.09	11.71	-0.10	-0.32
2	-1.66	10.14	-0.03	-0.09
3	-2.58	9.22	0.81	0.45
4	2.48	14.28	1.58	1.44

TABLE 16 (Continued)

No.	M_V	V_o	$(B-V)_o$	$(U-B)_o$
11	-5.65	6.15	-0.20	-0.95
1	-0.92	10.88	-0.18	-0.63
2	-0.76	11.04	-0.19	-0.69
12	-6.68	5.12	-0.19	-0.98
1	-1.16	10.64	-0.12	-0.42
2	2.19	13.99	-0.05	-0.14
13	-5.31	6.49	-0.18	-0.88
1	-0.49	11.31	-0.16	-0.55
2	-0.99	10.81	-0.21	-0.72
14	-2.78	9.02	1.95	2.15
1	0.78	12.58	0.35	0.03
2	2.25	14.05	0.66	0.20
3	0.38	12.18	0.23	-0.13
4	1.70	13.50	0.30	0.08
15	-5.09	6.71	-0.19	-0.95
1	0.01	11.81	0.01	0.00
2	-0.28	11.52	-0.14	-0.49
16	-4.94	6.86	1.85	1.98
Oo899	-1.15	10.65	1.27	1.26
1	0.82	12.62	-0.01	-0.04
2	-0.65	11.15	-0.12	-0.40
3	0.98	12.78	-0.04	-0.11
Oo1211	-1.12	10.68	-0.04	-0.11
17	-7.05	4.75	-0.14	-0.79
1	-0.68	11.12	-0.12	-0.39
2	-2.36	9.44	-0.23	-0.82
3	-2.21	9.59	-0.23	-0.82
18	-7.03	4.77	-0.13	-0.90
1	0.88	12.68	-0.15	-0.51
2	0.07	11.87	-0.07	-0.23
3	-0.21	11.59	-0.04	-0.13
Oo1166	-0.74	11.06	-0.16	-0.56
Oo1202	-1.50	10.30	-0.18	-0.64
19	-4.68	7.12	1.89	2.27
1	-0.92	10.88	0.01	0.01
2	-1.01	10.79	-0.16	-0.54
20	-5.14	6.66	1.98	2.38
1	-0.45	11.35	0.39	0.01
2	0.13	11.93	0.19	0.13
21	-5.44	6.36	1.82	2.01
1	0.60	12.40	0.39	0.01
2	2.19	13.99	0.24	0.12
3	0.72	12.52	0.84	0.52
22	-6.21	5.59	-0.09	-0.60
1	1.09	12.89	-0.01	-0.03
2	1.60	13.40	0.88	0.62
3	-2.65	9.15	-0.01	-0.03

TABLE 16 (Continued)

No.	M_V	V_o	$(B-V)_o$	$(U-B)_o$
23	-4.97	6.83	1.97	2.26
I	1.31	13.11	0.24	0.12
2	1.37	13.17	0.50	-0.05
24	-5.67	6.13	1.80	2.21
I	0.73	12.53	0.29	0.08
2	1.74	13.54	1.79	1.53
25	-7.41	4.39	-0.08	-0.45
I	-1.56	10.24	-0.17	-0.61
2	-0.19	11.61	-0.07	-0.23
3	-1.42	10.38	-0.21	-0.75
26	-5.10	6.70	-0.12	-0.87
Oo2203	2.81	14.61	0.50	0.05
Oo2188	1.98	13.78	0.32	0.05
1	0.13	11.93	-0.13	-0.46
2	0.66	12.46	-0.08	-0.24
27	-5.23	6.57	1.84	2.05
I	-0.02	11.78	0.00	-0.01
2	0.30	12.10	0.31	0.06
3	1.30	13.10	0.24	0.12
28	-7.38	4.42	0.12	-0.07
I	-2.55	9.25	-0.08	-0.27
2	-0.54	11.26	0.40	0.00
3	-2.29	9.51	0.85	0.54
4	-1.17	10.63	0.29	0.08
29	-5.21	6.59	1.83	1.79
I	0.16	11.96	-0.10	-0.32
2	1.37	13.17	0.72	0.32
Oo2349	-0.64	11.16	-0.19	-0.65
30	-4.46	7.34	2.05	2.09
I	1.45	13.25	0.01	0.00
2	0.13	11.93	-0.04	-0.12
31	-6.21	5.59	0.11	-0.34
I	0.34	12.14	-0.11	-0.37
2	-1.06	10.74	-0.20	-0.69
3	1.65	13.45	0.70	0.29
32	-6.94	4.86	-0.11	-0.61
I	0.22	12.02	-0.10	-0.33
2	0.93	12.73	0.36	0.03
3	-0.12	11.68	-0.13	-0.45
33	-5.12	6.68	1.79	1.93
I	1.25	13.05	0.39	0.01
2	2.34	14.14	1.68	1.68
34	-5.52	6.28	1.70	1.83
I	-1.26	10.54	-0.20	-0.69
2	-0.68	11.12	-0.10	-0.33

TABLE 16 (Continued)

No.	M_V	V_o	$(B-V)_o$	$(U-B)_o$
35	-6.98	4.82	-0.18	-0.96
1	-2.71	9.09	0.01	0.01
2	-2.83	8.97	-0.11	-0.35
36	-5.64	6.16	1.67	1.92
1	0.35	12.15	-0.08	-0.27
2	-2.57	9.23	-0.25	-0.89
3	-1.92	9.88	-0.22	-0.79
4	1.79	13.59	0.50	0.00
37	-5.74	6.06	-0.01	-0.40
1	1.04	12.84	0.50	-0.02
2	-1.13	10.67	-0.01	-0.03
38	-7.17	4.63	-0.15	-0.91
1	-1.27	10.53	-0.16	-0.55
2	3.98	15.78	0.94	0.76
3	-0.18	11.62	-0.17	-0.60
4	-1.03	10.77	-0.08	-0.27
39	-3.95	7.85	2.17	3.08
1	-0.09	11.71	0.01	0.01
2	-0.80	11.00	0.56	0.09
3	-1.62	10.18	0.28	-0.01
40	-6.59	5.21	0.10	-0.08
1	-0.38	11.42	-0.15	-0.51
2	2.90	14.70	1.75	1.90
3	2.80	14.60	1.79	2.43
4	1.12	12.92	-0.06	-0.17
5	-0.51	11.29	-0.13	-0.46
41	-6.71	5.09	-0.34	-1.15
1	-0.55	11.25	-0.09	-0.29
2	-0.04	11.76	0.75	0.39
42	-7.18	4.62	-0.04	-0.61
1	-1.31	10.49	-0.17	-0.60
2	0.82	12.62	-0.04	-0.11
3	-0.63	11.17	-0.08	-0.26
43	-6.39	5.41	-0.06	-0.49
1	-0.84	10.96	-0.15	-0.52
2	0.76	12.56	-0.04	-0.12
44	-6.45	5.35	-0.24	-0.92
1	-0.96	10.84	-0.19	-0.65
2	-0.71	11.09	-0.16	-0.56
45	-6.73	5.07	1.64	2.19
1	-1.14	10.66	-0.11	-0.35
2	-1.84	9.96	-0.09	-0.31
46	-5.79	6.01	-0.21	-0.89
1	-1.74	10.06	-0.11	-0.37
2	-0.56	11.24	-0.13	-0.45
3	-0.64	11.16	1.18	1.09

TABLE 16 (Continued)

No.	M_V	V_o	$(B-V)_o$	$(U-B)_o$
47	-6.66	5.14	0.05	-0.29
1	0.09	11.89	0.01	0.00
2	-1.37	10.43	0.23	0.12
3	-1.64	10.16	-0.13	-0.43
48	-6.88	4.92	-0.04	-0.53
1	-0.37	11.43	-0.14	-0.49
2	-2.77	9.03	-0.24	-0.85
49	-5.40	6.40	-0.19	-1.02
1	-0.89	10.91	-0.17	-0.60
2	-0.59	11.21	-0.17	-0.57
50	-5.99	5.81	0.04	-0.52
1	-1.84	9.96	-0.13	-0.43
2	-0.38	11.42	0.34	0.04
3	0.39	12.19	-0.13	-0.43
51	-7.74	4.06	0.16	-0.07

TABLE 17

O STARS AND FAINT NEIGHBORS OF THE GENERAL REGION

No.	M_V	V_o	$(B-V)_o$	$(U-B)_o$
1	-3.98	7.82	-0.50	-1.21
1 extrin.	0.16	11.96	0.59	-0.75
2	-0.51	11.29	0.93	0.73
2	-4.97	6.83	-0.42	-1.23
1	1.68	13.48	-0.06	-0.19
2	-2.75	9.05	-0.16	-0.56
3	-5.25	6.55	-0.51	-1.32
1	-2.64	9.16	-0.10	-0.33
4	-4.72	7.08	-0.25	-1.09
1	-2.97	8.83	-0.10	-0.32
2	-1.88	9.92	-0.03	-0.08
3	-0.25	11.55	-0.12	-0.41
4	-0.58	11.22	0.24	0.12
5	-6.31	5.49	-0.40	-1.26
1	-0.33	11.47	0.79	0.43
2	-1.74	10.06	-0.26	-0.90
6	-4.50	7.30	-0.36	-1.15
1	-1.21	10.59	-0.06	-0.18
2	-1.59	10.21	-0.15	-0.52
2a	-1.04	10.76	-0.09	-0.30
7	-4.78	7.02	-0.43	-1.26
3	-2.94	8.86	-0.30	-1.17
4	-2.21	9.59	-0.26	-0.93
8	-6.55	5.25	-0.36	-1.23
5	-1.53	10.27	-0.14	-1.08
6	-2.81	8.99	-0.28	-1.00
9	-6.48	5.32	-0.25	-1.13
1	-2.48	9.32	-0.27	-0.94
2	0.79	12.59	0.44	-0.07
10	-5.96	5.84	-0.48	-1.31
1	-1.53	10.27	-0.25	-0.89
2	-0.85	10.95	-0.16	-0.57
11	-4.80	7.00	-0.33	-1.16
1	-0.08	11.72	-0.12	-0.41
2	0.93	12.73	-0.07	-0.21
3	0.10	11.90	-0.06	-0.20
12	-6.94	4.86	-0.34	-1.12
1	-2.66	9.14	-0.27	-0.95
2	-2.73	9.07	-0.30	-1.06
13	-5.60	6.20	-0.38	-1.21
1	-0.43	11.37	-0.05	-0.17
2	-2.03	13.83	0.64	0.95
3	0.86	12.66	0.50	0.01

TABLE 17 (Continued)

No.	M_V	V_o	$(B-V)_o$	$(U-B)_o$
14	-5.43	6.37	-0.71	-1.49
1	-3.45	8.35	-0.13	-0.45
2	-2.10	9.70	0.25	0.11
15	-5.12	6.68	-0.39	-1.22
1	-0.70	11.10	0.02	0.02
2	-1.85	9.95	-0.08	-0.26
16	-6.58	5.22	-0.23	-1.11
1	-1.57	10.23	-0.11	-0.38
2	-0.92	10.88	-0.04	-0.11
17	-5.36	6.44	-0.31	-1.15
3	-1.50	10.30	-0.22	-0.79
4	-1.00	10.80	-0.05	-0.15
18	-6.24	5.56	-0.35	-1.18
1	-3.13	8.67	-0.27	-0.95
2	-3.06	8.74	-0.34	-1.20
3	-0.97	10.83	-0.01	-0.03
19	-4.66	7.14	-0.42	-1.21
1	-3.04	8.76	0.97	0.81
2	-2.56	9.24	-0.11	-0.37
20	-5.40	6.40	-0.42	-1.21
1	-1.27	10.53	-0.17	-0.60
2	-0.56	11.24	-0.18	-0.62
21	-4.63	7.17	-0.38	-1.20
1	-2.23	9.57	-0.02	-0.06
2	-1.82	9.98	-0.11	-0.35

TABLE 18

GIANTS-SUBGIANTS AND FAINT NEIGHBORS
OF THE GENERAL REGION

No.	M_V	V_o	$(B-V)_o$	$(U-B)_o$
1	-4.56	7.24	-0.20	-0.79
I	-0.73	11.07	-0.12	-0.41
2	0.25	12.05	0.05	0.06
2	-4.23	7.57	-0.26	-1.00
I	0.20	12.00	-0.02	-0.06
2	1.48	13.28	-0.04	-0.13
3	-4.71	7.09	-0.30	-1.04
I	1.09	12.89	-0.06	-0.18
2	1.36	13.16	0.32	0.05
4	-5.47	6.33	-0.37	-1.17
I	1.27	13.07	-0.21	-0.75
2	0.49	12.29	0.44	0.00
3	-0.18	11.62	0.38	0.02
4	0.95	12.75	0.89	0.64
5	-5.91	5.89	-0.75	-1.43
I	0.81	12.61	-0.20	-0.72
2	1.15	12.95	-0.07	-0.21
3	0.56	12.36	-0.07	-0.22
6	-4.42	7.38	-0.23	-0.94
I	-0.87	10.93	-0.22	-0.78
2	-0.47	11.33	-0.12	-0.40
7	-4.62	7.18	-0.26	-1.12
I	-0.65	11.15	-0.20	-0.72
2	-1.07	10.73	-0.20	-0.72
8	-4.76	7.04	-0.22	-0.96
I	-0.45	11.35	-0.19	-0.67
2	0.98	12.78	-0.21	-0.73
9	-2.87	8.93	-0.26	-0.86
I	0.07	11.87	-0.07	-0.23
2	-0.21	11.59	-0.04	-0.13
Ool166	-0.74	11.06	-0.16	-0.56
Ool202	-1.50	10.30	-0.18	-0.64
10	-4.65	7.15	-0.31	-0.99
I extrin.	0.02	11.82	-0.09	-1.25
2	0.32	12.12	1.95	1.89
epsilon	1.94	13.73	0.77	0.39
11	-5.33	6.47	-0.53	-1.27
I	0.14	11.94	-0.17	-0.60
2	-1.96	9.84	-0.12	-0.41

TABLE 18 (Continued)

No.	M_V	V_o	$(B-V)_o$	$(U-B)_o$
12	-5.63	6.17	-0.51	-1.12
1	-0.87	10.93	-0.11	-0.37
2	0.52	12.32	0.49	-0.10
13	-4.62	7.18	-0.28	-1.08
1	-1.01	12.81	-0.07	-0.21
2	-2.01	9.79	-0.04	-0.12
14	-3.37	8.43	-0.18	-0.91
1	0.14	11.94	-0.15	-0.51
2	2.57	14.37	0.44	0.00
15	-4.29	7.51	-0.23	-0.94
1	1.21	13.01	-0.01	-0.04
2	0.12	11.92	-0.14	-0.49
16	-4.94	6.86	-0.51	-1.27
1	0.74	12.54	-0.04	-0.09
2	1.39	13.19	0.36	0.46
3	-1.94	9.86	0.87	0.59
17	-6.52	5.28	-0.29	-1.05
1	-0.70	11.10	-0.14	-0.47
2	1.01	12.81	0.17	0.13
3	1.04	12.85	-0.21	-0.73

TABLE 19

STARS OF THE EXTREME NUCLEUS OF h PERSEI

No.	M_V	V_o	$(B-V)_o$	No.	M_V	V_o	$(B-V)_o$
1	-7.25	4.75	-0.14	47		15.20	0.09
2	-2.78	9.22	-0.09	48	1.90	13.90	0.04
3	1.73	13.73	0.32	49	2.35	14.35	0.23
4	0.38	12.38	0.50	50	1.03	13.03	0.02
5	-0.10	11.90	-0.04	51		15.71	0.13
6	-0.12	11.88	(-0.11)	52	0.98	12.98	0.26
7	-1.15	10.85	(-0.16)	53	3.02	15.02	0.07
8	1.76	13.76	0.32	54	2.28	14.28	0.11
9	-3.05	8.95	-0.07	55	-3.24	8.76	(-0.25)
10	-0.41	11.59	(-0.11)	56		15.77	0.09
11	-3.47	8.53	-0.20	57	3.14	15.14	0.26
12	-0.01	11.99	(-0.17)	58	1.67	13.67	(-0.12)
13	3.00	15.00	0.25	59	0.23	12.23	0.20
14	1.85	13.85	0.26	60	-3.15	8.85	(-0.21)
15	1.48	13.48	0.24	61	-1.45	10.57	-0.16
16	-0.45	11.55	(-0.08)	62		15.77	0.25
17	0.28	12.28	0.30	63	0.81	12.81	-0.03
18	0.99	12.99	0.83	64		16.14	0.10
19	0.79	12.79	0.73	65	1.82	13.82	0.03
20	0.06	12.06	-0.15	66	-1.29	10.71	(-0.17)
21	-3.58	8.42	(-0.31)	67		15.96	0.40
22	-4.28	7.72	-0.03	68	3.18	15.18	0.11
23	-4.04	7.96	-0.02	69	2.16	14.16	0.08
24	-2.24	9.76	-0.21	70	0.71	12.71	(0.00)
25	-2.37	9.63	-0.12	71	3.07	15.07	0.21
25b	0.45	12.45	-0.07	72	2.17	14.17	0.05
26	2.02	14.02	0.30	73	-0.90	11.10	(-0.22)
27	2.26	14.26	0.09	74	-0.88	11.12	(-0.22)
28	-3.41	8.59	-0.31	75	-1.09	10.91	(-0.05)
29	0.65	12.65	0.14	76		15.49	0.12
30	0.95	12.95	0.08	77		15.86	0.34
31	-1.41	10.59	(-0.19)	78	3.19	15.19	0.25
32	1.94	13.94	0.25	79	1.68	13.68	0.04
33	-2.51	9.49	(-0.32)	79b	1.60	13.60	-0.01
34	-3.46	8.54	(-0.27)	80		16.06	0.49
35	1.55	13.55	0.20	81	0.21	12.21	(-0.10)
36	1.97	13.97	0.17	82	-2.60	9.40	(-0.11)
37	-0.13	11.87	(0.49)	83	1.06	13.06	(0.01)
38		15.20	0.15	84	1.67	13.67	0.14
39	-0.03	11.97	(-0.17)	85	2.30	14.30	0.19
40	2.62	14.62	0.14	86	-2.45	9.55	(-0.23)
41	-0.39	11.61	(-0.09)	87		15.69	0.21
42	1.42	13.42	0.11	88	2.36	14.36	(0.50)
43	2.07	14.07	0.19	89	2.77	14.77	0.56
44	-0.38	11.62	-0.03	90		16.01	0.21
45	1.59	13.59	0.30	91		16.20	0.16
46	2.57	14.57	0.11	92	1.16	13.16	-0.10

TABLE 19 (Continued)

No.	M_V	V_o	$(B-V)_o$	No.	M_V	V_o	$(B-V)_o$
93	3.16	15.16	0.32	142	2.45	14.45	0.81
94		16.01	0.36	143	0.72	12.72	(-0.06)
95		15.59	0.00	144		16.23	0.09
96	0.81	12.81	(-0.03)	145		16.01	0.26
97	-1.23	10.77	(-0.23)	146	0.57	12.57	(-0.07)
98	0.70	12.70	(-0.01)	147		16.58	0.22
99	0.97	12.97	0.36	148	3.39	15.39	0.34
100	2.08	14.08	0.35	149	2.23	14.23	0.43
101		15.70	0.38	150		16.34	-0.04
102	3.32	15.32	0.38	151		15.94	0.59
103	2.29	14.29	(0.28)	152		16.18	0.31
104		16.21	0.29	153		16.33	0.23
105	3.21	15.21	0.63	154		15.68	0.80
106		16.49	0.05	155		16.43	0.07
107	0.43	12.43	(-0.07)	156		15.68	0.23
108	1.43	13.43	0.02	157		16.34	0.05
109	2.83	14.83	0.12	158		15.71	0.38
110	3.31	15.31	0.36	159		16.16	0.32
111	1.59	13.59	0.06	160		16.68	-0.19
112	0.77	12.77	(-0.04)	161		15.55	0.16
113		15.86	0.15	162	1.74	13.74	0.22
114	1.43	13.43	0.42	163		16.39	0.16
115		15.99	0.33	164		16.35	0.24
116		15.60	0.26	165	1.16	13.16	(-0.05)
117	2.64	14.64	0.25	166	3.48	15.48	0.47
118	2.68	14.68	0.16	167	2.60	14.60	0.96
119	-1.10	10.90	(-0.17)	168	1.42	13.42	1.31
120	1.20	13.20	0.00	169	3.21	15.21	0.23
121	3.25	15.25	0.53	170		15.51	0.37
122		15.99	0.09	171		15.81	0.15
123	3.20	15.20	0.09	172	2.92	14.92	0.18
124	0.60	12.60	-0.14	173	0.09	12.09	(0.01)
125	2.61	14.61	0.20	174	0.17	12.17	(-0.02)
126		15.31	0.53	175	2.06	14.06	0.05
127		16.03	0.26	176		16.08	0.22
128		16.62	-0.16	177		16.24	-0.40
129		16.69	-0.14	178	-1.37	10.63	(-0.19)
130		16.14	0.24	179		16.09	0.23
131	0.10	12.10	(-0.09)	180	2.57	14.57	0.28
132	1.90	13.90	0.12	181	2.51	14.51	0.33
133	0.12	12.12	0.31	182	3.08	15.08	0.28
134	1.40	13.40	0.28	183	3.02	15.02	0.29
135	3.12	15.12	0.33	184	2.82	14.82	0.51
136	1.44	13.44	1.24	185	1.74	13.74	0.22
137	-2.97	9.03	(-0.20)	186		15.80	0.21
138	1.48	13.48	0.17	187		16.40	0.19
139	2.36	14.36	0.00	188	0.20	12.20	(0.02)
140		15.55	0.18	189	2.09	14.09	0.04
141	1.53	13.53	0.02	190		16.10	0.46

TABLE 19 (Continued)

No.	M_V	V_o	$(B-V)_o$	No.	M_V	V_o	$(B-V)_o$
191	2.81	14.81	0.31	241		16.17	0.20
192	1.42	13.42	0.62	242		16.30	0.49
193	-2.54	9.46	(-0.21)	243		16.57	0.27
194	1.25	13.25	0.17	244	-1.56	10.44	(-0.18)
195	-0.50	11.50	(-0.04)	245	3.45	15.45	0.35
196	0.97	12.97	(0.35)	246	0.90	12.90	(-0.03)
197		16.81	-0.44	247		16.13	0.14
198		15.74	0.61	248	3.08	15.08	0.36
199	-2.55	9.45	(-0.17)	249	0.45	12.45	-0.23
200		16.26	-0.15	250	1.90	13.90	0.25
201	0.76	12.76	(-0.05)	251		15.90	0.34
202	-4.52	7.48	(-0.32)	252	-0.31	11.69	(-0.14)
203	1.47	13.47	0.06	253	2.33	14.33	0.29
204		15.94	0.13	254	1.73	13.73	0.13
205	-1.10	10.90	(-0.20)	255	1.99	13.99	0.02
206	1.95	13.95	0.17	256		16.03	0.43
207	1.16	13.16	(0.01)	257		16.24	0.36
208	1.16	13.16	0.08	258	2.71	14.71	0.38
209	1.81	13.81	0.02	259	-4.36	7.64	(-0.27)
210	3.14	15.14	0.35	260	0.70	12.70	0.18
211		16.12	0.30	261	1.46	13.46	0.15
212		16.49	0.45	262	3.27	15.27	0.46
213	2.02	14.02	0.15	263	-2.03	9.97	-0.15
214	Kodak	Star		264	-1.10	10.90	-0.07
215	2.03	14.03	0.11	264b	-0.81	11.19	-0.03
216		16.45	0.29	265	-2.76	9.24	0.00
217	2.69	14.69	0.38	266	-1.88	10.12	(-0.27)
218	0.02	12.02	(-0.10)	267	2.44	14.44	0.42
219	0.58	12.58	-0.16	268	-4.01	7.99	(-0.22)
220		16.13	0.24	269	0.69	12.69	0.24
221	3.17	15.17	0.31	270	-1.23	10.77	-0.17
222		16.28	0.22	271	1.47	13.47	0.30
223	1.42	13.42	0.03	272	-2.63	9.37	(-0.11)
224	-0.28	11.72	(-0.10)	273	-2.91	9.09	-0.13
225	2.41	14.41	0.16	274	1.88	13.88	0.28
226	2.93	14.93	0.96	275	0.29	12.29	1.36
227		15.79	0.45	276	3.15	15.15	0.35
228	1.99	13.99	0.42	277		15.73	0.13
229		16.99	-0.03	278	3.50	15.50	0.05
230		16.11	0.51	279	3.05	15.05	0.34
231	0.24	12.24	-0.16	280	0.40	12.40	(-0.10)
232		16.40	0.25	281		15.92	0.23
233	3.00	15.00	0.30	282		16.03	0.32
234	1.87	13.87	-0.06	283	-2.14	9.86	(-0.12)
235		16.02	0.33	284	-1.55	10.45	-0.14
236		16.83	-0.09	285	-0.67	11.33	-0.12
237		16.23	0.50	286	0.30	12.30	-0.16
238	3.06	15.06	0.54	287	2.99	14.99	0.38
239	3.54	15.54	0.48	288	0.40	12.40	(-0.06)
240	3.38	15.38	0.23	289	0.93	12.93	0.12

TABLE 19 (Continued)

No.	M_V	V_o	$(B-V)_o$	No.	M_V	V_o	$(B-V)_o$
290	-0.86	11.14	(-0.22)	300	-1.48	10.52	(-0.16)
291	1.09	13.09	1.14	301	0.86	12.86	(0.07)
292	0.67	12.67	(-0.03)	302	2.60	14.60	0.67
293		16.12	0.22	303	2.75	14.75	0.27
294	3.56	15.56	0.58	304	-3.07	8.93	-0.07
295		16.08	0.32	305	1.55	13.55	-0.03
296		16.39	0.20	306	-0.91	11.09	-0.07
297	-0.57	11.43	(-0.19)	307	1.83	13.83	0.81
298	-1.60	10.40	(-0.16)				
299	2.92	14.92	0.21				

TABLE 20

STARS OF THE EXTREME NUCLEUS OF chi PERSEI

No.	M_V	V_o	$(B-V)_o$	No.	M_V	V_o	$(B-V)_o$
1	-4.44	7.56	(-0.32)	48	2.65	14.65	0.36
2	3.39	15.39	-0.07	49	-1.84	10.16	(-0.19)
3	0.97	12.97	(-0.08)	50	2.20	14.20	0.61
4	2.86	14.86	0.48	51		15.97	0.08
5	2.41	14.41	0.34	52		16.46	-0.28
6	3.15	15.15	0.32	53		15.63	0.34
7		16.41	-0.04	54		16.18	0.22
8	1.82	13.82	0.50	55	0.51	12.51	(-0.11)
9		15.79	0.52	56		16.04	0.38
10	2.42	14.42	0.28	57		16.33	0.32
11	0.25	12.25	(-0.16)	58	2.90	14.90	1.03
12		15.52	0.63	59	1.72	13.72	1.18
13		15.64	0.61	60	-5.42	6.58	2.01
14		17.28	-0.02	61	0.15	12.15	-0.07
15	2.55	14.55	0.29	62	3.45	15.45	0.45
16	2.58	14.58	0.27	63	2.78	14.78	0.39
17	2.61	14.61	0.53	64	3.26	15.26	0.58
18	3.51	15.51	0.39	65	3.27	15.27	0.65
19		15.58	0.32	66	1.80	13.80	1.13
20	1.57	13.57	(-0.05)	67		15.76	0.58
21	0.41	12.41	-0.13	68	2.95	14.95	0.67
22		15.59	0.49	69	-4.49	7.51	-0.28
23	-0.81	11.19	(-0.19)	70	1.35	13.35	0.53
24		15.85	0.38	71		16.33	0.30
25	0.72	12.72	-0.08	72	2.21	14.21	0.24
26	0.43	12.43	-0.24	73	3.40	15.40	0.20
27	-0.54	11.46	(-0.16)	74	1.94	13.94	0.04
28	1.22	13.22	0.28	75		15.73	0.51
29	1.43	13.43	(0.00)	76	0.34	12.34	-0.15
30	-0.80	11.20	(-0.17)	77	0.38	12.38	-0.19
31	-5.15	6.85	(-0.27)	78		16.97	-0.05
32	0.82	12.82	0.50	79	3.13	15.13	0.44
33	3.06	15.06	0.17	80	-1.41	10.59	(-0.20)
34	1.80	13.80	0.58	81	3.24	15.24	0.26
35	1.45	13.45	0.06	82	-0.18	11.82	0.24
36	-4.27	7.73	-0.27	83	0.33	12.33	0.53
37	2.69	14.69	0.02	84	2.87	14.87	0.53
38	0.32	12.32	0.46	85		16.72	0.24
39	0.71	12.71	(-0.07)	86		16.98	0.00
40		15.83	0.22	87		16.47	0.68
41	3.06	15.06	0.32	88		16.08	0.28
42	-0.34	11.66	(-0.11)	89	0.45	12.45	(-0.06)
43	1.32	13.32	0.02	90	1.63	13.63	-1.04
44	3.18	15.18	0.39	91	1.90	13.90	0.65
45	2.61	14.61	0.45	92		16.71	0.32
46	-4.57	7.43	(-0.27)	93		15.65	0.38
47	2.00	14.00	-0.19	94	2.16	14.16	1.04

TABLE 20 (Continued)

No.	M_V	V_o	$(B-V)_o$	No.	M_V	V_o	$(B-V)_o$
95		17.33	-0.17	144	3.17	15.17	0.25
96		17.41	-0.43	145	2.82	14.82	0.44
97		15.75	0.35	146	3.35	15.35	0.33
98		15.56	0.92	147	-0.23	11.77	(-0.15)
99	1.39	13.39	(-0.03)	148	1.76	13.76	0.69
100		15.92	0.48	149	2.36	14.36	0.27
101	0.20	12.20	0.30	150	2.03	14.03	0.09
102		15.05	0.56	151	1.80	13.80	0.13
103		15.06	0.28	152	0.50	12.50	(-0.05)
104	2.58	14.58	0.30	153	3.06	15.06	0.28
105	2.50	14.50	0.35	154	1.45	13.45	-0.06
106	1.90	13.90	0.35	155	-0.60	11.40	(-0.19)
107	-1.41	10.59	-0.04	156	0.99	12.99	-0.09
108	-0.36	11.64	0.01	157	0.95	12.95	(0.48)
109	0.02	12.02	-0.14	158		16.71	0.00
110	0.56	12.56	-0.18	159	1.58	13.58	0.58
111	0.47	12.47	0.33	160	1.58	13.58	1.16
112		15.63	0.74	161	1.53	13.53	0.05
113	-0.63	11.37	(0.49)	162	1.72	13.72	0.16
114		16.33	0.07	163	2.23	14.23	0.06
115		16.61	0.06	164	3.03	15.03	0.16
116	2.41	14.41	(0.36)	165	-4.24	7.76	-0.33
117	2.86	14.86	0.51	166	1.56	13.56	-0.14
118		16.66	-0.10	167	1.35	13.35	(-0.07)
119	0.36	12.36	0.31	168	-2.05	9.95	(-0.23)
120	-3.64	8.36	(-0.22)	169		15.89	-0.10
121	2.05	14.05	(0.35)	170	2.61	14.61	0.33
122	2.74	14.74	(0.41)	171	-2.90	9.10	(-0.26)
123	-0.21	11.79	(-0.14)	172	3.25	15.25	0.31
124	-0.31	11.69	(-0.06)	172b	-3.29	8.71	-0.06
125	2.21	14.21	0.72	173	2.08	14.08	0.24
126	1.15	13.15	(-0.08)	174	-2.51	9.49	(-0.21)
127	2.31	14.31	0.04	175	2.37	14.37	0.33
128		15.90	0.42	176	3.40	15.40	0.35
129	2.43	14.43	0.35	177	0.19	12.19	-0.05
130	2.52	14.52	1.15	178	-1.21	10.79	-0.22
131		15.69	0.07	179	0.15	12.15	-0.10
132	-3.87	8.13	(-0.34)	180	-0.07	11.93	-0.19
133		15.95	0.04	181	1.96	13.96	0.36
134	2.25	14.25	0.11	182	-0.62	11.38	(-0.16)
135	1.58	13.58	(0.44)	183		15.65	0.04
136	0.95	12.95	(-0.09)	184		16.24	0.02
137		15.75	-0.14	185	-2.06	9.94	(-0.21)
138	1.67	13.67	0.65	186	-4.41	7.59	(-0.28)
139		15.91	0.27	187	-3.84	8.16	(-0.28)
140		16.24	0.12	188	-0.14	11.86	-0.03
141	-1.51	10.49	(-0.16)	189	-1.73	10.27	2.41
142	2.30	14.30	0.66	190	-5.69	6.31	-0.26
143		16.07	0.24	191	0.84	12.84	(-0.10)

TABLE 20 (Continued)

No.	M_V	V_o	$(B-V)_o$	No.	M_V	V_o	$(B-V)_o$
192	1.19	13.19	0.12	241		16.32	0.18
193		15.90	0.07	242	2.86	14.86	0.36
194	1.31	13.31	(0.00)	243	1.48	13.48	(-0.02)
195		15.33	0.34	244		16.08	0.25
196		15.66	0.16	245	-0.89	11.11	(-0.17)
197		16.41	-0.12	246		15.85	0.12
198	0.66	12.66	(-0.07)	247		16.27	0.07
199	3.17	15.17	0.39	248	-2.36	9.64	(-0.25)
200	1.63	13.63	-0.03	249	1.58	13.58	0.07
201	1.62	13.62	1.32	250	-0.43	11.57	(-0.16)
202		16.24	0.31	251	-0.91	11.09	(-0.13)
203	1.55	13.55	(0.50)	252	-0.01	11.99	(-0.10)
204		17.08	-0.23	253	3.28	15.28	0.33
205	0.49	12.49	(-0.09)	254	2.72	14.72	0.33
206		15.66	0.33	255		16.84	-0.59
207	2.61	14.61	0.33	256	2.45	14.45	0.26
208	1.59	13.59	(-0.04)	257	2.39	14.39	0.33
209	-2.03	9.97	(-0.23)	258	1.62	13.62	(-0.05)
210		16.45	0.03	259	2.04	14.04	0.15
211		16.39	0.03	260		15.97	0.33
212		15.57	0.53	261	3.37	15.37	0.37
213	2.93	14.93	0.37	262	1.57	13.57	(-0.06)
214	-2.12	9.88	(-0.24)	263	1.67	13.67	(-0.04)
215	3.24	15.24	0.39	264		15.84	0.45
216	2.73	14.73	0.33	265		15.98	0.40
217	2.53	14.53	0.32	266	1.88	13.88	0.36
218		15.73	0.20	267	3.57	15.57	0.36
219	-0.26	11.74	(-0.14)	268	3.37	15.37	0.32
220	2.40	14.40	0.17	269	1.24	13.24	(-0.02)
221	2.64	14.64	0.36	270	2.37	14.37	0.22
222	-1.41	10.59	(-0.22)	271	2.38	14.38	0.27
223	2.46	14.46	0.19	272		16.07	0.44
224	3.49	15.49	0.58	273	3.01	15.01	0.30
225	-2.79	9.21	-0.25	274		16.37	0.33
226	-0.28	11.72	-0.14	275		16.36	0.45
227	-4.41	7.59	-0.32	276	-2.55	9.45	(-0.17)
228	0.38	12.38	(-0.14)	277	0.41	12.41	0.13
229	0.96	12.96	0.13	278	2.12	14.12	0.38
230	3.20	15.20	0.11	279		16.04	0.25
231	0.91	12.91	(-0.01)	280	1.88	13.88	(0.01)
232	2.97	14.97	0.25	281		15.55	0.31
232b	2.23	14.23	(-0.27)	282	-0.67	11.33	(-0.15)
233	3.13	15.13	0.42	283		15.96	0.37
234		16.42	-0.12	284	2.78	14.78	0.35
235		16.27	0.19	285	3.04	15.04	0.12
236		15.86	0.22	286	0.66	12.66	(-0.10)
237	2.08	14.08	0.19	287		16.27	-0.21
238	-1.81	10.19	(-0.11)	288	2.52	14.52	0.22
239		15.91	0.34	289	0.29	12.29	(-0.11)
240	0.73	12.73	(-0.11)	290	3.41	15.41	0.60

TABLE 20 (Continued)

No.	M_V	V_o	$(B-V)_o$	No.	M_V	V_o	$(B-V)_o$
291	0.65	12.65	(-0.09)	297	1.49	13.49	(-0.03)
292	1.78	13.78	0.14	298	1.30	13.30	(-0.04)
293	-0.21	11.79	1.60	299		16.42	0.51
294	2.64	14.64	0.95	300		16.46	0.30
295	3.16	15.16	0.51	301		16.89	0.31
296	1.74	13.74	0.13				

APPENDIX II

FIGURES

FIGURE CAPTIONS

Fig. 1. - Identification chart for the supergiants and faint neighbors of the general region.

Fig. 2. - Identification chart for the O stars and faint neighbors of the general region.

Fig. 3. - Identification chart for the giants-subgiants and faint neighbors of the general region.

Fig. 4. - Identification chart for the stars of the extreme nucleus of h Persei. The circle is 6 minutes-of-arc in diameter.

Fig. 5. - Identification chart for the stars of the extreme nucleus of chi Persei. The circle is 6 minutes-of-arc in diameter.

Fig. 6. - Reddening and absorption as a function of the amount of interstellar absorbing material for stars of different intrinsic-color. The bold-lined curves represent integration results for HD214680, the sun, and δ Tauri. The U-B color-excess scale should be multiplied by 0.802 in order to produce agreement with observational reddening-trajectories.

Fig. 7. - Loci of constant quantities of interstellar dust in the $(E_{(U-B)}, (B-V)_o)$ plane. The dashed horizontal lines are asymptotes corresponding to infinitely red and infinitely blue stars (the first derivative of the spectral energy distribution approaches plus and minus infinity respectively, with the second derivative becoming positive at all finite wavelengths in either limit).

Fig. 8. - B-V color-excess as a function of intrinsic-color for various concentrations of interstellar absorbing matter. The same as Figure 7 substituting B-V for U-B.

Fig. 9 - Reddening-trajectories in the color-color diagram terminated on the intrinsic relationship for luminosity-class V stars.

Fig. 10. - Isocryptic-chart in $E_{(B-V)}$ (normalized to AOV stars) for h Persei.

Fig. 11. - Isocryptic-chart in $E_{(B-V)}$ (normalized to AOV stars) for chi Persei.

Fig. 12. - Color-color relation for unreddened supergiants. Open circles are Ia; half-filed are Iab; and filled are Ib. Curves are for black-bodies, class V, and class I. The class I curve for intermediate colors not in the range of the present study is from Arp (1958b) and is heuristic at the red extreme.

Fig. 13. - Color-color relation for O stars and giants-subgiants. Class II is on the left; III and IV are in the center; and the O stars are on the right. The curves are for class I, class V, and blackbodies.

Fig. 14. - Intrinsic B-V difference (supergiants minus dwarfs) versus spectral type. Filled circles are from the present study of h and chi Persei. Open circles are from M29 and nearby, supposed-unreddened, field supergiants (Johnson 1958). X points are from the Ib relation found by Kraft (1960a, b) from cepheids. Crosses are Feinstein's (1959) determination of the envelope of Sp versus B-V (uncorrected for reddening). The adopted mean relation is shown.

Fig. 15. - Absolute plot of $(B-V)_o$ versus Sp for the supergiants in the general region of h and chi Persei. Open circles are Ia; half-filled circles are Iab; and filled circles are Ib. The solid curve is the class V relation adopted by Arp (1958b). The dashed curve is the previous class I relation (Johnson 1958). The lazy-T curve is the class I relation from the present study.

Fig. 16. - Intrinsic-color versus spectral type data plot for giants, subgiants, and O stars in the region of h and chi Persei. Open circles are class II; filled circles are O stars and classes III and IV. The solid curve is adopted class V relation of Arp (1958b).

Fig. 17. - Intrinsic-color-apparent magnitude diagram for all bright-stars and faint-neighbors of the general region of h and chi Persei. Open circles are north of $57^{\circ}10'$; and filled circles are south. X points are luminosity class V B stars of the general region whose primary measurements are from Johnson and Morgan (1955) and Johnson and Hiltner (1956).

Fig. 18. - As in Figure 17 except open circles are west of 2^h18^m and filled circles are east. Both figures are separated for epoch 1855.

Fig. 19. - C-M diagram for class I stars of the present study; extrinsically-unreddened on the left and intrinsically-unreddened on the right. See text, section IVa, b and Vc.

Fig. 20. - Intrinsic C-M diagram of stars of the extreme nuclei of h (filled circles) and chi (open circles) Persei.

Fig. 21. - C-M diagram of all photoelectric and photographically-interpolated observations of the present study, corrected for reddening.

Fig. 22. - HR diagram of the bright-stars of the general region of h and chi Persei.

Fig. 23. - Luminosity function of the extreme nuclei of h and chi Persei. The solid histogram is for all stars; the dashed histogram is for the main-sequence. The solid curves are creation spectrums due to Schmidt (1959) for the case $n = 2$ and normalized to (1) the main-sequence histogram and (2) the total histogram. The dashed curve is a van Rhijn function normalized to the total histogram.

Fig. 24. - Schematic C-M diagrams of h and chi Persei compared to other clusters of the Galaxy and the Large and Small Magellanic Clouds.

Fig. 25. - Bolometric-Correction scales proposed by various authors. The solid curve is due to Popper (1959) and is symbolized by capital A. The center-line curve (B) is due to Oke (1961). The arrow-head curve is Arp's (1958) review indicated by C. The dashed curve (D) is Schmalberger's (1960) compilation. See text, section VIc for detailed descriptions of the mode of compilation of these proposals. The adopted relation is indicated by the following table.

$(B-V)_o$	Cls I	Cls II	Cls III	Cls IV	Cls V
-0.48 to -0.40	C+0.40	C+0.40	C+0.40	C+0.40	C+0.40
-0.40 to -0.22	D	D	D	D	D
-0.22 to 0.30	C	C	C	C	C
0.30 to 0.40	B	(B+C)/2	C	C	C
0.40 to 1.20	B	(B+A)/2	A	A	A
1.20 to --	A+0.23	A+0.23	A	A	A

The curves in the figure are labeled according to the luminosity class to which each applies.

Fig. 26. - Effective-temperature scales proposed by various authors. The solid curve (A) is due to Popper (1959); the dashed curve (B) is from Bless (1960); the center-lined curve (C) from Schmalberger (1960); the arrow-head curve (D) from Arp (1958b); the lazy-T curve (E) from Oke (1961). See text, section VIc for detailed descriptions of the mode of compilation of these proposals. The adopted scale is indicated by the following table.

$(B-V)_o$	Cls I	Cls II	Cls III	Cls IV	Cls V
-0.48 to -0.40	D-0.036	D-0.036	D-0.036	D-0.036	D-0.036
-0.40 to -0.22	C	C	C	C	C
-0.22 to 0.00	(B+A)/2	(B+A)/2	(B+A)/2	(B+A)/2	(B+A)/2
0.00 to 0.30	A	A	A	A	A
0.30 to 1.20	E	(E+A)/2	A	A	A
1.20 to 1.30	D+0.061	(D+A)/2+ 0.030	A	A	A
1.30 to --	D+0.061	$(D_I+D_V)/2$ + 0.030	D	D	D

The curves in the figure are labeled according to the luminosity class to which each applies.

Fig. 27. - M_{bol}- Log T_e diagram of h and chi Persei. Theoretical evolutionary tracks for gravitational-contraction, hydrogen burning, and helium burning are shown. See text, section VIc for authors of the individual tracks. The direction of superimposed arrow-heads indicate the direction of evolution. The initial chemical compositions assumed by the various authors are as follows.

Author	X	Y	Z	X_{cno}	A
Main-Sequence					
Henyey, Le Levier, and Levee (1959).	0.68	0.31	0.01	Z/4	
Schwarzschild and Harm (1958).	0.75	0.22	0.03	Z/7	
Hazelgrove and Hoyle (1956).	0.75	0.24			$6x10^{-5}$
Sakashita, Ōno, and Hayashi (1959).	0.90	0.08	0.02	Z/3	
Pre-Main-Sequence					
Henyey, Le Levier, and Levee (1955).	0.74	0.25	0.01		
Brownlee and Cox (1961) plus homology.	highly detailed pre-solar composition.				
Post-Main-Sequence					
Hayashi and Cameron (1961)	0.90	0.08	0.02	Z/3	
Mass-Loss-with-Mixing					
Massevitch (1958)	function of time with preservation of homogeneity.				

Detailed accounts of all figures are given in the text.

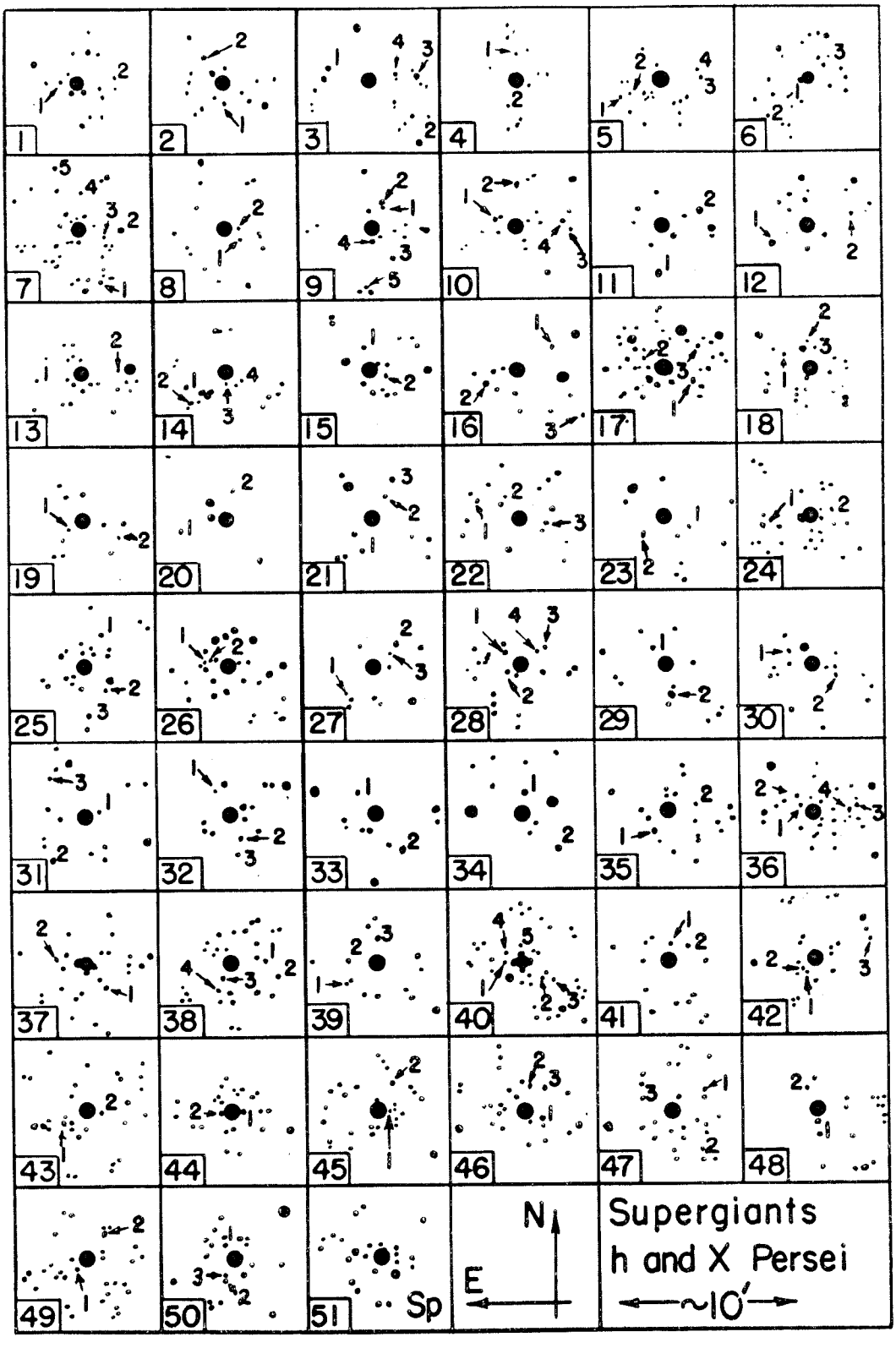
1
2
3
4
5
6
7
8
9
10
11
12
13
14
15
16
17
18
19
20
21
22
23
24
25
26
27
28
29
30
31
32
33
34
35
36
37
38
39
40
41
42
43
44
45
46
47
48
49
50
51
Sp
N
E
Supergiants
h and X Persei
~10'

Figure 1

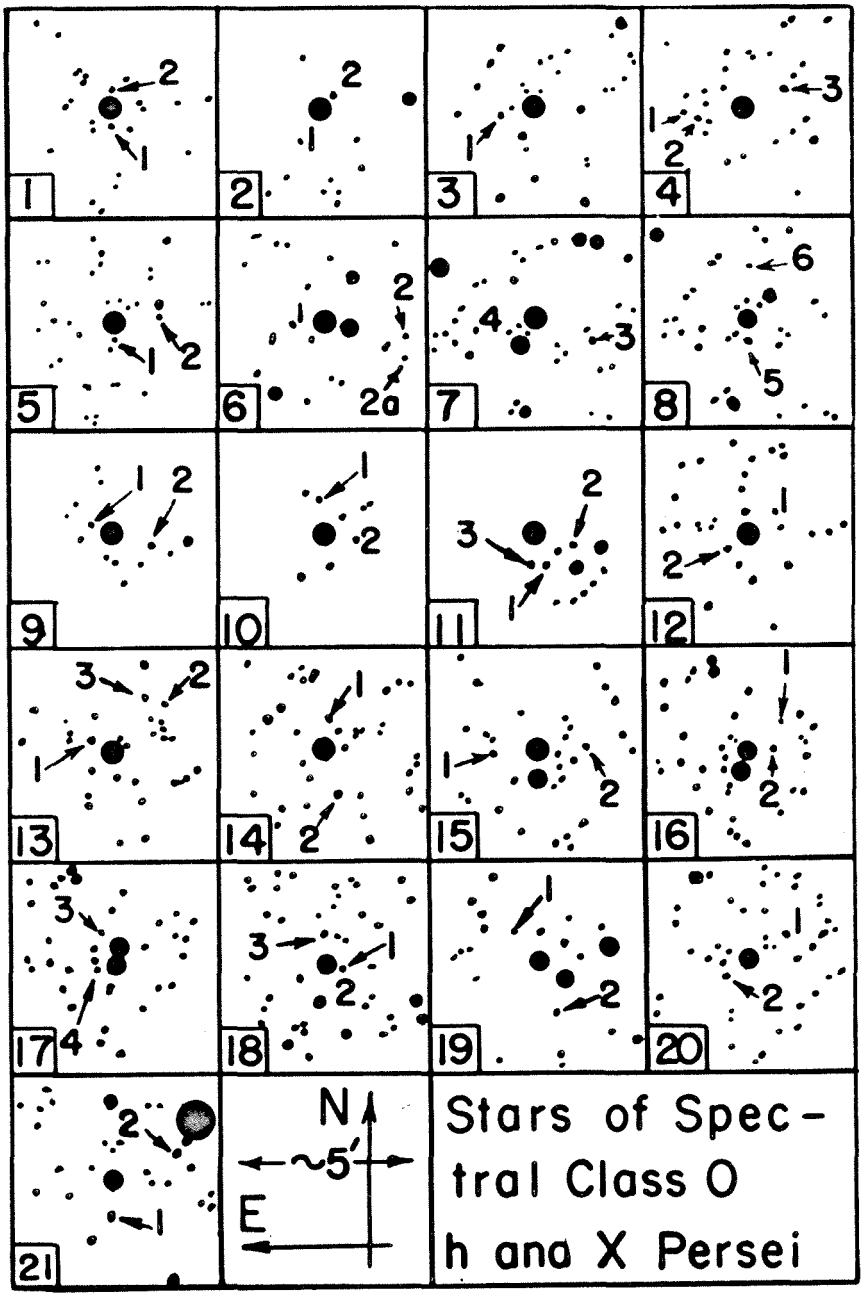
1
2
3
4
5
6
7
8
9
10
11
12
13
14
15
16
17
18
19
20
21
N
~5'
E
Stars of Spec-
tral Class O
h and X Persei

Figure 2

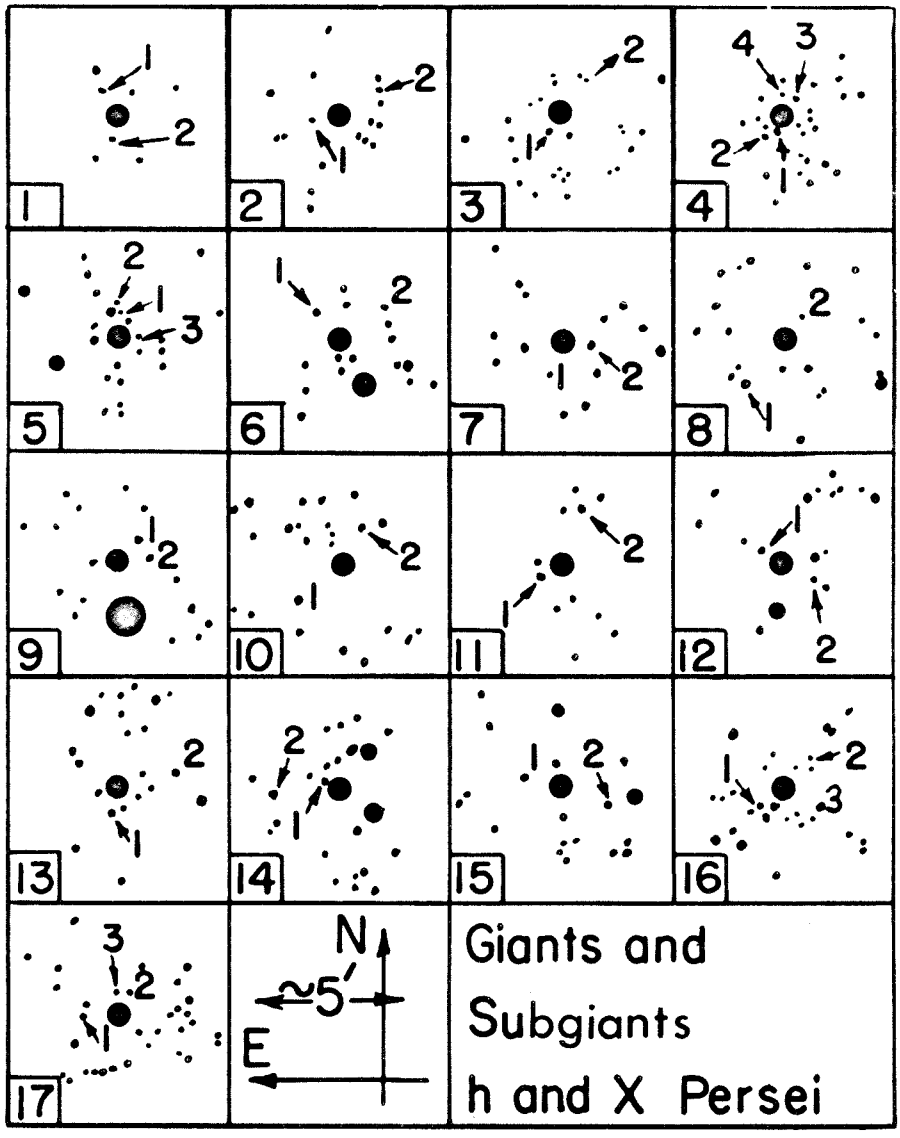
1
2
3
4
5
6
7
8
9
10
11
12
13
14
15
16
17
N
≃5′
E
Giants and
Subgiants
h and X Persei

Figure 3

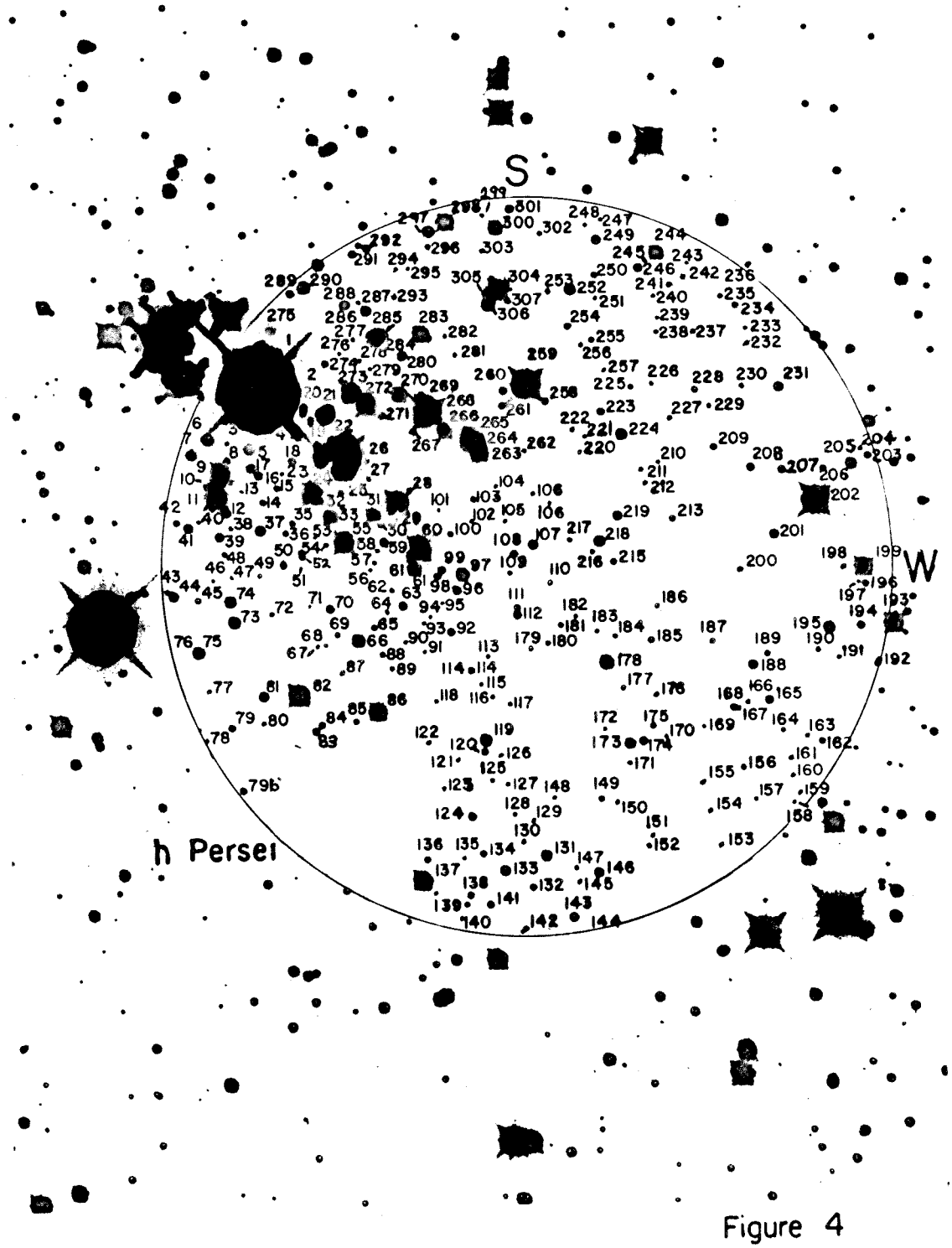

Figure 4

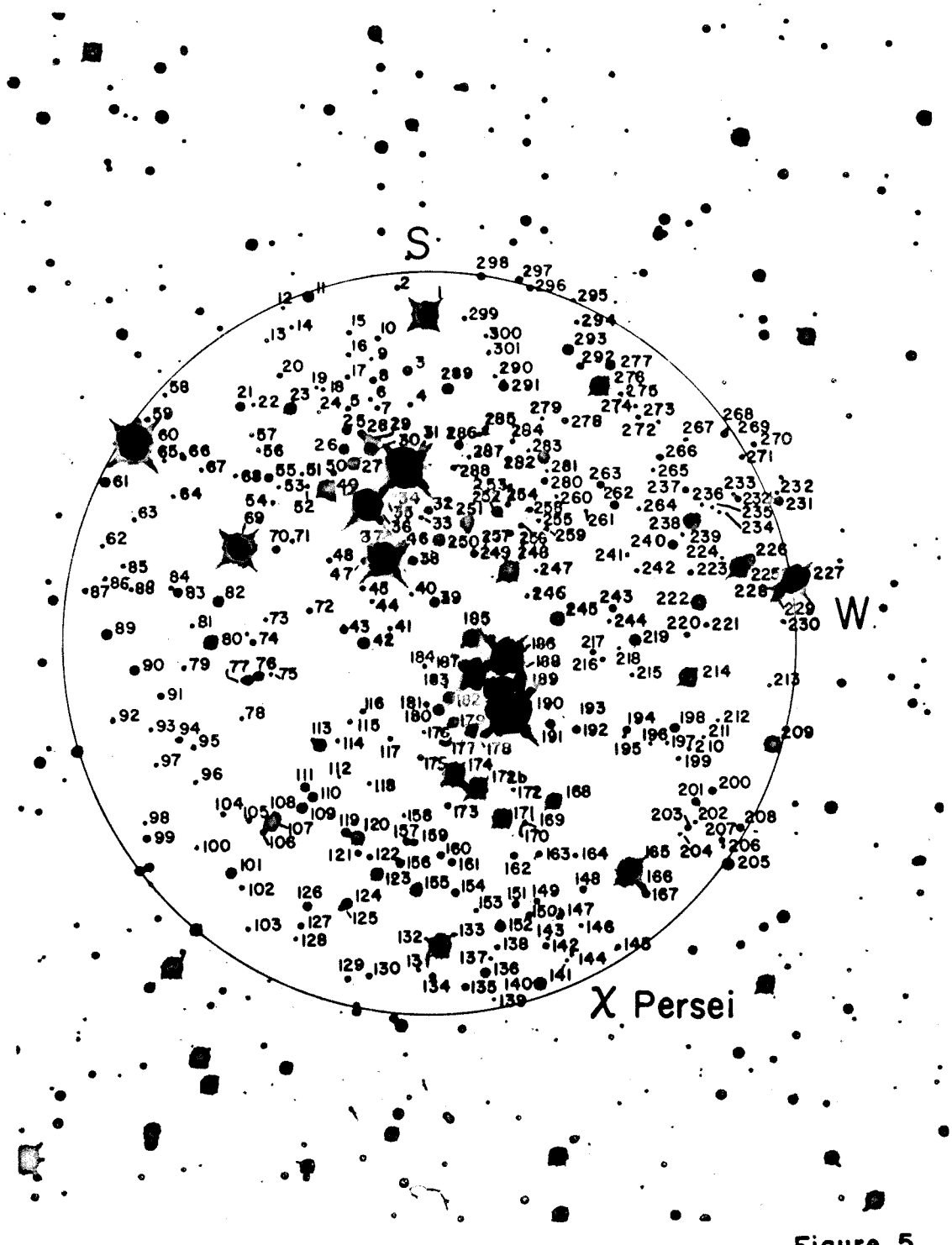

Figure 5

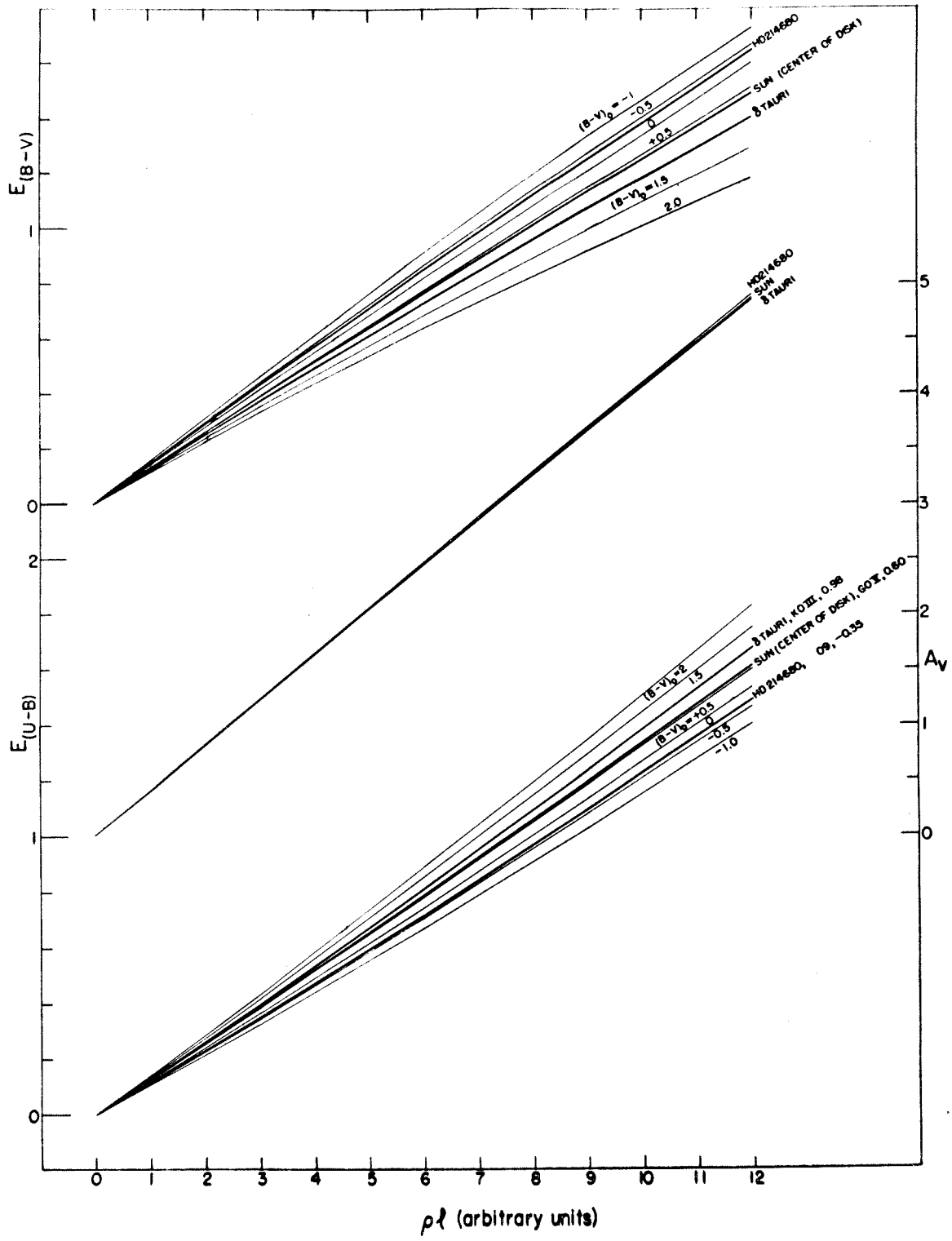
$E_{(B-V)}$
$E_{(U-B)}$
A_V
$\rho\ell$ (arbitrary units)
HD214680
SUN (CENTER OF DISK)
β TAURI
$(B-V)_0$ = -1
-0.5
0
+0.5
$(B-V)_0$ = 1.9
2.0
HD214680
SUN
β TAURI
β TAURI, K0 III, 0.98
SUN (CENTER OF DISK), G0 V, 0.60
HD 214680, O9, -0.35
$(B-V)_0$ = 2
1.5
$(B-V)_0$ = +0.5
0
-0.5
-1.0

Figure 6

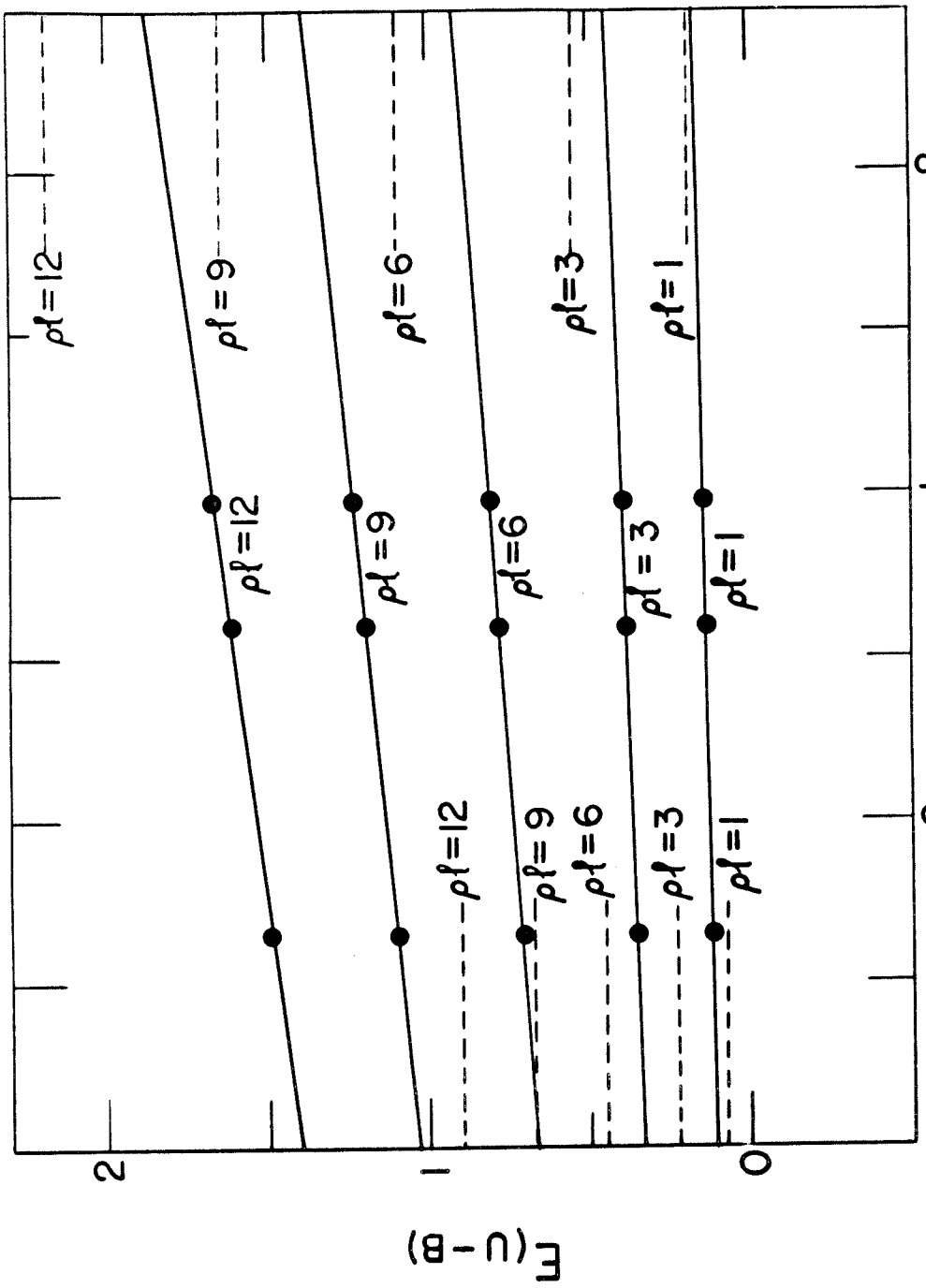
$\rho l = 12$
$\rho l = 9$
$\rho l = 6$
$\rho l = 3$
$\rho l = 1$
$\rho l = 12$
$\rho l = 9$
$\rho l = 6$
$\rho l = 3$
$\rho l = 1$
$\rho l = 12$
$\rho l = 9$
$\rho l = 6$
$\rho l = 3$
$\rho l = 1$
2
1
0
$m_{(U-B)}$
2
1
0
$(B-V)_0$

Figure 7

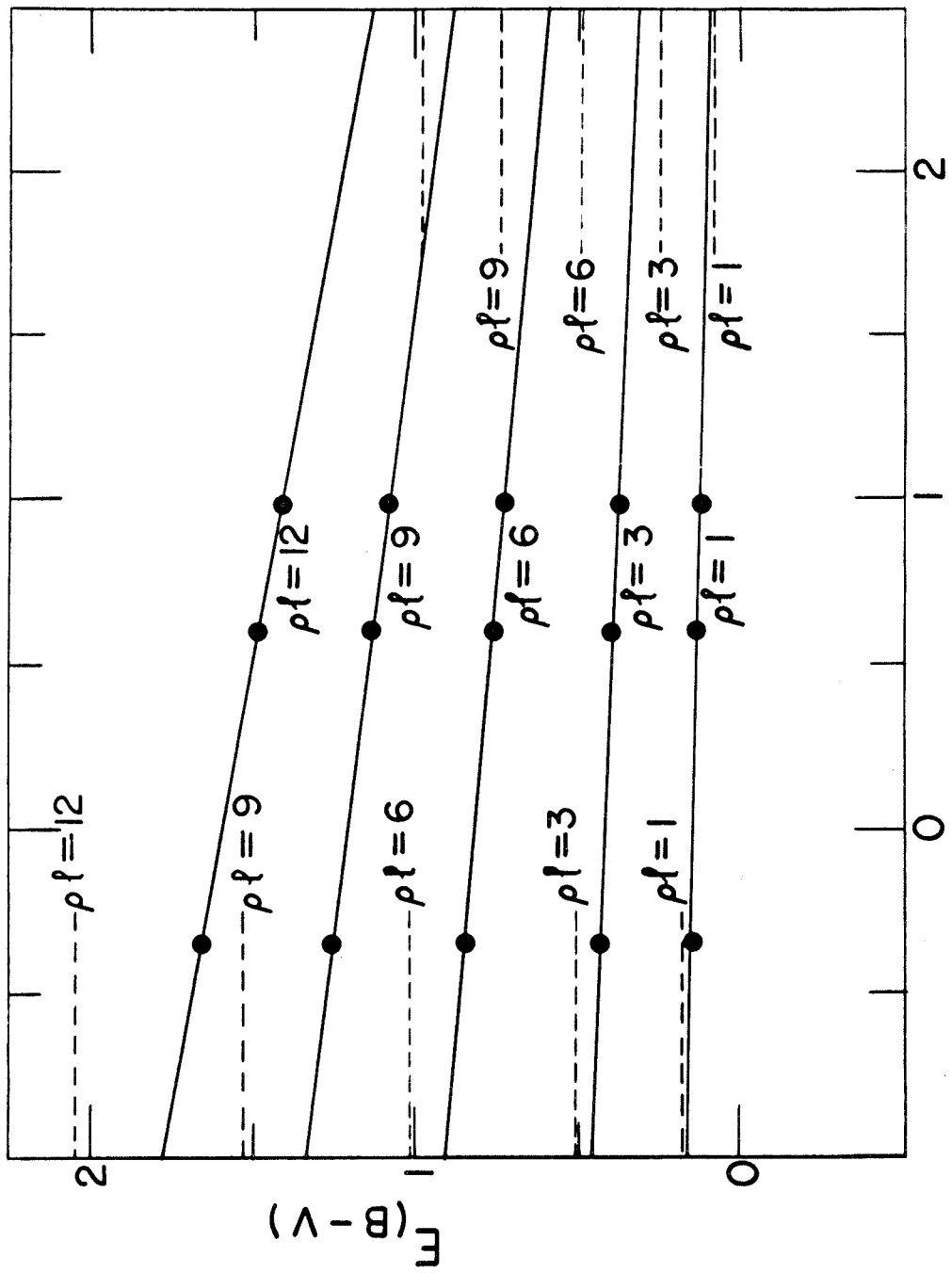

Figure 8

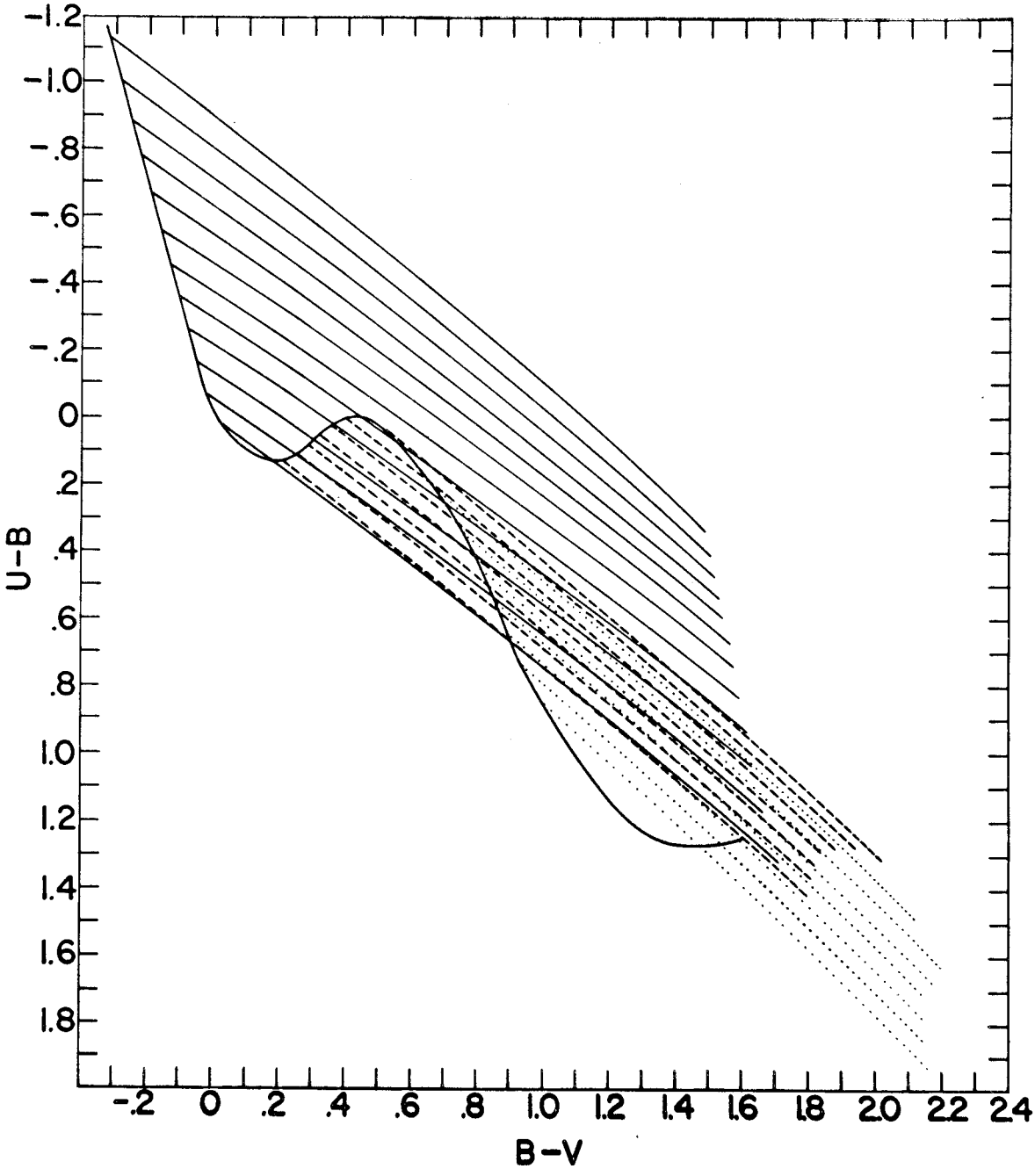

Figure 9

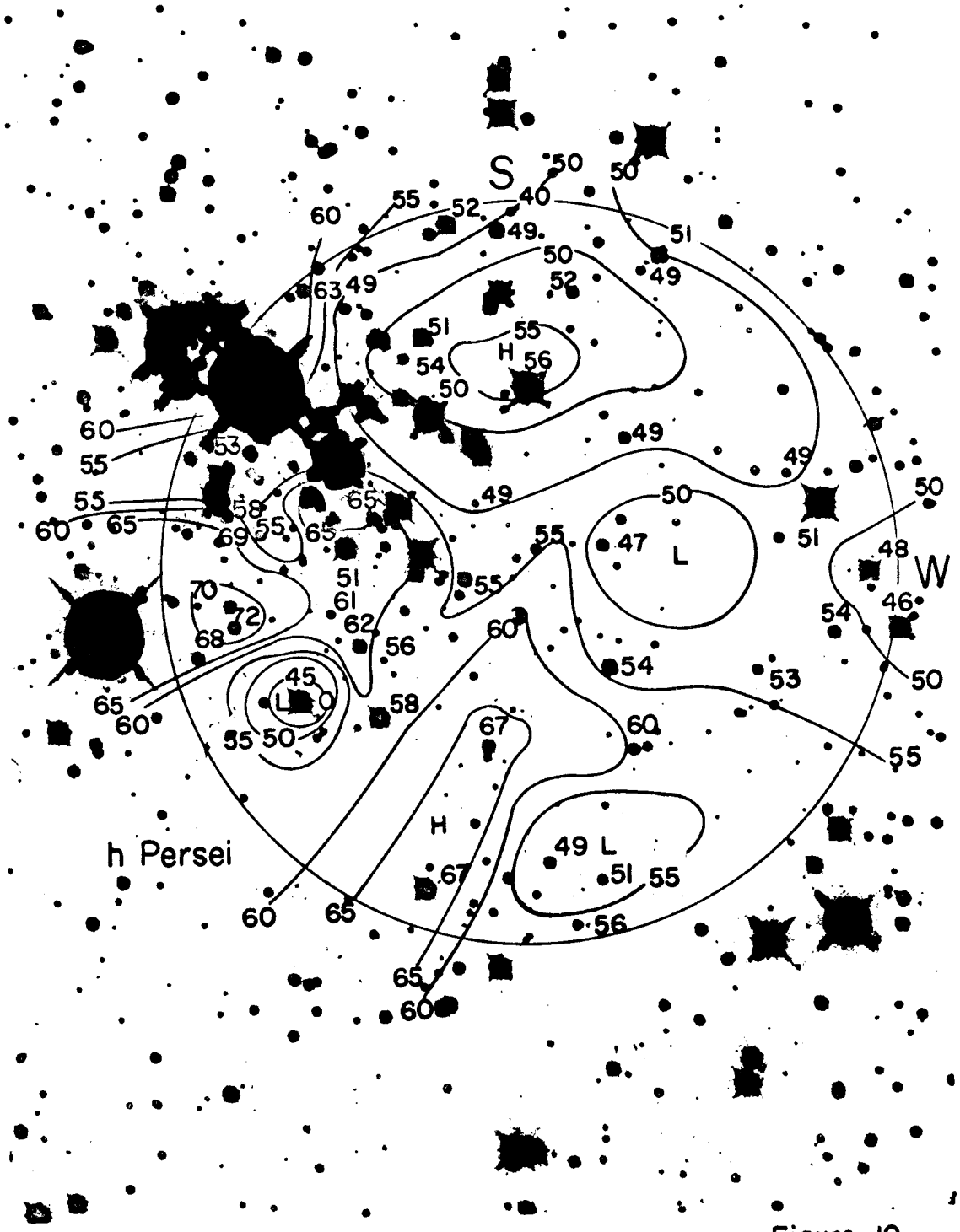
S
W
h Persei
H
L
50
50
40
60
55
52
49
51
50
52
49
63
49
51
55
H
56
54
50
60
53
55
49
49
49
55
58
65
65
50
60
65
69
55
65
47
L
51
48
W
55
51
70
61
72
62
55
54
46
68
56
60
54
53
50
45
L
65
60
58
55
50
67
60
55
H
49 L
67
51
55
60
65
56
65
60

Figure 10

+ +'s)

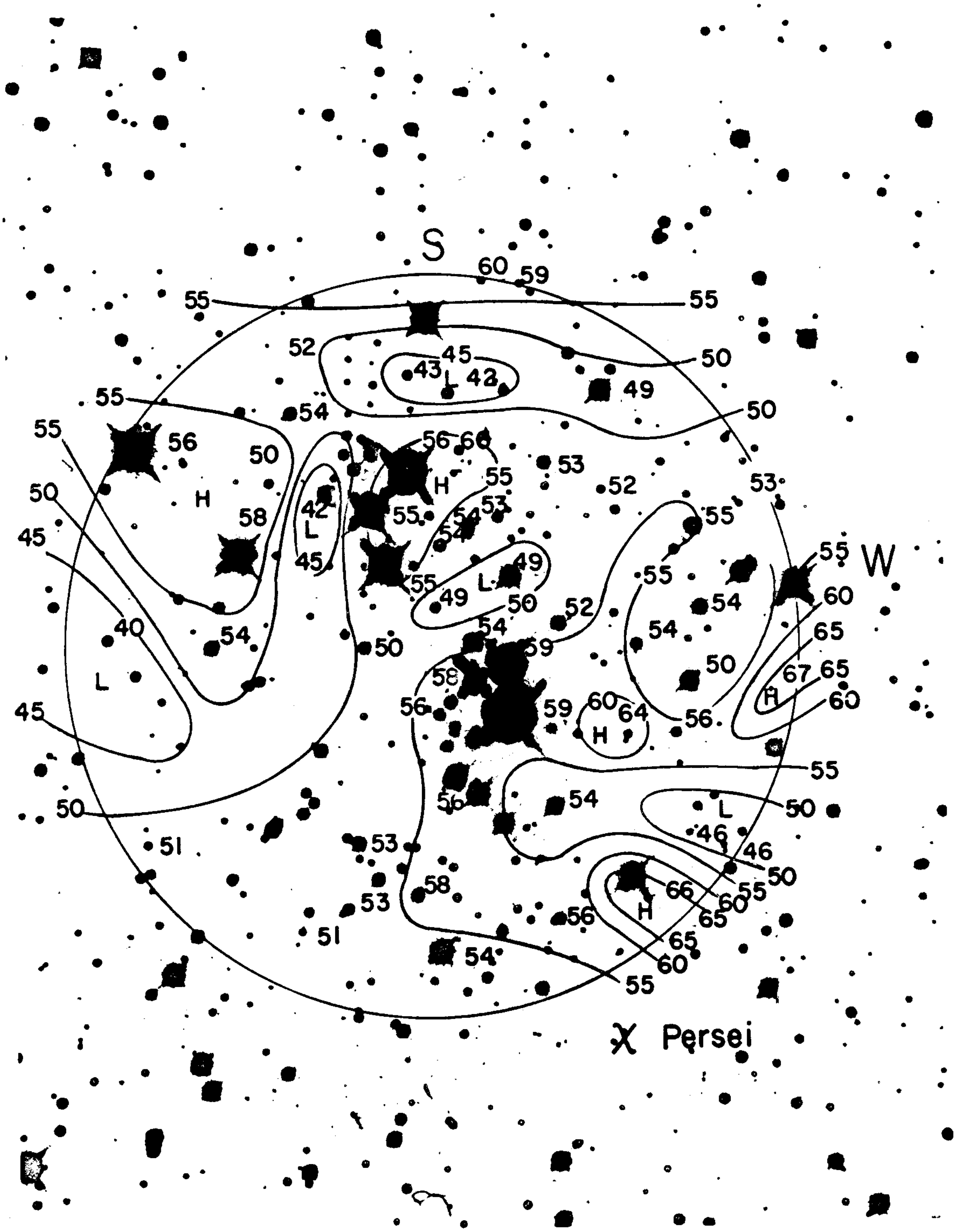

Figure 11

Figure 12

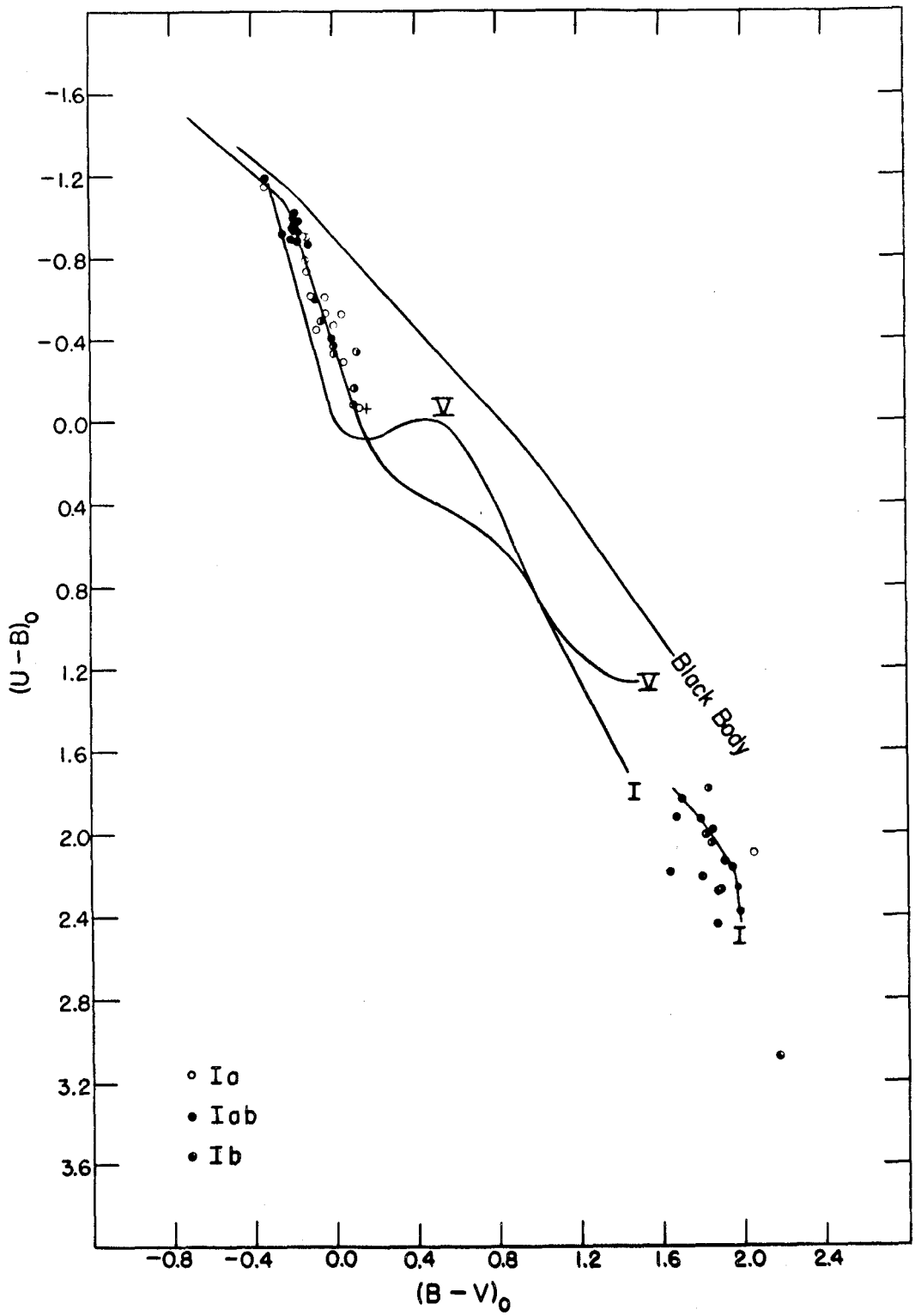
-1.6
-1.2
-0.8
-0.4
0.0
0.4
0.8
1.2
1.6
2.0
2.4
2.8
3.2
3.6
(U-B)0
-0.8
-0.4
0.0
0.4
0.8
1.2
1.6
2.0
2.4
(B-V)0
V
V
I
I
Black Body
° Ia
• Iab
• Ib

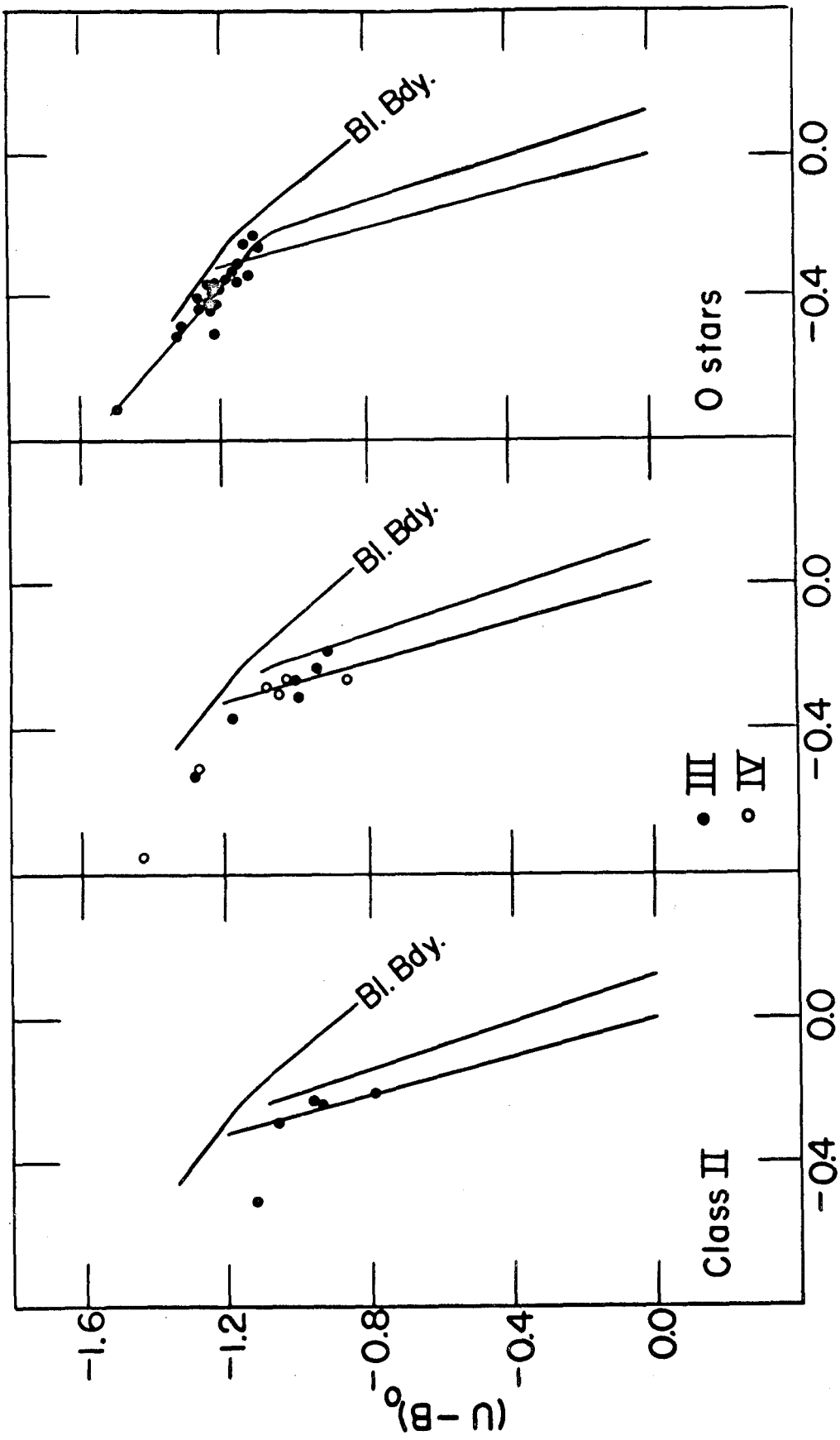
Bl. Bdy.
O stars
Bl. Bdy.
Bl. Bdy.
Class II
III
IV
$(U-B)_o$
$(B-V)_o$
-1.6
-1.2
-0.8
-0.4
0.0
-0.4
0.0

Figure 13

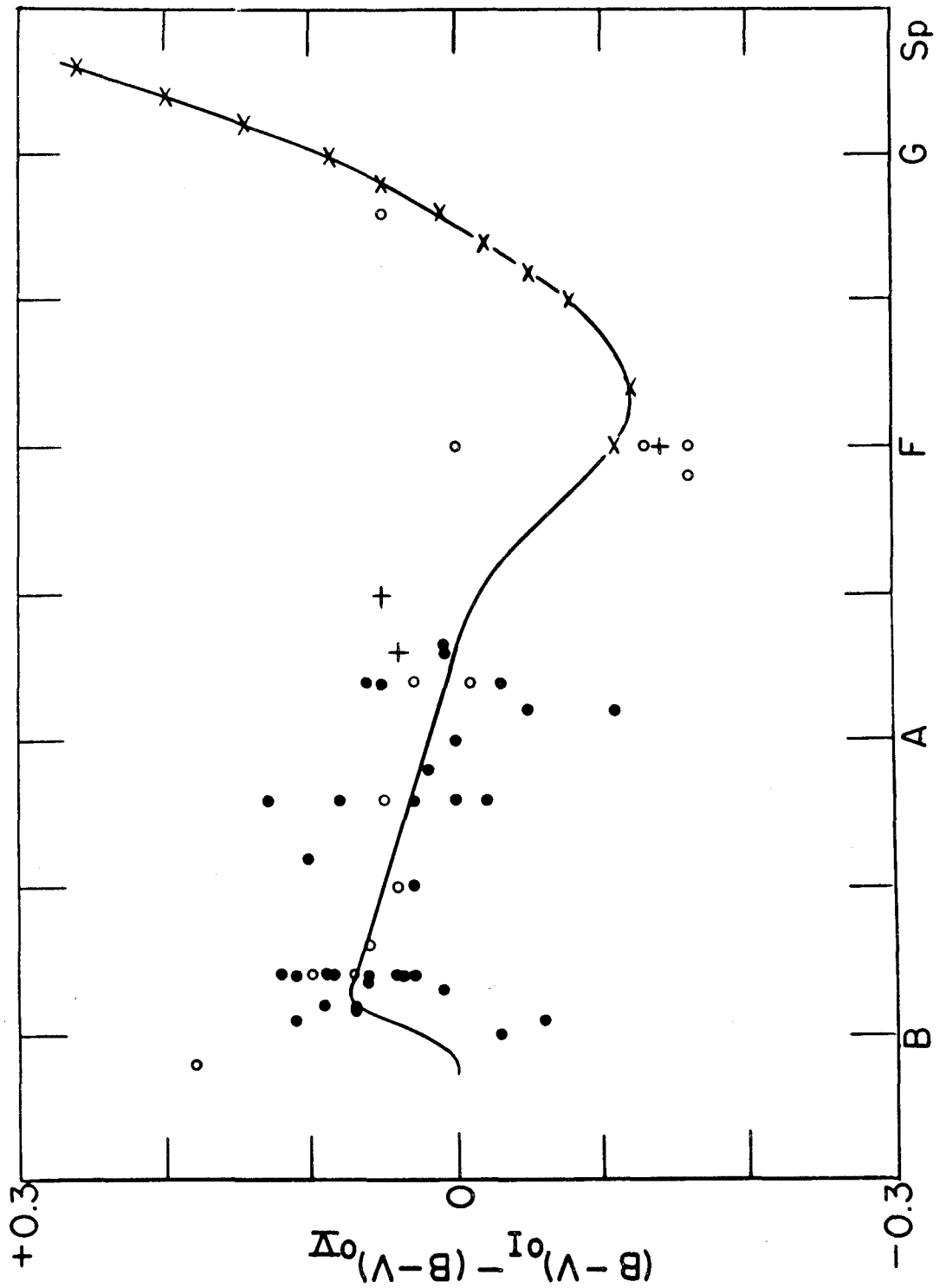

Figure 14

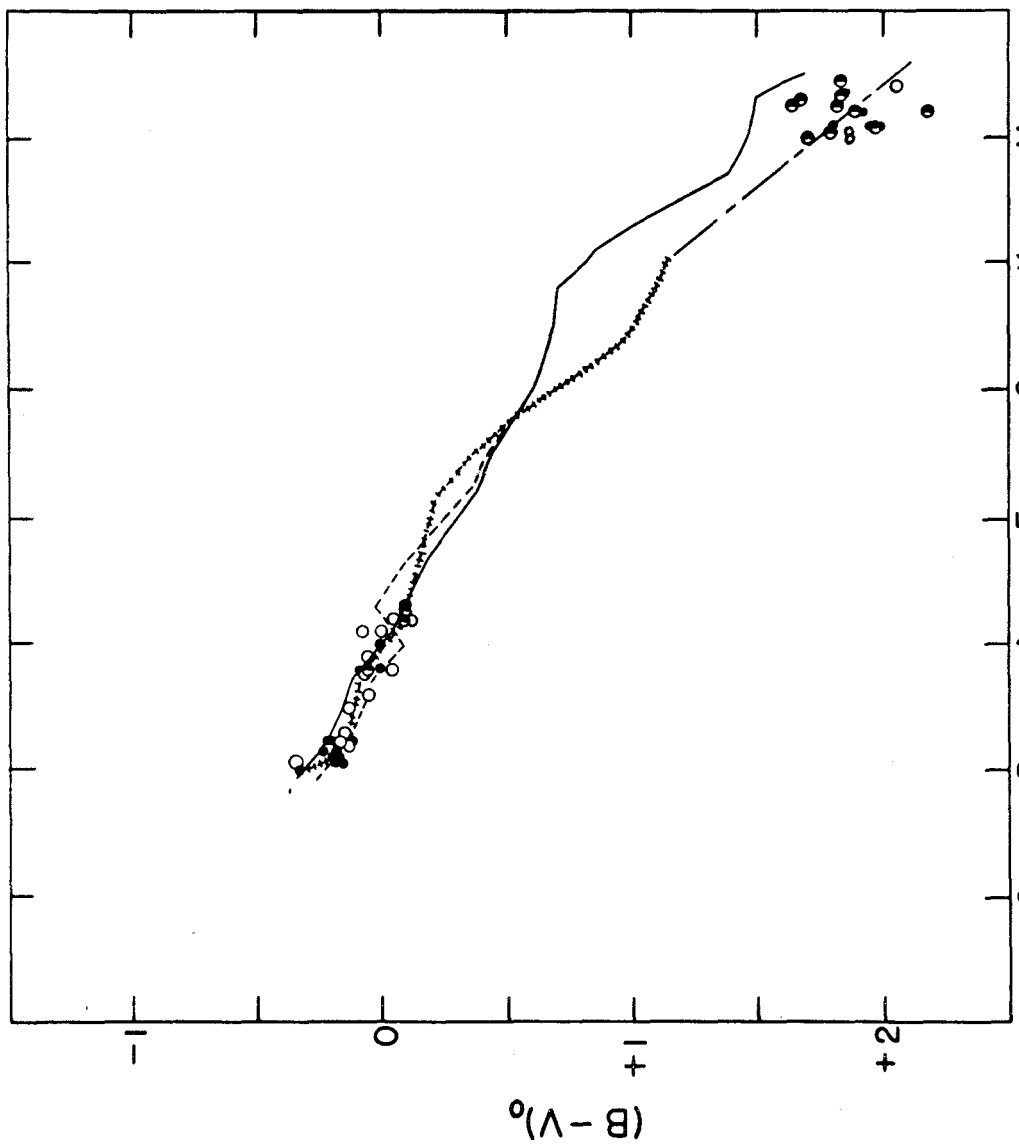

Figure 15

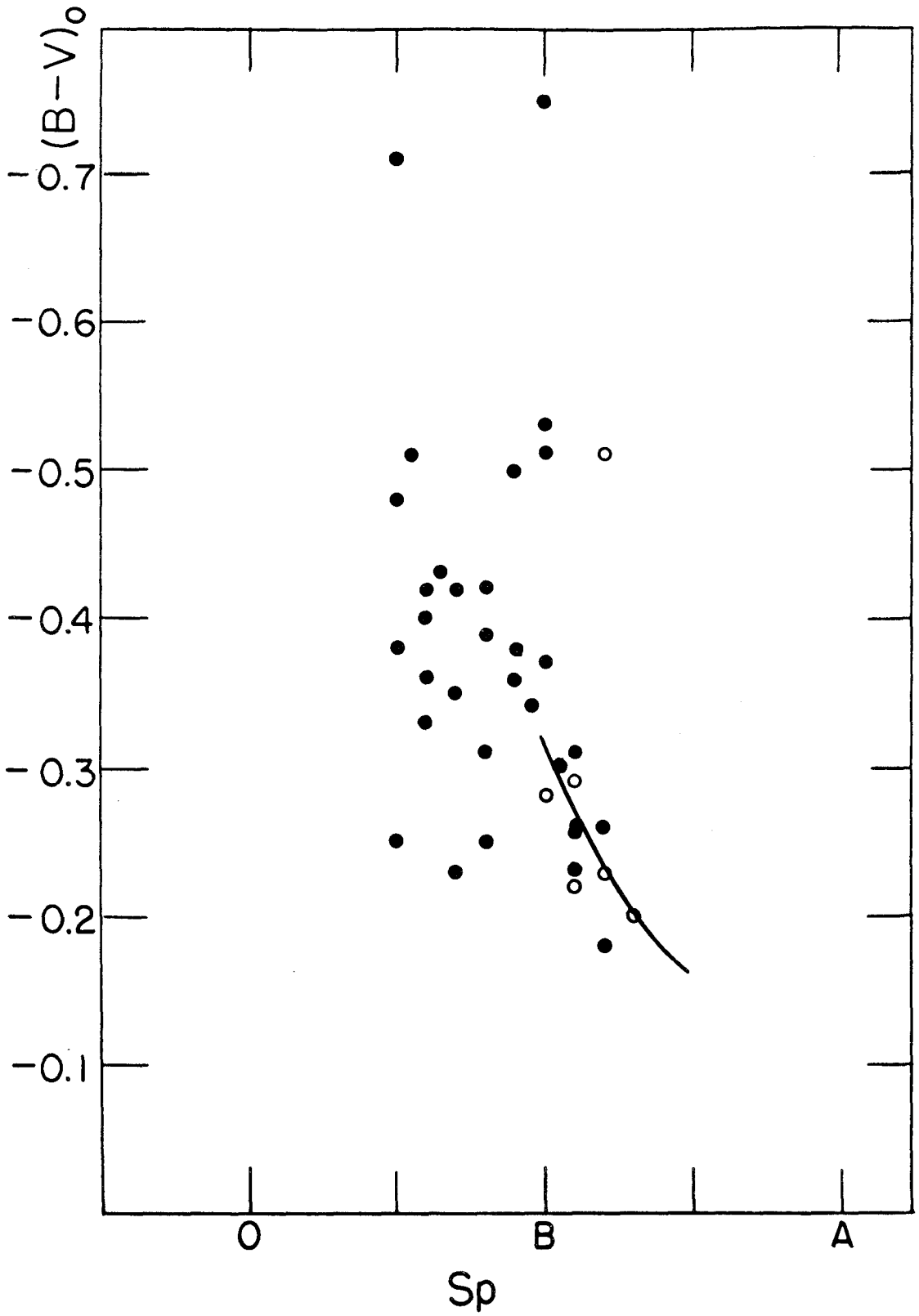

Figure 16

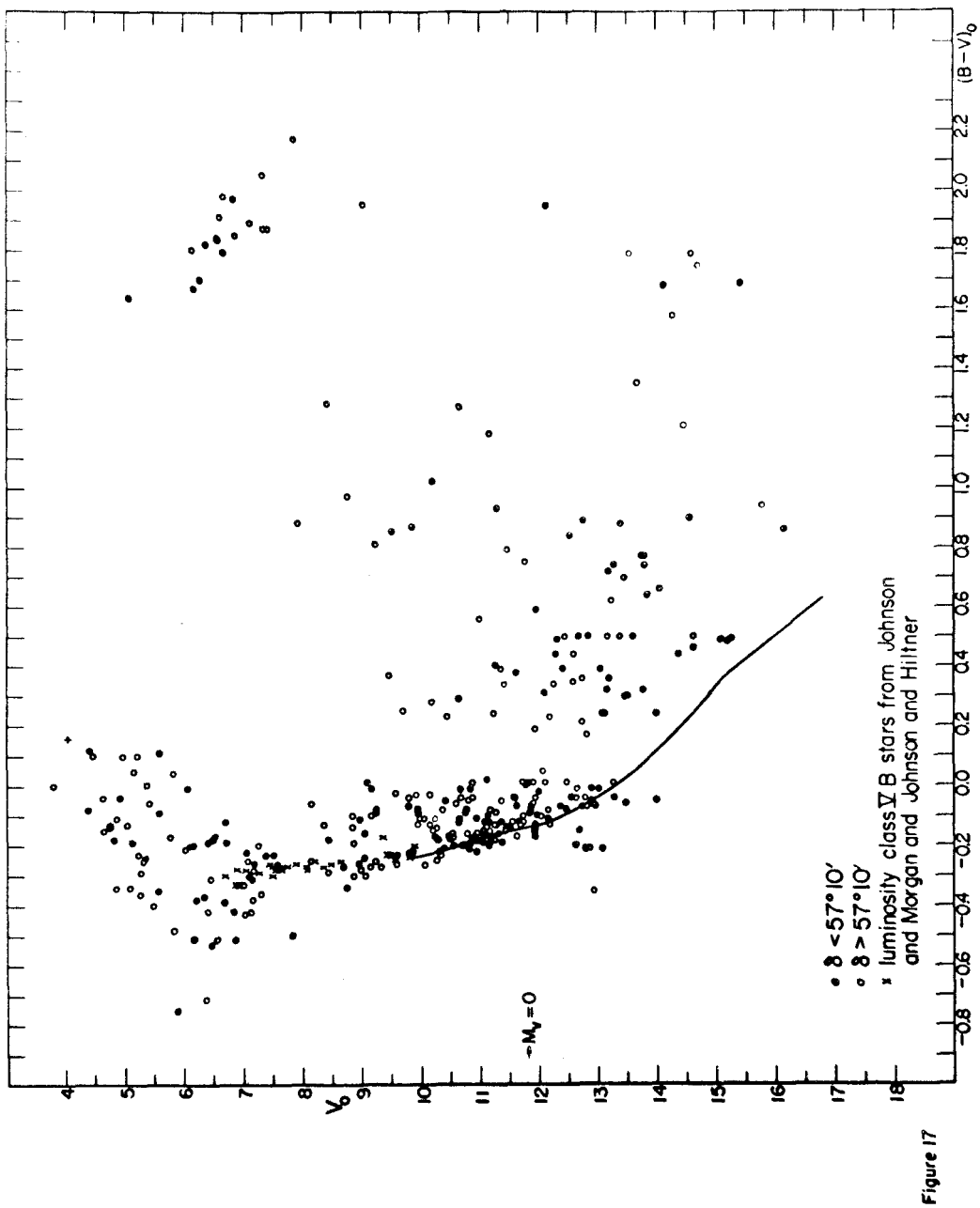
V_0
$(B-V)_0$
$-M_V=0$
• δ < 57° 10'
○ δ > 57° 10'
× luminosity class V B stars from Johnson and Morgan and Johnson and Hiltner

Figure 17

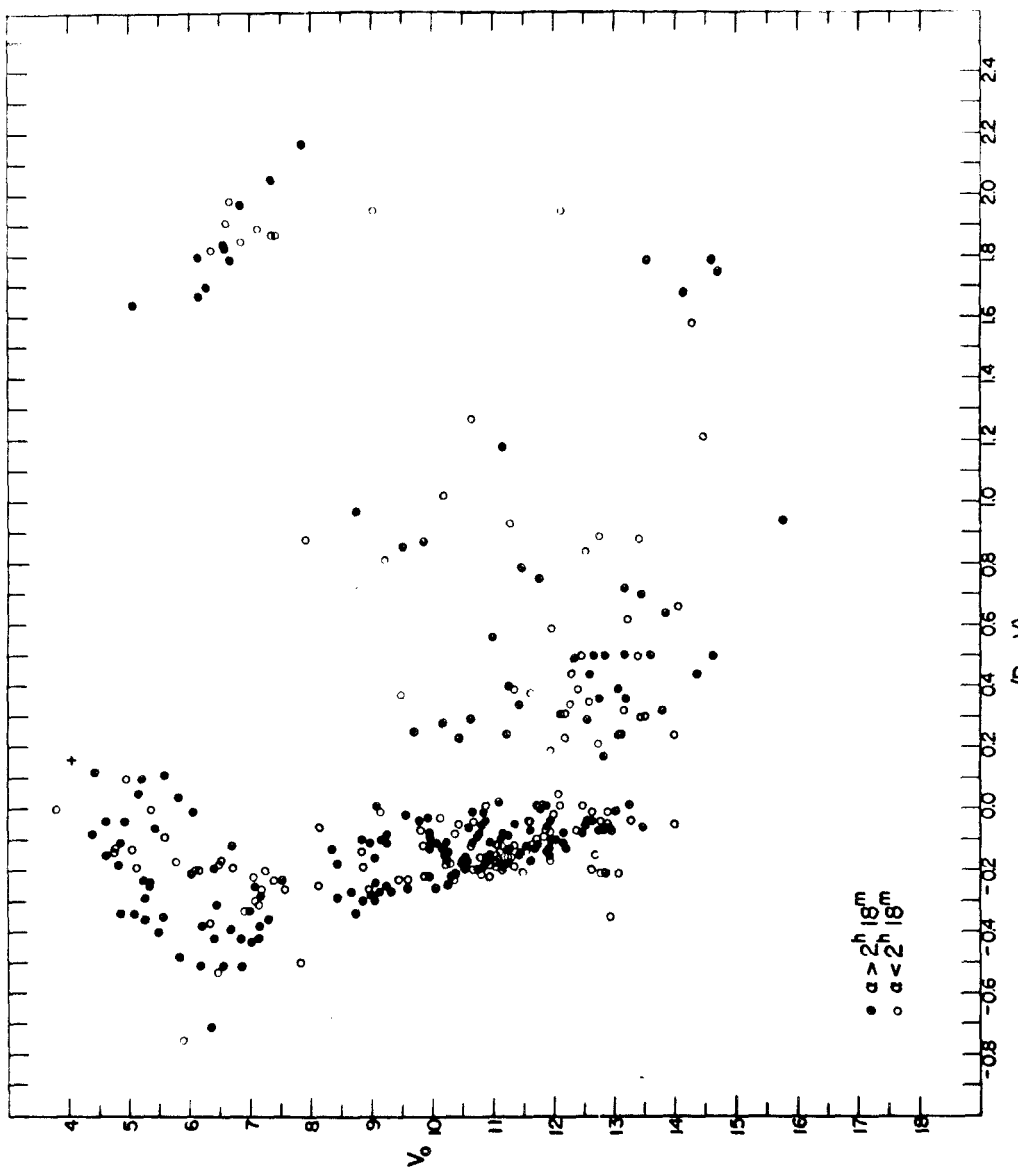

Figure 18

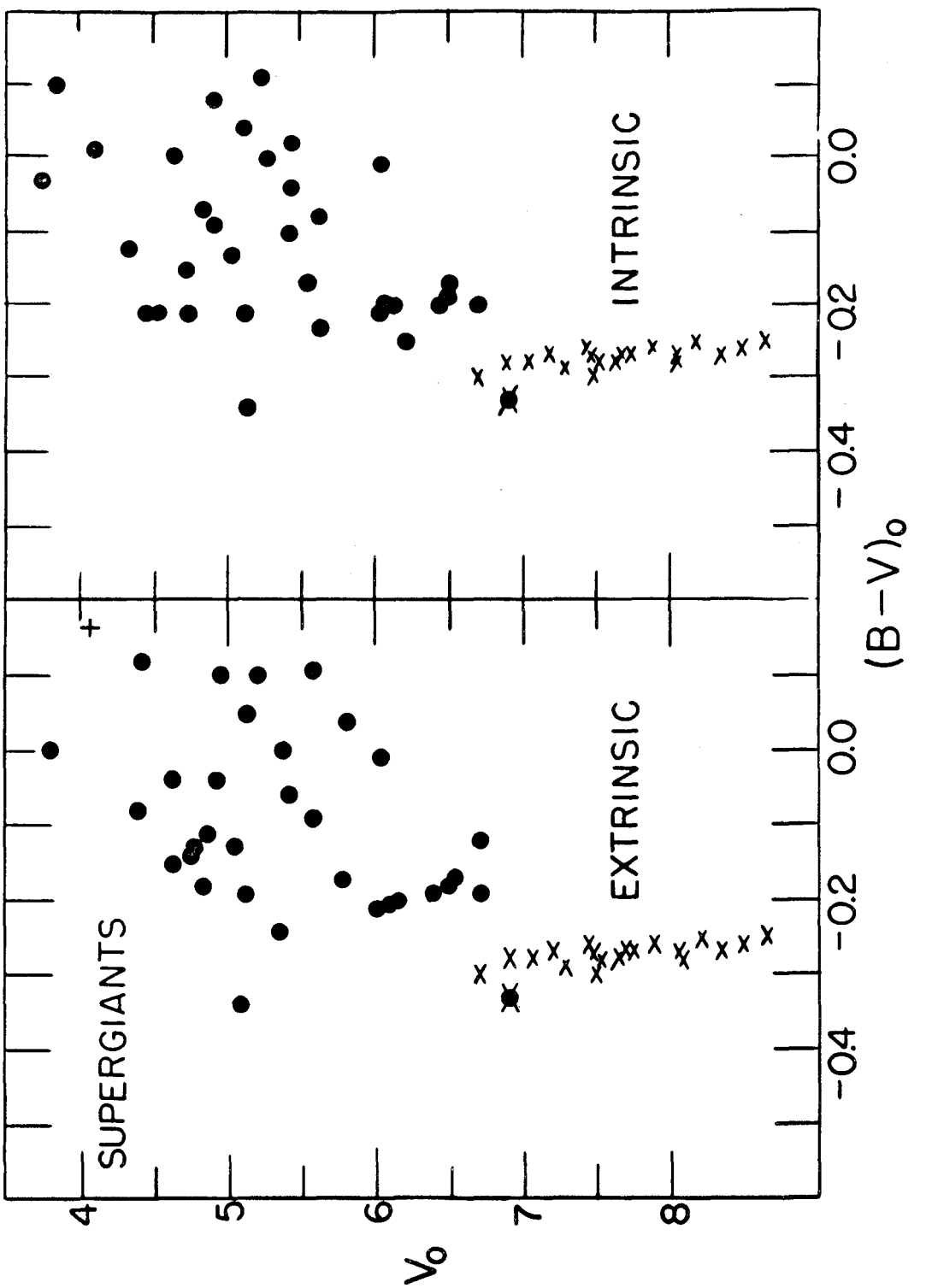
SUPERGIANTS
INTRINSIC
EXTRINSIC
V_o
$(B-V)_o$
4
5
6
7
8
-0.4
-0.2
0.0
-0.4
-0.2
0.0

Figure 19

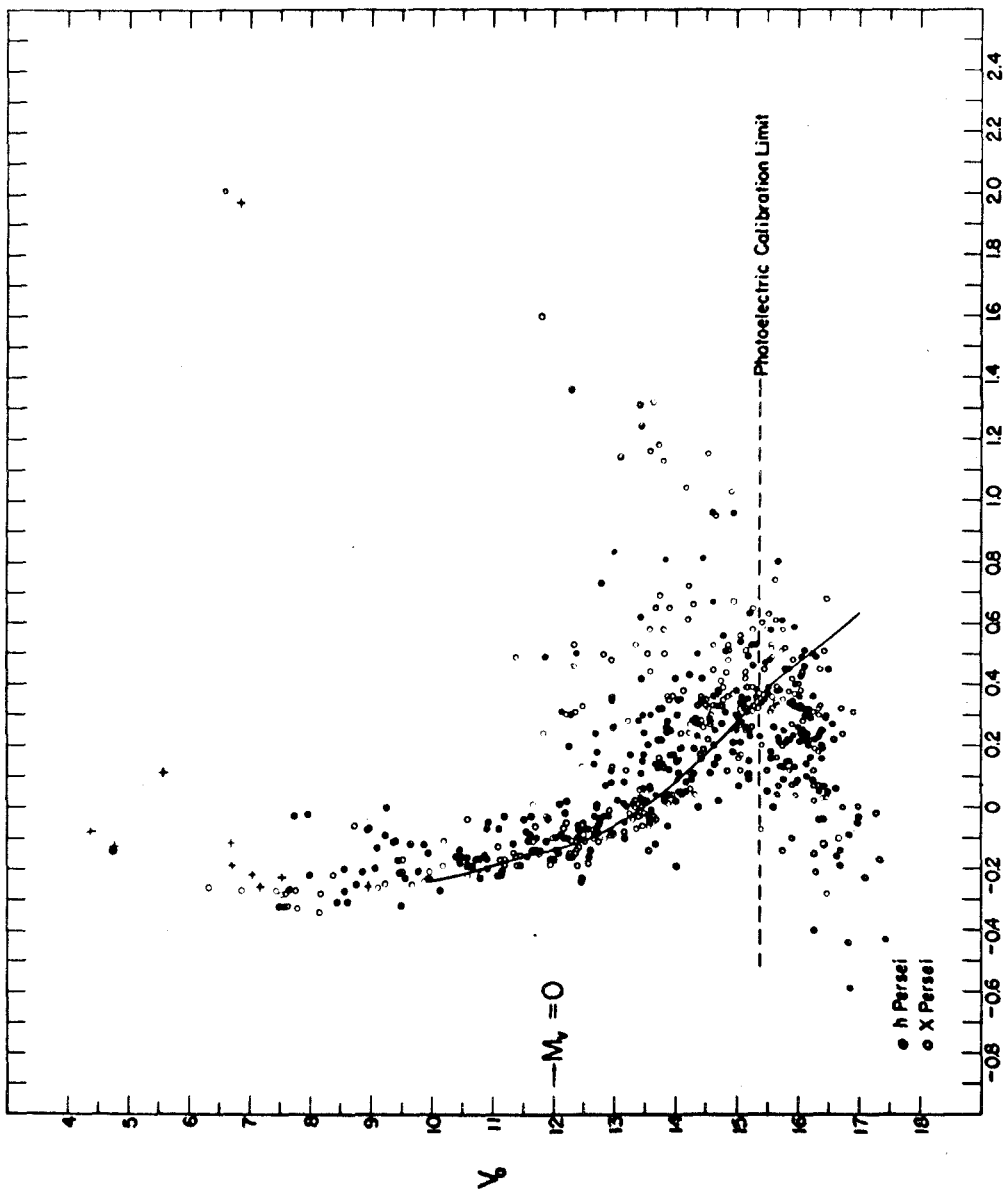
Photoelectric Calibration Limit
—M_v = 0
h Persei
χ Persei
V_0
$(B-V)_0$

Figure 20

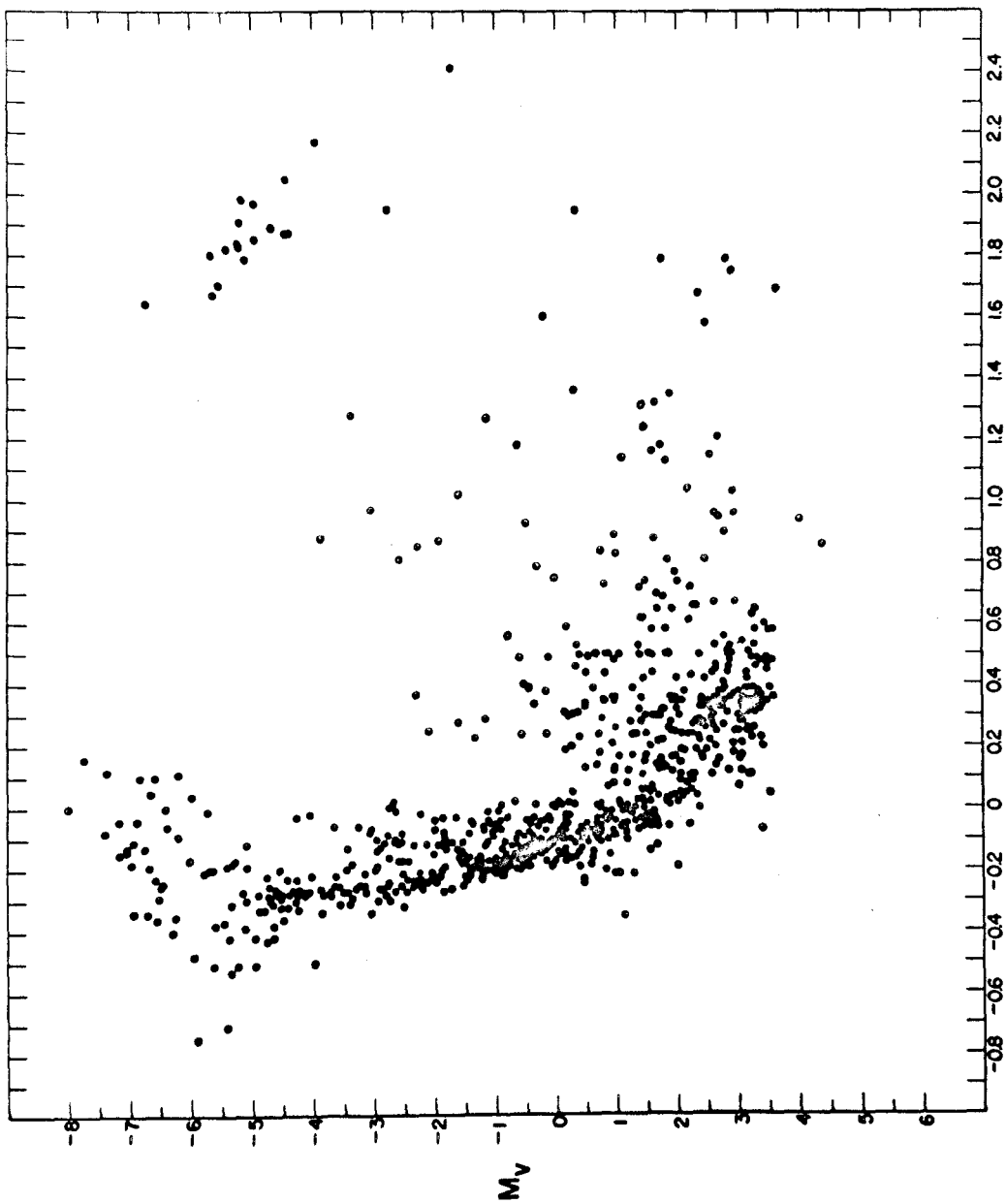
-8
-7
-6
-5
-4
-3
-2
-1
0
1
2
3
4
5
6
M_V
-0.8
-0.6
-0.4
-0.2
0
0.2
0.4
0.6
0.8
1.0
1.2
1.4
1.6
1.8
2.0
2.2
2.4
$(B-V)_0$

Figure 21

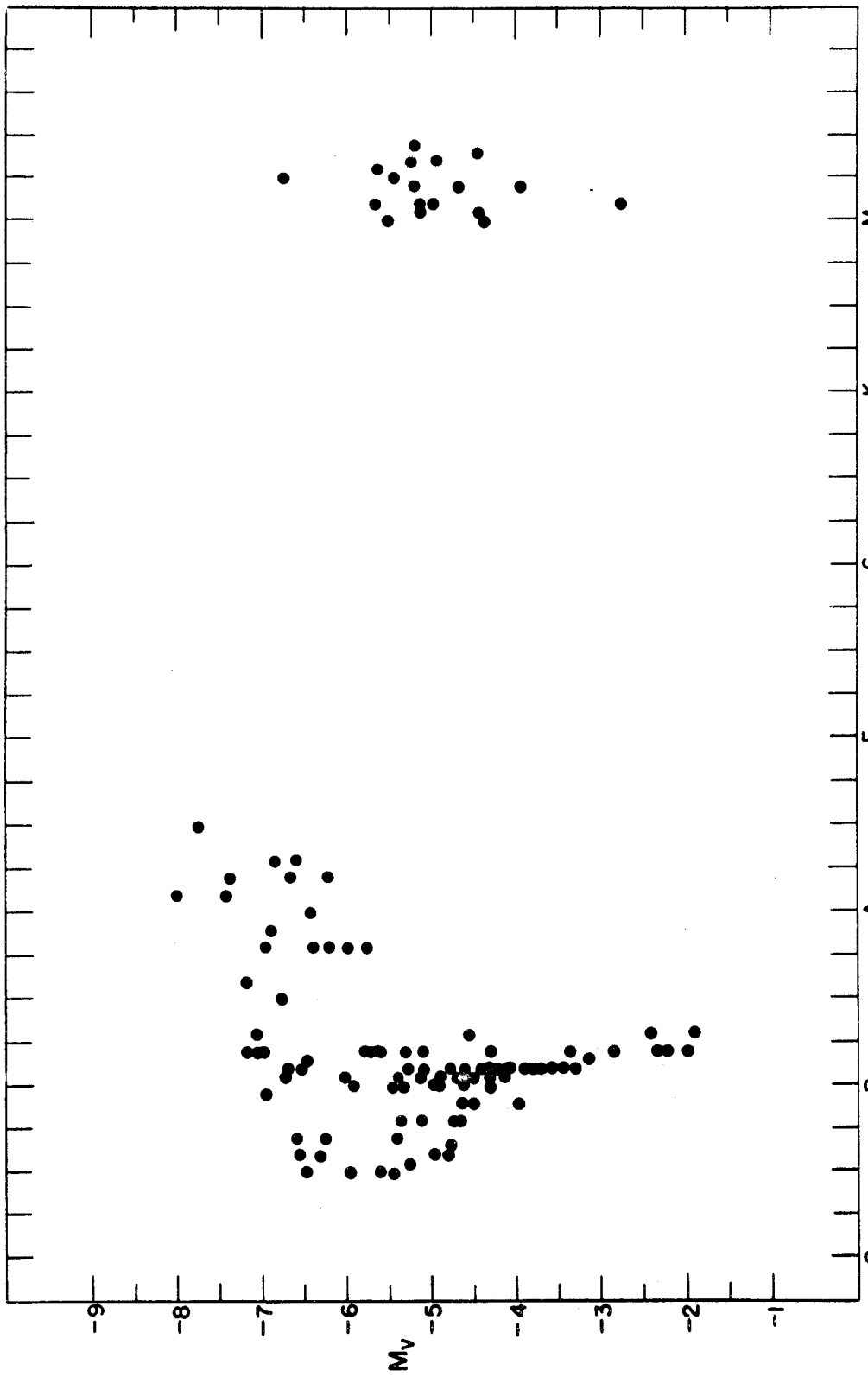

Figure 22

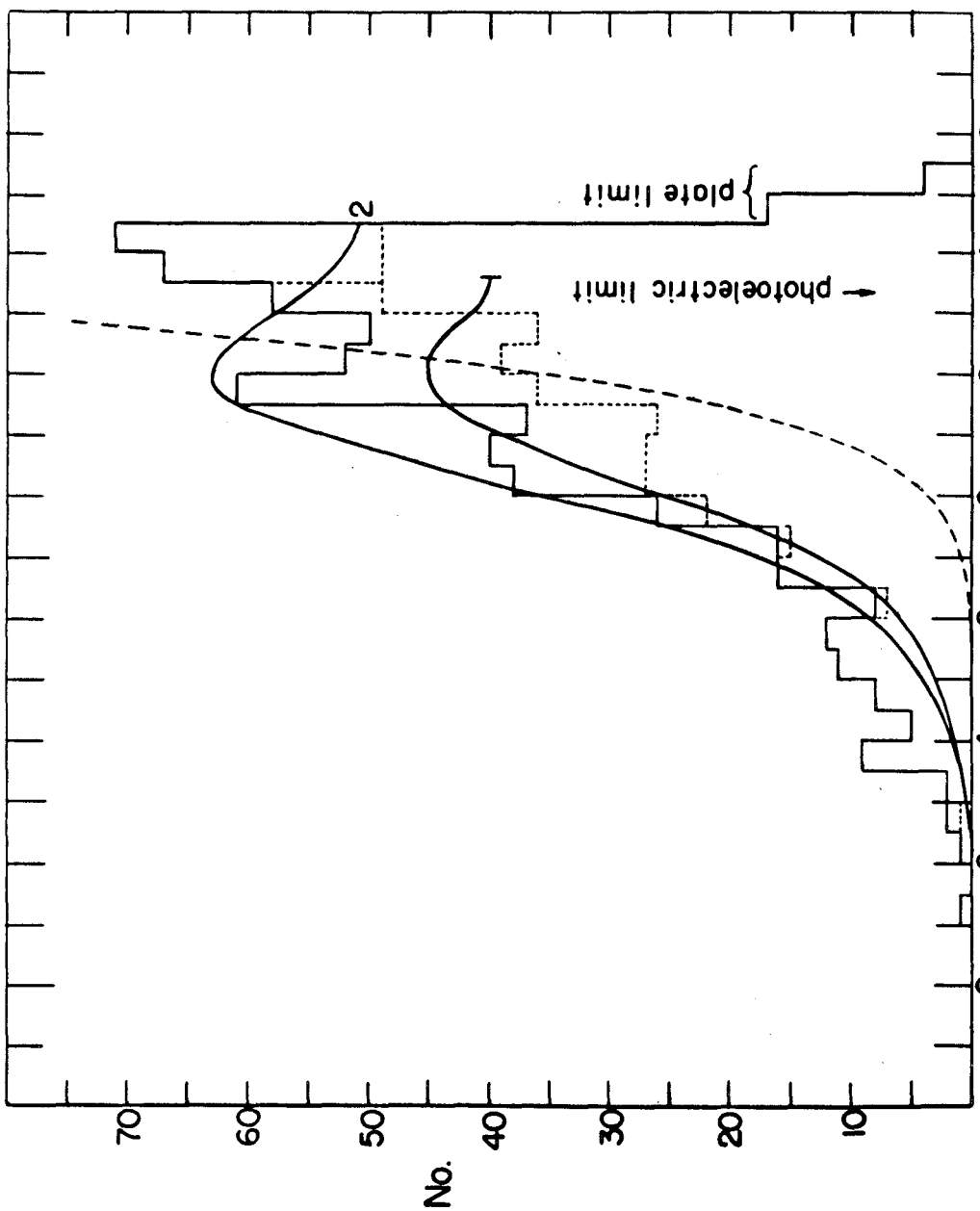
No.
70
60
50
40
30
20
10
M_V
-8
-6
-4
-2
0
2
4
6
2
photoelectric limit
plate limit

Figure 23

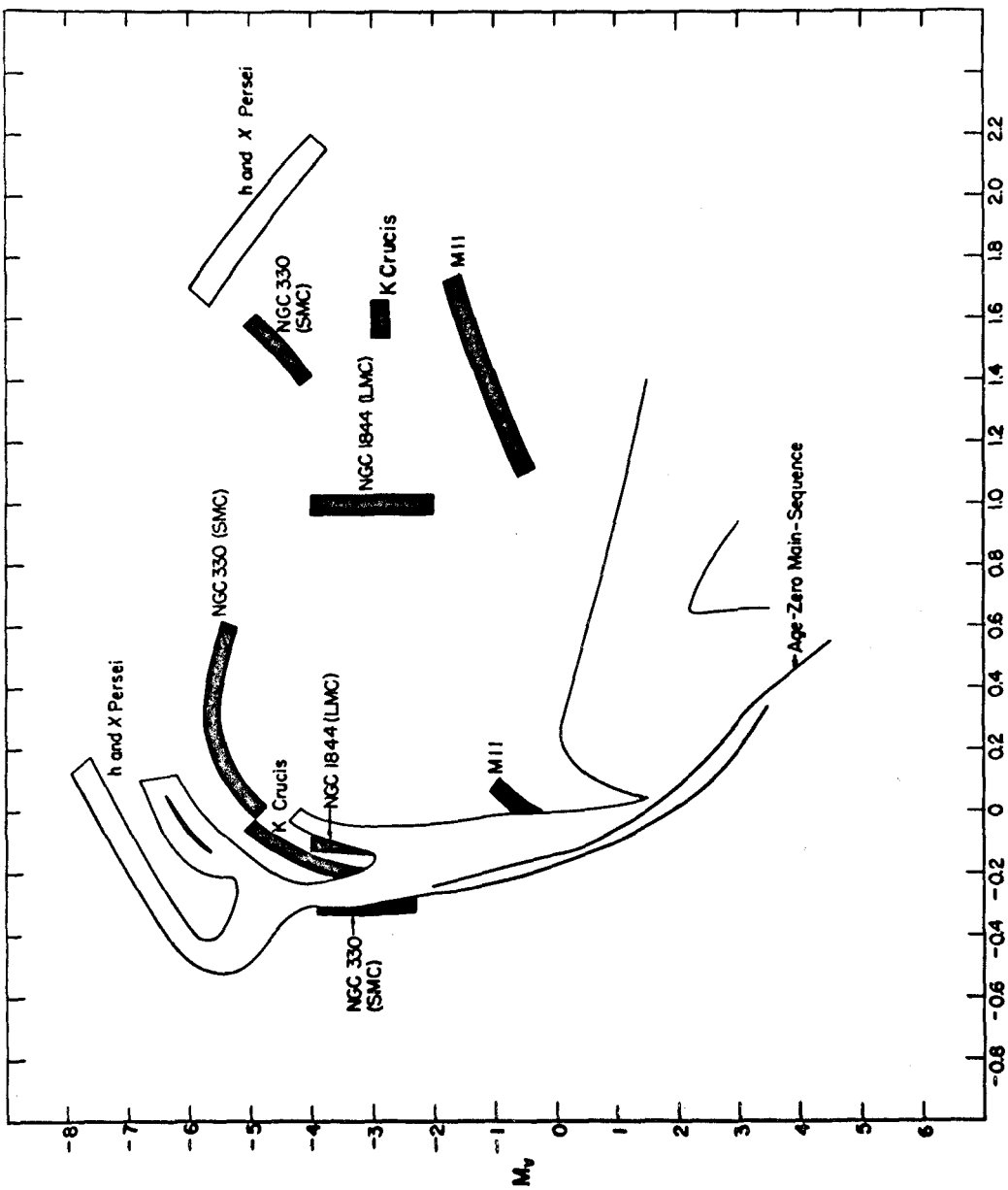
h and X Persei
NGC 330 (SMC)
K Crucis
NGC 1844 (LMC)
M11
Age-Zero Main-Sequence
M_V
$(B-V)_o$

Figure 24

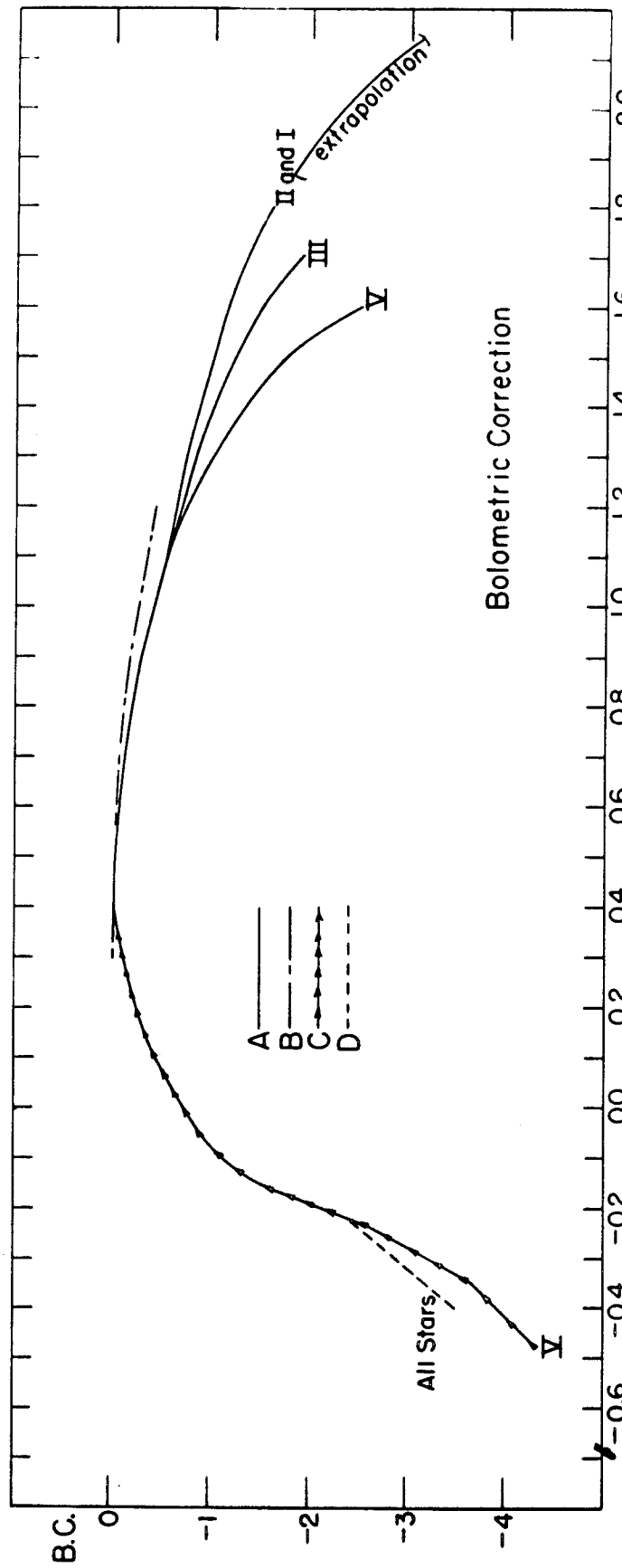
Bolometric Correction
B.C.
0
-1
-2
-3
-4
-0.6
-0.4
-0.2
0.0
0.2
0.4
0.6
0.8
1.0
1.2
1.4
1.6
1.8
2.0
$(B-V)_o$
II and I
extrapolation
III
V
A
B
C
D
All Stars
V

Figure 25

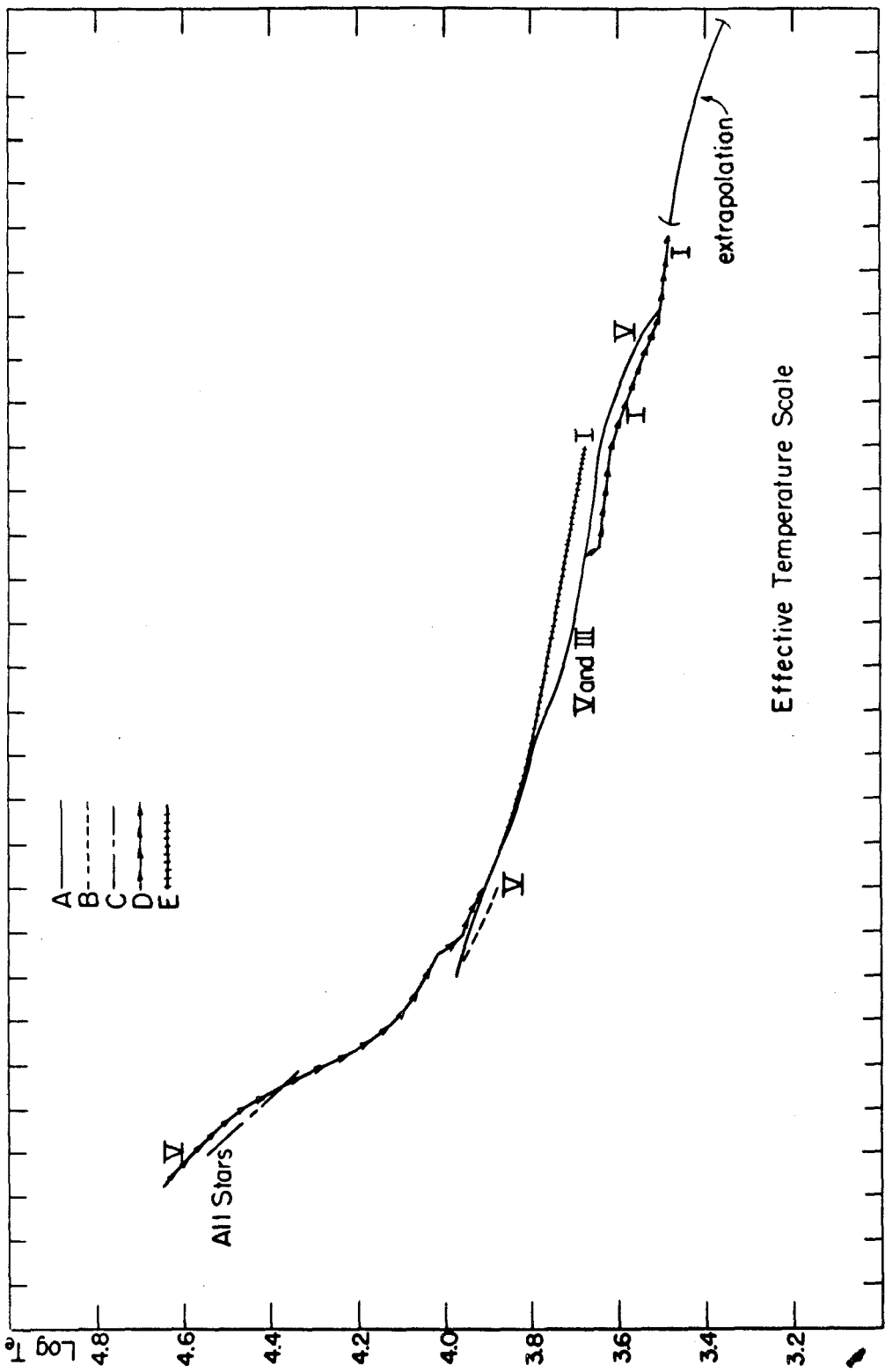
log T_e
4.8
4.6
4.4
4.2
4.0
3.8
3.6
3.4
3.2
-0.6
-0.4
-0.2
0.0
0.2
0.4
0.6
0.8
1.0
1.2
1.4
1.6
1.8
2.0
(B-V)_0
Effective Temperature Scale
A
B
C
D
E
All Stars
V
V
V and III
I
V
I
I
extrapolation

Figure 26

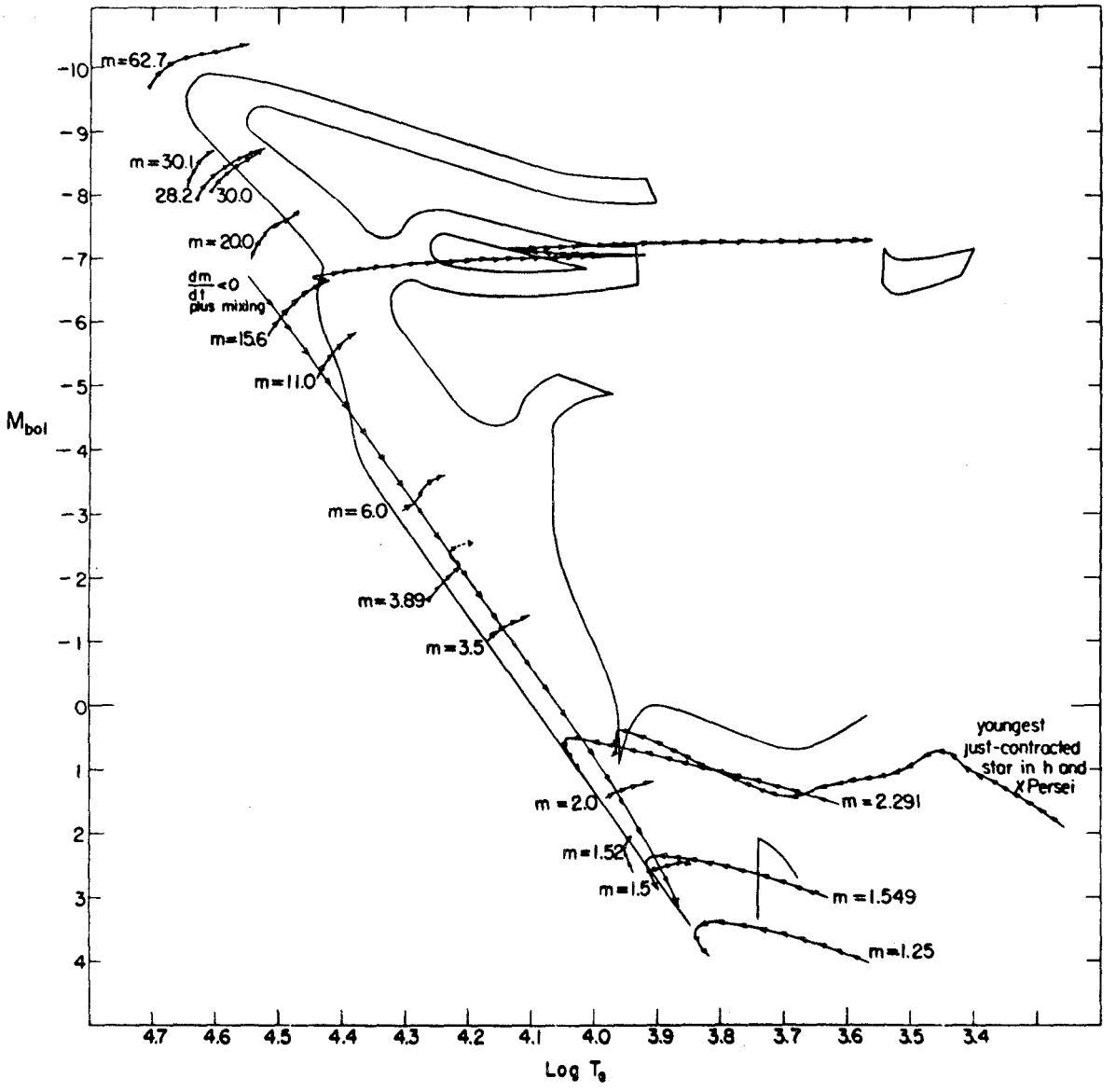
m=62.7
m=30.1
28.2
30.0
m=20.0
dm/dt <0
plus mixing
m=15.6
m=11.0
m=6.0
m=3.89
m=3.5
m=2.0
m=1.52
m=1.5
m=2.291
m=1.549
m=1.25
youngest
just-contracted
star in h and
χ Persei
M_bol
Log T_e
-10
-9
-8
-7
-6
-5
-4
-3
-2
-1
0
1
2
3
4
4.7
4.6
4.5
4.4
4.3
4.2
4.1
4.0
3.9
3.8
3.7
3.6
3.5
3.4

Figure 27